SAINT PETERSBURG STATE UNIVERSITY

As a manuscript

Iakovleva Diana Andreevna

INFLUENCE OF OCEANIC ADVECTION ON THE FORMATION OF THE THERMOHALINE STRUCTURE OF THE NORWEGIAN, IRMINGER, LABRADOR SEAS AND ON THE DEVELOPMENT OF DEEP CONVECTION

Scientific specialty 1.6.17. Oceanology

THESIS

for an academic degree

candidate of geographical sciences

Translation from Russian

Scientific supervisor:

candidate of geographical sciences

Bashmachnikov Igor Lvovich

Saint Petersburg

2025

TABLE OF CONTENTS

INTRODUCTION

Relevance of the research topic and the degree of its development

Oceanic heat advection largely determines the variability of the climate system of the North Atlantic and the Nordic Seas. In particular, oceanic heat advection makes a significant contribution to the variability of the heat content of the upper ocean layer and affects the air temperature of the above-mentioned and adjacent regions, and also affects the intensity of deep convection in the Labrador, Irminger, Norwegian and Greenland seas. The intensity of convection determines the intensity of the return deep flow of the Atlantic meridional overturning circulation (AMOC) and affects the intensity of the AMOC.

The AMOC, in turn, characterizes the intensity of the meridional transfer of oceanic heat in the Atlantic and is largely responsible for the formation of climatic variability in the subpolar and polar latitudes of the Northern Hemisphere. Previous studies have identified periods of weakening and strengthening of the AMOC. From the 1960s to the 1980s, there was a weakening of the AMOC (Caesar et al., 2021; Chen and Tung, 2018; Frajka -Williams et al., 2019; McCarthy et al., 2020). In the second half of the 1990s, the AMOC began to strengthen (Alekseev et al., 2021; Karcher et al, 2003), which peaked in the mid-2000s with a local decline in the mid-1990s (Chen and Tung, 2018). Since the mid-2000s, the AMOC intensity has begun to decline, which also covers the 2010s (Chen and Tung, 2018; McCarthy et al., 2020). The intensity of the AMOC is associated, among other things, with changes in the intensity of deep convection in the Labrador and Irminger Seas (Kuznetsova and Bashmachnikov, 2023). If earlier the volume of deep waters that formed in the Labrador Sea (Yashayaev, 2007) was the most significant for changing the intensity of the AMOC, then by the mid-2010s the area of deep convection in the eastern part of the Subpolar Gyre (in the Irminger Sea and in the area south of Cape Farewell) exceeded the area of the deep convection region of the Labrador Sea, and the volumes of deep waters became comparable (Lozier et al., 2019; Rühs et al., 2021). Deep convection in the subpolar regions of the Atlantic (in the Labrador and Irminger Seas) is caused by cold winters and the presence of pronounced cyclonic circulation in these waters (Yashayaev, 2007; Gladyshev et al., 2018). In the Irminger Sea, increased heat loss from the ocean to the atmosphere did not always lead to increased deep convection (Gladyshev et al., 2016a), and intense convection could occur even with moderate heat loss from the ocean (de Jong et al., 2012). In the Norwegian Sea, on the contrary, deep convection, which was episodically observed in the central part of the Lofoten Basin, was determined, first of all, by the intensity of heat transfer from the ocean to the atmosphere (Fedorov et al., 2021).

The nature of atmospheric circulation affects not only local heat exchange, but also the variability of the intensity of ocean water transport, thereby indirectly changing the ocean surface

temperature (Visbeck et al., 2003). For example, there are numerous studies on the dependence of the speed of ocean currents and their heat transfer in the North Atlantic on the magnitude of atmospheric circulation indices, in particular, the North Atlantic Oscillation (NAO) index (Barrier et al., 2014; Desbruyères et al., 2015; Raj et al., 2018; Iakovleva and Bashmachnikov, 2021).

Purpose and objectives

The aim of the work is to assess the nature and causes of variability of oceanic heat advection into the Norwegian Sea, Irminger Sea and Labrador Sea, as well as the influence of oceanic heat transport on deep convection.

Tasks:

1. To identify the nature and causes of interannual variability of oceanic heat advection into the Norwegian Sea and its influence on the heat content of the upper layer of the sea.
2. To highlight the nature and causes of interannual variability of oceanic heat advection in the Irminger Sea and its influence on the heat content of the upper sea layer and deep convection.
3. To identify the nature and causes of interannual variability of oceanic heat advection in the Labrador Sea and its influence on the upper sea heat content and deep convection.
4. To identify the features of mutual variability of oceanic heat advection into the seas of the Subpolar Gyre of the North Atlantic and the Nordic Seas in connection with the variability of atmospheric circulation in the region.

Scientific novelty

The scientific novelty of the work consists of the following three main research results.

The dependence of deep convection of the Irminger Sea on oceanic heat advection has been revealed. Previously, it was believed that the main contribution to the variability of deep convection in the region is made by the intensity of ocean-atmosphere heat exchange.

Dominant cycles of 2–4 and 5–8 years in duration have been identified in the interannual variability of the heat content of the upper 500-meter layer of the Labrador Sea, and the role of oceanic advection and atmospheric circulation in the formation of these cycles has been revealed.

It is shown that the cause of the interannual variability in the intensity of Atlantic water heat advection into the Nordic Seas, including both branches of the Norwegian Current, is the change in the sea level gradient through the Norwegian Current, which, in turn, is determined by both the Ekman surge and the local rotor of the wind field.

Theoretical and practical significance of the work

The theoretical significance of the work is to identify a possible mechanism for AMOC stabilization. It was previously shown that convection in the Irminger Sea plays a leading role in the long-term variability of the AMOC (Losier et al., 2019, Kuznetsova and Bashmachnikov, 2023). The dissertation shows that the intensity of deep convection in the Irminger Sea decreases with increasing convergence of oceanic heat in the sea, primarily due to advection by the Irminger Current. This suggests that there is a negative feedback between the intensity of convection in the Irminger Sea and the intensity of the AMOC.

The practical significance of the work is the significant influence of oceanic heat transfer from the tropical to the subpolar regions of the Atlantic and further north, and the significant influence of this transfer on the climate of vast territories. The Atlantic Ocean is responsible for about a quarter of the total (oceanic and atmospheric) heat transfer to the polar latitudes of the Northern Hemisphere (Buckley and Marshall, 2016). Monitoring the variability of incoming Atlantic waters as a major factor (Beszczynska-Moller et al., 2012; Aksenov and Ivanov, 2018) of the variability of the thermohaline structure of the Arctic Ocean is extremely important for the possibility of predicting large-scale climate changes in the Northern Hemisphere. Warm Atlantic waters of the AMOC enter the Norwegian Sea and further into other seas of the Arctic Ocean, including the seas of the Russian sector of the Arctic. Atlantic waters spread from west to east, moving along the continental slope and penetrating into the trenches and bays of the Barents, Kara and Laptev seas (Gakkel et al., 1970). Further to the east, only a weak branch of the Atlantic water flow penetrates, going into the Beaufort Sea (Gakkel et al., 1970). The flow of Atlantic waters influences changes in the air temperature of the Arctic (Semenov, 2008; Mokhov et al., 2008; Walczowski et al., 2012), on the area of ice cover in the Barents and Kara Seas (Semenov, 2008; Ivanov et al., 2014; Alekseev et al., 2015), on the climate of the European part of Russia (Mokhov et al., 2008), and also on the climate of Europe (Mokhov et al., 2008).

By influencing the restructuring of the vertical structure of North Atlantic waters, heat and salt flows directly affect the intensity of the influx of biogenic substances into the upper illuminated layer and the intensity of phytoplankton development, which, in turn, determines the development of subsequent trophic links, the bioproductivity of the water area, the variability of oxygen and carbon dioxide flows in the ocean-atmosphere system and the variability of the descending flows of organic carbon into the deep layers of the ocean (Billet et al., 1986). The increase in ice-free water surface and the destruction of water stratification in Arctic regions is another factor that leads to an increase in photosynthesis processes in these waters (Ardyna et al., 2014), and as a consequence – to an increase in bioproductivity. Advection of waters by the Norwegian Current (Atlantic waters) transports phytoplankton and nutrients from areas with higher productivity in temperate and subpolar latitudes to

polar regions, helping to maintain a higher level of primary production there (Vernet et al., 2019; Oziel et al., 2020).

Degree of reliability and testing of results

On the topic of the dissertation research, 6 articles have been published (3 in Russian, 3 in English). All articles have been published in periodicals indexed in the Russian Science Citation Index and Web of Science/Scopus. List of published works on the topic of the dissertation:

1. **Iakovleva D. A.**, Bashmachnikov I. L. Interannual variations of heat and freshwater contents in the cold water dome of the Labrador Sea // Vestnik of Saint Petersburg University. Earth Sciences. – 2019. – V. 64. – №. 1. – P. 136-158.
2. **Iakovleva D. A.**, Bashmachnikov I. L On the seesaw in interannual variability of upper ocean heat advection between the North Atlantic Subpolar Gyre and the Nordic Seas // Dynamics of Atmospheres and Oceans. – 2021. – V. 96. – P. 101263.
3. Fedorov A. M., Bashmachnikov I. L., **Iakovleva D. A.**, Kuznetcova D. A. and Raj R. P. Deep convection in the Subpolar Gyre: Do we have enough data to estimate its intensity? // Dynamics of Atmospheres and Oceans. – 2023. – V. 101. – P. 101338.
4. **Iakovleva D. A.**, Bashmachnikov I. L., Kuznetsova D. A. Impact of the Atlantic Meridional Overturning Circulation on upper water temperature of the North Atlantic and the Atlantic sector of the Arctic Ocean // Oceanology. – V. 63. – №. 2. – P. 149-156.
5. **Iakovleva D. A.**, Bashmachnikov I. L. The role of regional atmospheric circulation in interannual variability of the ocean heat advection in the Nordic Seas // Izvestiya, Atmospheric and Oceanic Physics. – 2023. – V. 59. – №. 5. – P. 470-478.
6. **Iakovleva D. A**, Bashmachnikov I. L, Diansky N. A. Coherence of deep convection in the Irminger Sea with oceanic heat advection // Oceanology. – 2023. – V. 63. – №. 1. – P. S1–S10.

The results of the dissertation research were presented at 14 conferences, of which 9 were all-Russian and 5 were international. Below is a list of published abstracts of conference reports:

1. **Iakovleva D. A.**, Bashmachnikov I. L. Trends and cyclicities of heat content in the central regions of the Labrador Sea. Sixteenth All-Russian Open Conference "Modern Problems of Remote Sensing of the Earth from Space" IKI RAS (Moscow), November 12-16, 2018.
2. **Iakovleva D. A.**, Bashmachnikov I. L. Trends and cyclicities of heat content and fresh water in the cold water dome of the Larbrador Sea. II All-Russian Conference "Hydrometeorology and Ecology: Achievements and Development Prospects" (St. Petersburg), December 19-20, 2018.

3. **Iakovleva D. A.**, Bashmachnikov I. L. Relationship between interannual variability of the heat content of the upper layer of the Labrador Sea and the North Atlantic Oscillation (NAO) index. IV All-Russian Scientific Conference of Young Scientists "Integrated Studies of the World Ocean" (Sevastopol), April 22-26, 2019.
4. **Iakovleva D. A.**, Bashmachnikov I. L. Redistribution of heat transport in the North Atlantic in connection with the variability of the North Atlantic Oscillation phase. Seventeenth All-Russian Open Conference "Modern Problems of Remote Sensing of the Earth from Space" IKI RAS (Moscow), November 11-15, 2019.
5. Bashmachnikov I. L., Fedorov A. M., **Iakovleva D. A.**, Vesman A. V. Interannual variability of deep convection intensity in the subpolar seas of the North Atlantic and Arctic Ocean. III All-Russian Conference "Hydrometeorology and Ecology: Achievements and Development Prospects" (St. Petersburg), December 18-19, 2019.
6. **Iakovleva D.A.**, Bashmachnikov I.L. Redistribution of the meridional oceanic heat flux in the North Atlantic depending on the NAO phase. III All-Russian Conference "Hydrometeorology and Ecology: Achievements and Development Prospects" (St. Petersburg), December 18-19, 2019.
7. **Iakovleva D.**, Bashmachnikov I. Variations of oceanic and atmospheric heat fluxes in the North Atlantic and their link to the North Atlantic Oscillation Index. EGU General Assembly 2020 (Vienna, Austria), 4–8 May 2020.
8. **Iakovleva D. A.**, Bashmachnikov I. L., Golubkin P. A. Mechanism of formation of deep convection in the Irminger Sea. V All-Russian scientific conference of young scientists "Comprehensive studies of the World Ocean" (Kalingrad), May 18-22, 2020.
9. **Iakovleva D. A.**, Bashmachnikov I. L. Relationship of spatiotemporal variability of water temperature in the North Atlantic and Arctic Oceans with the AMOC. The Nineteenth International Conference "Modern Problems of Remote Sensing of the Earth from Space (Physical Foundations, Methods and Technologies for Monitoring the Environment, Potentially Hazardous Phenomena and Objects)" (Moscow), November 15-19, 2021.
10. **Iakovleva D. A.**, Bashmachnikov I. L. Heat balance of the subpolar North Atlantic. VI All-Russian scientific conference of young scientists "Comprehensive studies of the World Ocean" (Moscow), April 18-24, 2021.
11. **Iakovleva D.**, Bashmachnikov I. The heat balance shapes deep convection in the Irminger Sea. EGU General Assembly 2021 (Vienna, Austria), 19–30 April 2021.
12. **Iakovleva D. A.**, Bashmachnikov I. L. Causes of interannual variability of deep convection intensity in the Irminger Sea. All-Russian scientific conference "Seas of Russia: Year of Science

and Technology in the Russian Federation – UN Decade of Ocean Sciences" (Sevastopol), September 21-24, 2021.

13. Fedorov A. M., Bashmachnikov I. L., **Iakovleva D. A.**, Kuznetcova D. A. and Raj R. P. Deep convection in the Subpolar Gyre, how much data is needed to estimate its intensity? EGU General Assembly 2022 (Vienna, Austria), 23–27 May 2022.
14. **Iakovleva D. A.,** Bashmachnikov I. L. Causes of interannual variability of oceanic heat flux at the Svinoy section. Twentieth International Conference "Modern Problems of Remote Sensing of the Earth from Space (Physical Foundations, Methods and Technologies for Monitoring the Environment, Potentially Hazardous Phenomena and Objects)" (Moscow), November 14-18, 2022.
15. **Iakovleva D. A.**, Bashmachnikov I. L. Changes in ocean-atmosphere heat fluxes and wind speed with changes in AMOC intensity. VII All-Russian Scientific Conference of Young Scientists "Integrated Studies of the World Ocean" (St. Petersburg), May 15-19, 2023.

Individual results obtained within the framework of this work were recognized with awards:

1. Prize-winner in the III All-Russian competition of student scientific papers on Arctic topics of the National Arctic Scientific and Educational Consortium (2019)
2. Prize winner olympiads Petropolitan Science (Re)Search, St. Petersburg State University (2019)
3. Prize-winner of the competition of term papers, diploma and scientific papers 2018-2019, dedicated to the 200th anniversary of the discovery of Antarctica by Russian sailors (2020)

Personal contribution of the author

The author's personal contribution consists of choosing methods, writing scripts for data processing, calculations and data visualization, analysis of the obtained results, writing the text of articles and the text of the dissertation.

Structure of the dissertation

The dissertation corresponds to the following points of the specialty passport 1.6.17. Oceanology (geographical sciences): external forces acting on the ocean, and flows of matter and energy; processes of formation of water masses, their spatio-temporal structure, hydrophysical fields of the World Ocean.

The dissertation consists of an introduction, six chapters, a conclusion, a list of abbreviations, a list of references including 150 references, and three appendices. The work is presented on 89 pages, including 27 figures and 9 tables.

Introduction. The relevance of the work is described, the goals and objectives of the dissertation are formulated, the novelty, theoretical and practical significance of this work, the degree of reliability and testing of the results are indicated, the main scientific results and provisions submitted for defense are presented.

Chapter 1. A physical and geographical description of the study area is given. Literary sources devoted primarily to the study of heat content and oceanic heat fluxes in the northern part of the North Atlantic and in the Nordic Seas, as well as the study of the AMOC, are analyzed in detail. A brief overview of the main indices of atmospheric and oceanic circulation is given.

Chapter 2. Presents a description of the data arrays on the basis of which this study was conducted, provides cross-validation of data from various sources, and provides the main calculation formulas used in the work.

Chapter 3. The main causes of variability of oceanic heat advection into the Norwegian Sea are presented. It is shown that oceanic heat advection into the Norwegian Sea is determined by the change in the sea level gradient through the Norwegian Current, which in turn is determined by both the Ekman surge and the local rotor of the wind field.

Chapter 4. The relationship between heat content, heat balance and deep convection in the Irminger Sea is investigated. The leading influence of oceanic heat transfer on deep convection in the Irminger Sea is proven.

Chapter 5. The nature of interannual variability of heat content and freshwater content in the Labrador Sea is studied, the main cyclicities are identified, the relationship of these cyclicities with the North Atlantic Oscillation index is revealed, and the mechanisms of this relationship, including oceanic advection, are described. The influence of heat content on deep convection in the Labrador Sea is considered.

Chapter 6. The relationship between the water temperature of the North Atlantic and the Atlantic sector of the Arctic Ocean with the variability of the AMOC intensity is considered. The antiphase nature of the oceanic heat transfer to the Nordic Seas and to the Labrador and Irminger Seas and the relationship of this phenomenon with the NAO phase are revealed.

The conclusion contains the main findings of the dissertation.

Acknowledgments

The author thanks his scientific supervisor, candidate of geographical sciences Igor Lvovich Bashmachnikov, for his work, patience and motivation, as well as his parents and grandmother.

The research obtained as a result of this work received financial support from:

- Grant of the Russian Science Foundation No. 17-17-01151, project “Dynamics of deep convection in subpolar and polar regions of the ocean in conditions of changing climate, its connection with fresh water and heat flows, and influence on the Atlantic meridional thermohaline circulation”
- Grant of Saint Petersburg State University No. 94033410, project “Atlantic Gateway to the Arctic: Ocean Circulation as a Factor of Long-Term Variability of Arctic Climate and the State of Polar Ecosystems”
- Project of the Ministry of Science and Higher Education of the Russian Federation No. 13.2251.21.0006 (identifier RF-225121X0006, agreement No. 075-10-2021-104 in the information system "Electronic Budget" of the Russian Federation) "The Arctic region in the Earth's climate system and its transformation under global warming"

Main scientific results

1. The intensity of the Irminger Sea convection is determined primarily by the convergence of oceanic heat advection (correlation coefficient -0.57); i.e., the less heat is transferred to the sea with the recirculating waters of the Irminger Current over the previous period, the greater will be the maximum convection depth (Iakovleva et al., 2023 p. S8).
2. The water transport at the Svinoy section is determined by the sea level gradient, which is formed primarily by the Ekman surge. The correlation of the variability of the sea level gradient caused by the combined variability of the Ekman surge magnitude and the local wind field rotor significantly correlates with the water transport (0.57) and with the oceanic heat flux (0.50) (Iakovleva and Bashmachnikov, 2023, p. 547).
3. It is shown that despite similar variability of the convection depth in the Labrador and Irminger Seas of the Subpolar Gyre, significant differences are observed in some years. Thus, during the winters of 2003/2004-2005/2006, convection weakened in the Irminger Sea (the convection depth was 400 and 600 m), while in the Labrador Sea, convection increased (the convection depth was 1200-1600 m). This suggests that in addition to the factors that have a joint effect on the convection depth in both seas, regional factors also have a significant effect on the convection depth. (Fedorov et al., 2023, p. 5).
4. Wavelet analysis of heat content and freshwater content allows us to identify two dominant interannual cycles: 5–8 years long (throughout the entire observation period) and 2–4 years long (since 2000). Wavelet coherence showed the significance of the relationship for 5–8 year and 2 year cycles with similar cycles of the NAO index (Iakovleva and Bashmachnikov, 2019, pp. 153–154).

5. Based on the analysis of several data sets with different time series durations, it was shown that the AMOC forms the second mode of the EOF of the upper layer temperature of the North Atlantic and the Atlantic sector of the Arctic Ocean, the contribution of which is 20–27% of the total water temperature variance (Iakovleva et al. 2023, p. 178).
6. A strong influence of the AMOC on the upper layers of the central part of the Irminger Sea has been revealed, where the variability of the AMOC intensity observed in recent decades can lead to an amplitude of temperature fluctuations in the upper 100-meter sea layer of 1.5–2 °C. This significantly affects the intensity of convection in this key region (Iakovleva et al. 2023, p. 178).
7. In the Subpolar Gyre, there is a high correlation between the upper ocean heat content and the NAO index, caused by changes in the regional atmospheric circulation: for the Irminger Sea from 0.40 to 0.65, and for the Labrador Sea from 0.30 to 0.70 (depending on the data set). It is shown that at low values of the NAO index, not only an increased heat loss from the sea surface is observed, but also a weaker regional heat convergence with oceanic transport. The latter is the result of a decrease in heat transport by the Irminger Current and an increase in the influx of cold water with the East Greenland Current and the Baffin Bay Current. Numerical estimates show that a change in the intensity of oceanic heat advection almost doubles the effect of ocean-atmosphere heat exchange in response to the NAO effect (Iakovleva and Bashmachnikov, 2021, p. 9).

Provisions submitted for defense

1. The flow of Atlantic waters and the advection of oceanic heat into the Norwegian Sea are determined by a regional anomaly in the atmospheric pressure field, which leads to a change in the sea level gradient due to the Ekman surge, as well as an increase in the local rotor of the wind field.
2. A high dependence of the interannual variability of heat content and deep convection in the Irminger Sea on the intensity of oceanic heat advection, primarily associated with the recirculating waters of the Irminger Current, was revealed.
3. In the interannual variability of the heat content of the upper 500-meter layer of the Labrador Sea, dominant cycles of 5–8 years duration have been identified, which are caused by variability in oceanic heat advection and ocean-atmosphere heat exchange and are associated with variability in the North Atlantic Oscillation index.

CHAPTER 1. PHYSICAL AND GEOGRAPHICAL DESCRIPTION OF THE STUDY AREA

The study area (Fig. 1.1) is the seas of the Subpolar Gyre of the North Atlantic Ocean and the Nordic Seas of the Arctic Ocean. The seas of the Subpolar Gyre of the Atlantic Ocean include the Labrador Sea and the Irminger Sea. According to the Soviet nomenclature, the Nordic Seas of the Arctic Ocean include the Norwegian, Greenland, Barents and White seas (Treshnikov et al., 1967). In particular, the Norwegian Sea is considered in this work from the Nordic Seas.

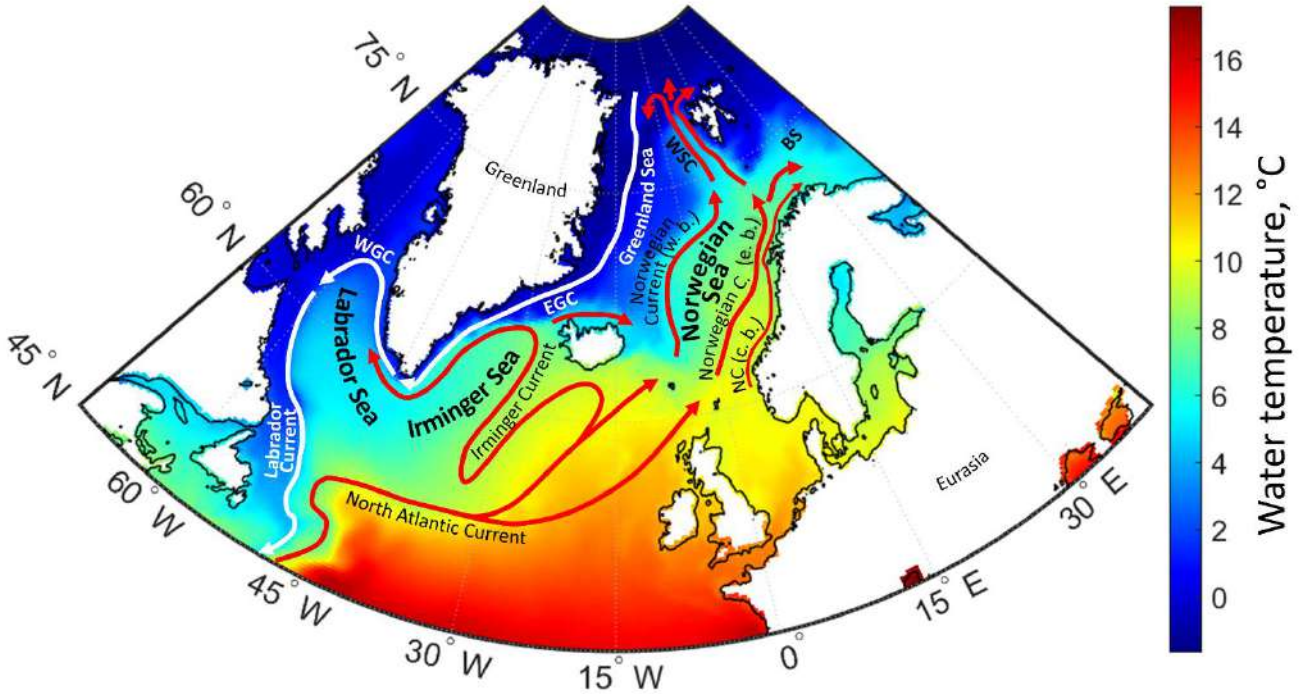

Figure 1.1. Map of the study area: spatial distribution of surface water temperature averaged over 1993-2020 based on ARMOR-3D data. BS – the Barents Sea, EGC – the East Greenland Current, NC (c. b.) – the coastal branch of Norwegian Current, Norwegian C. (e. b.) – the eastern branch of Norwegian Current, Norwegian Current (w. b.) – the western branch of Norwegian Current, WGC – the West Greenland Current, WSC – the West Spitsbergen Current.

1.1 Atlantic meridional overturning circulation

The processes occurring in the Subpolar Gyre have a significant impact on the intensity of the Atlantic meridional overturning circulation (AMOC) (Rhein et al., 2011; Lozier et al., 2019; Kuznetsova and Bashmachnikov, 2021). The AMOC characterizes the generalized mass (heat, salt) transport in the meridional direction. Heat advection by the upper branch of the AMOC to the subpolar regions of the North Atlantic is redistributed in the Iceland Basin between the two main continuations of the North Atlantic Current: the Irminger Current, which transports heat to the Subpolar Gyre, and the Norwegian

Current, which transports heat through the Nordic Seas. A relatively small fraction of the total heat flux also enters the Norwegian Current with one of the continuations of the Irminger Current, which goes around Iceland from the west (the so-called North Iceland Irminger Current).

Atlantic waters enter the Nordic Seas through the Faroe–Shetland Strait, where the flow forms the eastern and western branches of the Norwegian Current, which carry warm waters further into the Arctic Basin. Atlantic waters account for two thirds of the total inflow of waters entering the Arctic Basin (Gakkel et al., 1970). The eastern branch is mainly formed by the Shetland branch of the North Atlantic Current with an average water transport of 3–4 Sv (1 Sv = 10^6 m^3/s), and the western branch is formed by the North Iceland Irminger Current with an average water transport of less than 1 Sv and the Faroe branch of the North Atlantic Current with an average water transport of 3–4 Sv (Hansen et al., 2008).

The lower branch of the AMOC, the AMOC return deep current, is formed in areas of deep convection in the Irminger, Labrador, and Greenland seas, where intense heat loss from the ocean is observed in winter. It has long been believed that the variability of the volume of deep water generated in the Labrador Sea (Yashayaev, 2007) is one of the most significant factors of AMOC variability. Variability in the volume of deep water generated in the Irminger Sea is a much more important source of interannual variability of the AMOC (Kuznetsova and Bashmachnikov, 2021; Lozier et al., 2019). With a rather low convection intensity until the early 2000s, by the mid-2010s the deep convection area of the eastern Subpolar Gyre (in the Irminger Sea and in the area south of Cape Farewell) exceeded the deep convection area of the Labrador Sea for the first time since the 1950s, and the volume of newly formed intermediate water masses became comparable to that of the Labrador Sea. According to literary sources, this situation persisted at least until the late 2010s (Rühs et al., 2021).

The possible influence of the AMOC on the temperature of Atlantic waters in the Arctic Ocean follows from the observed nature of the transfer of temperature anomalies by the surface current system of the North Atlantic. In particular, it has been shown that the variability of the temperature of the North Atlantic Current waters in the Faroe-Shetland Strait can penetrate far into the Eurasian Basin of the Arctic Ocean (Alekseev et al., 2019; Karcher et al., 2003; Polyakov et al., 2000). It is also possible to trace the spread of sea surface temperature anomalies from the tropical North Atlantic to the Fram Strait (over a period of approximately 4 years) and further along the edge of the Eurasian Basin shelf to the central regions of the Arctic Ocean (Alekseev et al., 2021). It is assumed that such a spread of temperature anomalies in the ocean is supported by large-scale mechanisms of ocean-atmosphere interaction, which, in turn, lead to an increase in atmospheric heat transport to the Arctic, which has a significant impact on the interannual variability of sea ice extent of the Arctic Ocean (Alekseev et al., 2017).

The dynamics of the AMOC in the North Atlantic can be reliably estimated since the beginning of the operation of the transatlantic RAPID observational array in the first half of the 2000s (Volkov et al., 2020). Since the first half of the 1990s, the AMOC dynamics can be estimated from the results of joint processing of satellite altimetry and Argo float data, from individual observations of currents in some years, and also using indirect indicators (Caesar et al., 2021; Chen and Tung, 2018; Frajka-Williams et al., 2019; McCarthy et al., 2020). All available data indicate a process of gradual weakening of the AMOC from the 1960s to the 1980s. Then, in the second half of the 1990s, there was a short-term strengthening of the AMOC. During this period, the volume, temperature and salinity of Atlantic waters in the Nordic Seas, and, somewhat later, in the Eurasian Basin of the Arctic Ocean, increased and remained high relative to the climatic average until the mid-1990s (Alekseev et al., 2021; Karcher et al., 2003). Since the mid-1990s, a local decrease in the intensity of the AMOC has been observed (Chen and Tung, 2018), which was accompanied by a decrease in the heat flux and flow of the West Spitsbergen Current (Karcher et al., 2003). In the mid-2000s, a local maximum of the AMOC was observed, after which a fairly rapid decrease in the AMOC intensity began, which continued until the 2010s noted also according to direct observations on the RAPID section (26° N) (Chen and Tung, 2018; McCarthy et al., 2020). It was accompanied by a decrease in deep convection in the Labrador and Irminger Seas (Bashmachnikov et al., 2019) and a weakening of the Subpolar Gyre currents (the Labrador, the East Greenland, the West Greenland and the Irminger currents) (Belonenko et al., 2018). Then, the AMOC water transport stabilized at lower values. The vast majority of modern climate models predict a long-term trend towards a further slowdown of the AMOC, on average by 30% by the end of the 21st century (Visbeck, 2007). This trend may be superimposed on the previously noted decadal and intra-decadal oscillations.

Of course, the AMOC is only one of the mechanisms that can regulate variations in the oceanic heat flux in the subpolar and polar regions. Based on the analysis of natural and model data, many researchers associate the increase in the intensity of heat transfer to the north through the Nordic Seas in the 1990s with a regional increase in atmospheric cyclonic circulation over the basin and a weakening of heat transfer by the ocean surface in this area (Alekseev et al., 2017; Karcher et al., 2003). The intensity of heat fluxes in this region is also associated with the influence of large-scale atmospheric structures characterized by the North Atlantic Oscillation (NAO) index, the East Atlantic Oscillation (EAO) index and the Wangerheim-Giers circulation index (Karcher et al., 2003, Vesman et al., 2023). On the other hand, NAO variability and AMOC dynamics are presumably linked through numerous direct and feedback mechanisms (see, e.g., Alekseev et al., 2017; Våge et al., 2011a).

1.2 Atmospheric and oceanic circulation indices

North Atlantic Oscillation (NAO)

The NAO is the main mode of variability of the atmospheric circulation of the North Atlantic. The NAO index is the difference in atmospheric pressure between the Azores High and the Icelandic Low. Sometimes the negative and positive phases of the NAO are studied as separate weather conditions due to a certain shift of the above-mentioned centers of action between the positive and negative phases of the NAO (Barrier et al., 2015). Alternatively, the angular index of the NAO (the Angle NAO Index) (Wang et al., 2012) determines the zonal migration of the Icelandic Low relative to the actual position of the Azores High. On interannual time scales, the angular NAO index is quite closely related to the classical NAO index.

The NAO affects heat fluxes (heat content) differently in different regions of the North Atlantic (Marshall et al., 2001; Visbeck et al., 2003; Levermann and Born, 2007; Barrier et al., 2015; Belonenko et al., 2018; Iakovleva and Bashmachnikov, 2019). During the positive phase of the NAO, westerly winds pass through the Labrador Sea and are deflected northward over the eastern Norwegian Sea (see, e.g., Visbeck et al., 2003). Warmer air prevails over the Norwegian Sea, while cold and dry conditions are observed over the Labrador Sea due to the strengthening of northwesterly winds from the Canadian Archipelago. As a result, heat loss from the Labrador Sea surface increases, while that from the Norwegian Sea decreases. When the NAO is in a negative phase, westerly winds are generally concentrated further south, but pass northward over the eastern Subpolar Gyre. Then, warm and humid conditions prevail over the Labrador and Irminger Seas, while cold and dry air over the Norwegian Sea is caused by the strengthening of polar northwesterly winds from the Greenland Sea. During our study period, the NAO index was predominantly positive. Its increasing trend since the 1970s reversed in the early 1990s, followed by a new increase after 2010 (see Luo et al., 2011; Wang et al., 2012). The corresponding variability of heat content in the upper Labrador Sea, with an increase since 1993 and a decrease after 2010, is presumably related to changes in the atmospheric circulation regime controlled by the NAO index (Yashayaev et al., 2015; Yashayaev and Seidov, 2015; Iakovleva and Bashmachnikov, 2019).

Variability in the intensity of ocean water transport is also shaped by the nature of atmospheric forcing, regulating ocean-atmosphere heat fluxes within and outside the studied regions through changes in sea surface temperature (Visbeck et al., 2003). In particular, the NAO has a significant impact on the velocity of ocean currents and heat transport, which is still not fully understood. When the NAO index is positive, the transport in the southern part of the Norwegian Current increases. An increase in oceanic heat advection in the Nordic Seas was observed from 1993 to 2016, when the positive phase of the NAO dominated (Raj et al., 2018). However, a significant part of the thermohaline anomalies of the Atlantic

water inflow recirculates around the Nordic Seas (Eldvik et al., 2009), which reduces correlations with the direct impact of the NAO in the Nordic Seas on decadal time scales.

East Atlantic Oscillation (EAO)

In the work (Wallace and Gutzler, 1981) the EAO is characterized by three centers: one located to the southwest of the Canary Islands (25° N and 25° W), another to the west of Great Britain (55° N and 20° W) and the third near the Black Sea (50° N and 40° E). In a later work (Nesterov, 2009) it is noted that during the positive phase of the EAO, the negative surface pressure anomaly is widespread in the North Atlantic north of 30° N (the maximum is to the east of Newfoundland). During the positive phase of the EAO (Nesterov, 2009), a dipole structure of surface pressure anomalies is formed (the center of the positive anomaly is between Iceland and Great Britain, the negative one is in the eastern part of the Tropical Atlantic).

In winter, during the positive phase of the EAO, the zonal circulation type dominates over the Atlantic-European region, whereas during the negative phase of the EAO, the meridional circulation type dominates (Mikhailova and Yurovsky, 2016). The authors (Mikhailova and Yurovsky, 2016) also note that during the positive phase of the EAO, the jet stream over the North Atlantic shifts to the southern (34-38° N) and central (42-46° N) positions, while during the negative phase of the EAO, an increase in the jet stream is observed in its northern position (54-58° N). In winter, during the positive phase of the EAO, the jet stream is located in the central and southern position, thereby increasing cyclonic activity in the temperate latitudes and decreasing in the polar latitudes (Mikhailova and Yurovsky, 2016). During the negative phase of the EAO, an anomalous anticyclonic circulation is formed over the North Atlantic, the jet stream is in a northern position, thus cyclonic activity increases in polar latitudes and decreases in temperate latitudes (Mikhailova and Yurovsky, 2016).

Arctic Oceanic Oscillation (AOO)

The intensity of oceanic advection of heat and salt, which influence the formation of the thermohaline regime in the Labrador Sea, is characterized, among other things, by the Arctic Ocean Oscillation Index (AOOI). The intensity of advection of cold and fresh Arctic waters into the sea can be characterized by the phase of the AOO index. It is calculated as the difference in sea levels between the central part of the Beaufort anticyclonic gyre and the last closed current line around the dome of cold freshened waters forming there (Proshutinsky et al., 2015). When the AOO index is positive, freshened surface water, like ice, accumulates in the Canadian part of the Arctic Basin. During periods of negative index values, an increase in cyclonic circulation is observed in the central and Eurasian parts of the Arctic Basin and an intensification of the water transport of freshened waters and ice through the Fram/Denmark and Davis Straits. The interannual variability of the AOO index is dominated by 10–14-year cyclicity (Proshutinsky et al., 2015).

Arctic Oscillation (AO)

The influence of the Arctic on the climate of the Labrador and Irminger Seas and the Nordic Seas depends on the degree of closure of the tropospheric and stratospheric circulation in the polar regions. This closure is determined by the AO index, which is the difference in air pressure in the central Arctic and in the region of 37–45° N, and characterizes the intensity of the leading mode of atmospheric pressure oscillations in the entire Northern Hemisphere. When the AO index decreases, the polar anticyclonic vortex over the Arctic weakens and the exchange of air masses between the Arctic and temperate latitudes intensifies. At low values of the AO index, colder weather is observed over the northwestern part of the Labrador Sea, and warmer weather is observed over the southeastern part (Bingyi and Jia, 2002). The AO index correlates well with the NAO index, and the NAO is often called a regional manifestation of the AO. The interannual variability of the AO index exhibits approximately the same cyclicities as the NAO index: 2.5–3.5, 6–8 and 12–20 years (Jevrejeva et al., 2003).

Atlantic Multidecadal Oscillation (AMO)

The temperature of the waters brought by the Irminger Current is associated with the AMO index, which is the average anomaly of the sea surface temperature in the North Atlantic between 0 and 70° N (Drinkwater et al., 2014). The AMO index has a pronounced cyclicity with cold and warm phases lasting 10–20 and 60–80 years, and the temperature difference between the extremes reaches 1 °C. During the warm phase of the AMO index, the number and intensity of tropical storms also increase, but in temperate latitudes the number of storms is weakly associated with the phases of this index. Its value increased from the 1990s to 2000, after which it began to decrease (Yashayaev et al., 2015).

East Atlantic/Western Russia Pattern (EAWRP)

The positive phase of the EAWRP is associated with positive height anomalies located over Europe and northern China, and negative height anomalies located over the central North Atlantic and the northern Caspian Sea. During the positive (negative) phase of the EAWR, wetter (drier) conditions are observed over eastern China, and drier (wetter) conditions prevail over central Europe and the Mediterranean region. The positive (negative) phase of the EAWR is also associated with above-average (below-average) temperatures over eastern Asia and below-average (above-average) temperatures over western Russia and northeastern Africa (Barnston and Livezey, 1987).

Tropical/Northern Hemisphere Pattern (TNHP)

The positive phase of the TNHR model is associated with below-average surface temperatures across the western and central United States and across central and eastern Canada (Mo and Livezey, 1986). Above-average precipitation is also observed in the central and eastern subtropical North Pacific,

and below-average precipitation is observed in the western United States, Cuba, the Bahamas, and much of the central North Atlantic Ocean (Mo and Livezey, 1986).

Polar/Eurasia Pattern (PEP)

The positive phase of PEP reflects negative height anomalies over the polar region and positive anomalies over northern China and Mongolia. The positive phase reflects a strengthened circumpolar vortex, while the negative phase reflects a weaker-than-average polar vortex. PEP is mainly associated with above-average temperatures over eastern Siberia and below-average temperatures over eastern China. PEP is also associated with above-average precipitation over the polar region north of Scandinavia.

Scandinavian Pattern (SP)

SP has a major circulation center over Scandinavia and weaker centers of opposite sign over western Europe and eastern Russia/western Mongolia. The positive phase of SP is associated with positive height anomalies, sometimes reflecting large blocking anticyclones, over Scandinavia and western Russia, while the negative phase of this pattern is associated with negative height anomalies in these regions (Barnston and Livezey, 1987).

The positive phase of PEP is associated with below-average temperatures in central Russia and western Europe. This period also sees higher than average precipitation in central and southern Europe and lower than average precipitation in Scandinavia.

1.3 Norwegian Sea

For the seas of the Russian Arctic, as well as for Europe, the influence of Atlantic waters, which are part of the AMOC and which enter more northern areas through the Norwegian Sea, is important. The Norwegian Sea belongs to the Nordic Seas and is a marginal sea of the Arctic Ocean. The main circulation in the Norwegian Sea is the Norwegian Current.

In the southern part of the Norwegian Sea, regular oceanographic observations are carried out at the Svinoy transect (around 66° N), which crosses all three branches of the Norwegian Current. The average water transport of Norwegian Current waters through the Svinoy transect is 7–9 Sv (Orvik et al., 2001; Hansen et al., 2008), and if only Atlantic waters are taken into account, it is 3–4 Sv (Hansen et al., 2015). The total water transport remains virtually unchanged up to the Fram Strait, where, according to buoy stations at 78° N, the average water transport is 7 Sv with 3 Sv of Atlantic waters (Schauer et al., 2004; Beszczynska-Moller et al., 2011). Atlantic waters are observed throughout the Norwegian Current from the surface to a depth of 400–600 m (Latarius and Quadfasel, 2016). However, the temperature of the Atlantic waters decreases as they move north due to heat exchange with the

atmosphere and mixing with cold Greenland waters. Thus, Atlantic waters in the Svinoy section are distinguished as waters with a salinity above 35 and a temperature above 5 °C (Orvik et al., 2001), or waters with a salinity above 34.95 and a temperature above 3 °C (Latarius and Quadfasel, 2016), or only by temperature above 4 °C (Hansen et al., 2015). The Atlantic waters in the Fram Strait already have a 2 °C isotherm (Beszczynska-Moller et al., 2011).

Attempts to relate the water transport through the Svinoy section to the values of the main index of atmospheric circulation in the North Atlantic – the North Atlantic Oscillation (NAO) – did not show a stable significant relationship. Thus, a significant relationship was observed with the water transport of the eastern branch of Atlantic waters for April 1996 – February 1999, which was associated with variability of the westerly winds, but not for April 1995 – April 1996 (Orvik et al., 2001). Some increase in the velocity of the eastern branch of the Norwegian Current with an increase in the NAO was found on composite maps of satellite altimetry (Raj et al., 2018). Summer values of water transport through the Svinoy section were highly and significantly correlated with the NAO index for February–April (0.75) (Mork and Blindheim, 2000), but the reasons for such an interseasonal relationship are unclear and therefore the relationship itself seems questionable. These results indicate that the NAO is, at a minimum, not the only factor determining the intensity of the northward Atlantic water flux in this region. Other authors have investigated the relationship between the water transport of the Norwegian Current branches and the local wind field. Thus, Orvik and Skagseth (2003) found a high correlation (0.88) between the zonally integrated wind stress rotor at 55° N and the water transport of the eastern branch of the Norwegian Current at 62° N, with a water transport lag of 15 months. Further research (Orvik, 2022) showed that the position of the zero rotor line of the wind field, which separates the subpolar and subtropical oceanic gyres in the eastern Atlantic, plays a major role in the dynamics of the eastern branch of the Norwegian Current. The position of the zero rotor line of the wind field is largely determined by the values of the East Atlantic Oscillation index (East Atlantic Pattern – EAP). The oceanic heat flux of Atlantic waters, the lower boundary of which is determined by the 4 °C isotherm, averages 125 TW at a base temperature of 0 °C (Hansen et al., 2015), while the total oceanic heat flux at the same base temperature is approximately 200 TW (Lebedev et al., 2019). This flux increased by approximately 18% over 20 years (from 1993 to 2013), with the largest changes occurring between 2003 and 2006 (Hansen et al., 2015). This was associated with an increase in the temperature of the Faroe Current waters, which increased by 1 °C from the mid-1990s to the early 2000s (Hansen et al., 2015). After this, the heat flux began to decrease, and Orvik (2022) found no significant trends in oceanic heat advection by the eastern branch of the Norwegian Current over the period 1995–2020. Variability in the intensity of heat advection by the eastern branch of the Norwegian Current through the Svinoy transect was determined by variability in water transport rather than water temperature.

In general, according to ARGO floats, the surface layer of the waters of the Norwegian and Greenland Seas has been warming, at least for the period 2005–2014, since the influx of warm Atlantic waters into the Norwegian and Greenland Seas was greater than the outflow (Lebedev et al., 2019). A significant role in the redistribution of heat and the increase in the temperature of the Norwegian-Greenland region is played by the heat transfer by eddies from the eastern branch of the Norwegian Current to the central regions of the Lofoten Basin (Bashmachnikov et al., 2023). This flow accounts for approximately 30% of the total heat influx into the Nordic Seas with the eastern branch of the Norwegian Current.

On days when the mixed layer maximum in the Lofoten Basin of the Norwegian Sea is at its extreme, two low pressure areas above sea level are formed – the Icelandic Low and the area over the Scandinavian Peninsula (Fedorov et al., 2021). The low pressure above sea level in the Scandinavian region forms strong northerly and north-easterly winds over the Lofoten Basin during this period (Fedorov et al., 2021). Also, the heat loss from the sea increases almost twice as much as the climatic average for the same dates (Fedorov et al., 2021).

1.4 Labrador Sea

The Labrador Sea is one of the subpolar seas of the North Atlantic, a place where cold and freshened polar waters interact with warm and salty subtropical waters. It is one of the few areas where deep winter convection (reaching depths of 2000 m) is observed and where the deep water masses of the North Atlantic are formed. Spreading south, these waters form a significant part of the return deep flux of the Atlantic meridional thermohaline circulation, which is one of the long-term climate-forming factors (Buckley and Marshall, 2016).

In the Labrador Sea, deep convection occurs during fairly intense autumn-winter cooling (thermal convection) and intensifies during salinization of the surface layer during ice formation (salinity convection). With relatively stable thermohaline characteristics of the deep layers, changes in temperature and salinity of the surface layer during the warm period of the year determine the intensity of water stratification by the beginning of autumn-winter cooling, creating conditions for further development of convective mixing.

Cold freshened Arctic waters (with a temperature of less than 2 °C and a salinity of 33–34) enter the Labrador Sea from the Arctic Ocean through the Davis Strait and with the East Greenland Current. In the latter case, these waters are already modified due to mixing with warm Atlantic waters in the Denmark Strait and the Irminger Sea. The East and West Greenland Currents have a complex structure. In addition to modified Arctic waters, these currents also carry modified Irminger Current waters (with a temperature of more than 4 °C and a salinity of more than 34.9). The Irminger Current waters can be

traced in the Labrador Sea at depths of about 500 m and partially penetrate into the central parts of the sea (Yashayaev, 2007). This is associated with intense eddy transport from the southwestern continental slope of Greenland (Chanut et al., 2008). The waters of the East Greenland Current, merging with Arctic waters coming from the Davis Strait and with freshened waters of Hudson Bay, form the Labrador Current. From the south, a small amount of subtropical Atlantic water enters the Labrador Sea due to transfrontal exchange via the North Atlantic Current.

Horizontal heat and salt fluxes, as well as vertical heat and fresh water exchange with the atmosphere, form the main characteristics and distribution patterns of surface water masses in the Labrador Sea. The upper layers of the Subpolar Cyclonic Gyre of the sea are occupied by the subpolar surface water mass (SPWM). The surface fraction of the SPWM (100–200 m) is characterized by low salinity of 34.7–34.85 and temperature of 2–4 °C. It is especially pronounced in the western and central parts of the sea. The lower fraction of the SPWM (200–500 m) has increased salinity values of 34.77–34.92 and temperature of 3–5 °C, and is especially pronounced in the eastern and southern parts of the sea. Both fractions are formed by mixing, in different proportions, fresh and cold waters of the Greenland and Labrador Currents with warmer and saltier waters of the Irminger Current (McCartney and Talley, 1982; Khatiwala et al., 2002; Yashayaev, 2007; Brambilla et al., 2008; Rhein et al., 2011). The intermediate and deep water masses in the Labrador Sea include the “classical” Labrador Sea Water (CLSW) with a temperature of 2.95°C and a salinity of 34.86, and its lighter fraction, the Upper Labrador Sea Water (ULSW) with a temperature of 3.5 °C and a salinity of 34.80. It is assumed that the ULSW is formed in a zone of intense eddy activity in the southwestern Labrador Sea (possibly in the Labrador Current) and is drawn into the West Coastal Deep Current (Stramma et al., 2004; Yashayaev, 2007). Both fractions of the Labrador Sea water mass are formed during deep convection. The deepest layers of the Labrador Sea are occupied by the North Atlantic Deep Water (NADW) with a temperature of 1.30–2.55 °C and a salinity of 34.87–34.96. It is formed as a result of the removal and modification of deep waters from the Greenland Sea through the Denmark Strait and the Faroe–Shetland Strait (Khatiwala et al., 2002; Yashayaev, 2007; Yashayaev and Clarke, 2008; Rhein et al., 2011; Jenkins et al., 2015).

Since the 1960s, several periods have been identified in the interannual variability of the thermohaline regime of the Labrador Sea in the literature. The coldest and freshest deep waters were observed in 1987–1994. This is due to the severe winters of this period, during which intense deep convection was observed (Curry and McCartney, 1996; Yashayaev, 2007). Anomalously warm and salty waters were observed in 1962–1971, 1977–1983, and 1994–2006 (Yashayaev, 2007). After 1998–1999, a decrease in the density of the Labrador water mass formed as a result of winter convection was noted. During these years, instead of the “classic” Labrador water mass, the lighter upper type of ULSW was predominantly formed (Yashayaev, 2007).

The observed relationship between changes in the characteristics of the deep Labrador waters formed in winter and the NAO index indicates a significant role of atmospheric processes in shaping the characteristics of the Labrador Sea waters. Thus, the period 1962–1971 (during which weak convective mixing and insignificant renewal of the deep Labrador waters, increasingly warm and salty, were recorded) was characterized by predominantly negative values of the NAO index. Conversely, the periods 1972–1976 and 1988–1994 (when the Labrador Sea waters were the coldest and most freshened) were characterized by predominantly positive values of the NAO indices (Yashayaev, 2007). From 1990 to 2010, the NAO index had a general downward trend (Yashayaev et al., 2015), indicating an increase in the influence of temperate air masses on the climate of the Labrador Sea. In 2010–2015, the decrease in the NAO index changed to the opposite trend (Yashayaev et al., 2015). In the interannual variability of the NAO index, which is quite chaotic, quasi-two-year, quasi-four-year, five-seven-year, quasi-twenty-year cyclicities are manifested (Pozo-Vazqueza et al., 2000; Bashmachnikov et al., 2013).

1.5 Irminger Sea

The Irminger Sea is one of several areas in the North Atlantic where North Atlantic Deep Water forms that is dense enough to form part of the deep return flow of the Atlantic Meridional Overturning Circulation (AMOC).

Deep convection in the subpolar regions of the Atlantic is caused by cold winters and the presence of pronounced cyclonic circulation in these waters (Yashayaev, 2007; Gladyshev et al., 2018). The average heat loss in the Irminger Sea in winter is high (100–200 W/m^2), although less than in the Labrador Sea (200–250 W/m^2) (Pickart et al., 2003a; Pickart et al., 2003b). In the eastern part of the Subpolar Gyre, the Irminger Current transports warm and salty Atlantic waters north along the Reykjanes Ridge. The Irminger Current water transport in its northern part varies, according to various estimates, between 7–14 Sv (Gladyshev et al., 2017; Le Bras et al., 2018) and 19±3 Sv (Våge et al., 2011a; Fried and de Jong, 2022) (1 Sv = 10^6 m^3/s). The estimate of the Atlantic water transport at the southern boundary of the Irminger Sea (58° N, 32–44° W) is somewhat smaller and, according to various data sets (ARMOR-3D, ORAS5, SODA3.4.2, SODA3.12.2), is within 4–6 Sv (Iakovleva and Bashmachnikov, 2021). In the western part of the Subpolar Gyre, along the continental slope of Greenland, the East Greenland Current transports, according to various estimates, 18–23 Sv, which includes a flux of fresher and colder polar water and warmer and saltier recirculating waters of the Irminger Current (Gladyshev et al., 2017; Le Bras et al., 2018). According to various estimates, the slope branch of the East Greenland Current transports 3.5–15 Sv of polar waters (Gladyshev et al., 2017; Le Bras et al., 2018). The shelf branch of the East Greenland Current has a water transport of 1–2 Sv, transporting the bulk of meltwater, including freshwater runoff from Greenland glaciers and sea ice melt

(Bacon et al., 2002; Gladyshev et al., 2017). These waters, as a rule, do not extend beyond the Greenland shelf and have little effect on the central regions of the Irminger Sea (Dukhovskoy et al., 2019). The recirculating waters of the Irminger Current of the East Greenland Current are actively involved in the central part of the cyclonic gyre of the Irminger Sea. It was the changes in the characteristics of the recirculating waters of the Irminger Current that led to the increase in salinity in the central part of the Irminger Sea during the mid- and late 1990s (Iakovleva and Bashmachnikov, 2021; Yang et al., 2016). At the same time, there was a strong warming of the eastern part of the Subpolar Gyre in the 1990s – 2000s (Desbruyères et al., 2015). Developing these studies, in this paper we show that long-term variability of deep convection in the Irminger Sea is primarily shaped by variability of oceanic heat advection rather than variability of local ocean-atmosphere heat and moisture exchange.

The upper layer of the deep waters of the Irminger Sea (approximately from 500 to 1500 m) is formed by the upper or deep intermediate water masses of the Irminger Sea, depending on the intensity of local convection (Le Bras et al., 2020). These waters have the same density as the water masses formed by moderate convection in the Labrador Sea. However, the waters of the Irminger Sea are slightly warmer and saltier (Pickart et al., 2003b). Below, to 2500 m, the denser Labrador water mass dominates, entering the Irminger Sea after intense convection in the Labrador Sea (Yashayaev, 2007). Even deeper, in the bottom layers, Icelandic-Shetland waters and Denmark Strait waters predominate (Eldevik et al., 2009; Våge et al., 2011b; Chafik and Rossby, 2019). They are the result of the transformation of the densest waters formed by deep convection in the Greenland Sea, in the relatively shallow sills of the Faroe-Shetland and Denmark Straits (Mastropole et al., 2017).

Deep convection in the Irminger Sea was not considered significant until recently. In the late 1990s, Pickart et al. (2003b) noted that convection in the Irminger Sea could, in some years, reach 1800 m, comparable to the intensity of deep convection in the Labrador Sea. Further observations showed that deep convection in the Irminger Sea reached depths of 700–1000 m or more quite regularly in the 1990s and 2010s, although such deep mixing occurred only occasionally in the 2000s (winters of 2008 and 2009) (de Jong et al., 2012; Gladyshev et al., 2016b; Gladyshev et al., 2016a; Bashmachnikov et al., 2019; Våge et al., 2009). It was also noted that by the mid-2010s the total amount of intermediate water in the Irminger Sea in the Subpolar Gyre was increasing (Rühs et al., 2021). Deep convection in the Irminger Sea was usually localized in relatively small areas of the water area, but in some winters the convection region covered almost the entire central part of the sea (Gladyshev et al., 2016a; Fedorov et al., 2018; Bashmachnikov et al., 2018; Le Bras et al., 2020). Some recent studies have recognized the great climatic significance of deep convection in the Irminger Sea, which largely determines the long-term variability of the AMOC (Sarafanov et al., 2012; Lozier et al., 2019; Petit et al., 2020; Kuznetsova and Bashmachnikov, 2021). In addition to classical convection in the central part of the basin, deep mixing was also observed due to hydrostatic instability during the Ekman transfrontal transport of denser

surface recirculating waters of the Irminger Current into the region of less dense polar waters of the East Greenland Current (Le Bras et al., 2020), as well as the cascading water transport of cold shelf waters down the Greenland continental slope (Falina et al., 2012). However, the authors of the above-cited works noted that these factors most likely have a limited effect on the formation of the deep waters of the Irminger Sea.

Changes in convection intensity in the Irminger Sea are often associated with variability in the upper sea temperature (Yashayaev and Loder, 2016; Piron et al., 2017; Zunino et al., 2020). Following the Nansen hypothesis (Nansen, 1912), many studies consider the interannual variability of winter ocean-atmosphere heat exchange as the main driver of variability in the upper ocean heat content, as well as the convection depth (Pickart et al., 2003a; Pickart et al., 2003b; de Jong et al., 2012; Yashayaev and Loder, 2016; Yashayaev et al., 2015). The increase in heat loss in winter is associated with a change in the structure of regional atmospheric circulation, which is most closely related to the location of the center of the Icelandic Low (Bakalian et al., 2007). Its position, in particular, influences the frequency of occurrence of strong westerly katabatic winds from the southern tip of Greenland. The oceanic heat loss in the area of their influence can reach 400–700 W/m^2. Such episodes usually last no more than 3 days, but can recur several times a month (Pickart et al., 2003a; Gladyshev et al., 2016b; Josey et al., 2019). The frequency of penetration of catabatic winds into the central part of the Irminger Sea increases at high positive values of the NAO index, when the Icelandic Low not only intensifies, but also shifts to the northeast, towards Iceland (Pickart et al., 2003a; Våge et al., 2008). As a result, heat loss from the Irminger Sea increases with increasing NAO index. Intensification of atmospheric forcing enhances cyclonic circulation in the Subpolar Gyre, which contributes to the rise of the pycnocline in the central part of the gyre, reducing the integral buoyancy reserve in the upper ocean layer, which favors convective mixing (Våge et al., 2011a; Desbruyères et al., 2015). The opposite effect is observed with an increase in the East Atlantic Oscillation index.

However, the variability of convection intensity may not always be directly related to the heat exchange between the ocean and the atmosphere. Thus, in the winter of 2009, intense convection (up to 1000 m) was observed with a fairly moderate heat loss by the ocean, reaching 150 W/m^2 only in mid-winter (de Jong et al., 2012). On the other hand, in the winter of 2011, despite the very intense heat loss from the ocean surface, sometimes exceeding 650 W/m^2, convection in the Irminger Sea did not reach even 400 m (Gladyshev et al., 2016a). These discrepancies, in principle, can be explained by the influence of the convection intensity of past years. Thus, it was noted that a well-mixed layer at middle depths, formed as a result of convection in the current year, creates conditions for deeper mixing of waters over the next 2–3 years (Gladyshev et al., 2016a). Below, we show that the above-mentioned features of the interannual variability of convection development can only be explained by the variability of the intensity of oceanic heat advection to the central regions of the Irminger Sea.

CHAPTER 2. DATA AND METHODS OF ANALYSIS

For this work, water temperature, water salinity and current velocity component data were obtained from the following 4-dimensional datasets: ARMOR-3D, SODA3.4.2, SODA3.12.2, ORAS4, ORAS5 and GLORYS (Table 2.1).

ARMOR-3D[1] is a combined in-situ and satellite dataset. In this dataset, four-dimensional thermohaline fields are presented on a regular grid with a horizontal resolution of 1/4°, at standard oceanographic horizons and with a time resolution of 1 month (Larnicol et al., 2006; Buongiorno Nardelli et al., 2012). The time interval of the ARMOR-3D array is limited from below by the beginning of high-quality observations of satellite altimeters (i.e. 1993). The data sources are:

1. temperature (T) and salinity (S) profiles obtained from ARGO buoys, CTD probes, XBT bathythermographs, weather buoys and other platforms (data from the World Ocean Data Base, as well as other arrays);
2. sea level anomalies obtained from satellite altimetry data with a spatial resolution of 1/4° (the SSALTO/DUACS center);
3. upper mixed layer (UML) temperature based on satellite and in situ reanalysis observations Reinolds with 1° spatial resolution.

The developers of the ARMOR-3D array obtained three-dimensional temperature and salinity fields at the nodes of a regular grid in two stages. First, regression dependences of temperature and salinity at different horizons on SST and sea level anomalies were found. For this purpose, in-situ subsatellite observations of temperature and salinity were used. The specified dependences were used to construct "synthetic" temperature and salinity profiles at each point of a regular grid to a depth of 1500 m. Secondly, the "synthetic" and in-situ determined vertical temperature and salinity profiles are jointly interpolated by the optimal interpolation method to the points of a regular grid. In this case, the weighting coefficients of each profile are inversely proportional to the calculated errors in determining the thermohaline characteristics in a profile of this type (for profiles obtained *in-situ*, the errors are smaller than for "synthetic" ones), and also depend on the distance between the profile and the grid node. The advantage of this array over the results of optimal interpolation using only *in-situ data* vertical profiles in the upper ocean layer consists in additional use of satellite information. Thus, in the work (Larnicol et al., 2006) it is stated that when using this method, the accuracy of temperature field reconstruction increases by an average of 25%.

[1]http://marine.copernicus.eu/

Reanalysis SODA3 ocean (versions 4.2 and 12.2, Simple Ocean Data Assimilation, 1980–2018)[2] provides monthly data with a horizontal resolution of 0.5×0.5°. The reanalysis is based on the ocean general circulation model MOM5 with the ice block SIS1. The model assimilates in-situ temperature and salinity profiles from the World Ocean Database, SST observations from the International Comprehensive Ocean- Atmosphere Data Set (ICOADS), as well as SST remote sensing data (Carton et al., 2018). The two versions of SODA used in this study differ in their atmospheric forcing: SODA3.4.2 assimilates the ERA-Interim atmospheric reanalysis, while SODA3.12.2 assimilates the JRA-55DO reanalysis.

ORAS5 (Ocean ReAnalysis System 5, 1958–2018)[3] — is a global oceanic ensemble eddy-resolving reanalysis with a time resolution of one month and a horizontal resolution of 1×1° (Zuo et al., 2019). The reanalysis is based on the NEMO 3.4.1 ocean model. The model assimilates SST from the HadISST2 and OSTIA operational datasets, sea ice concentration from the OSTIA dataset, sea level anomalies from AVISO DT2014, and in-situ vertical profiles from the EN4. Depending on the modeling period, the model uses the ERA-40 (before 1979), ERA-Interim (from 1979 to 2015) and ECMWF NWP (since 2015) atmospheric reanalysis.

Oceanic ORAS4 reanalysis (Ocean Re-Analysis System 4, 1958–2017)[4] is based on the NEMO V3.0 ocean model. The reanalysis has a spatial resolution of 1° × 1° (Balmaseda et al., 2013). Depending on the modeling period, either ERA-40 (1957 to 1989), ERA- Interim (1989 to 2009), or ECMWF NWP (since 2010) atmospheric reanalysis data are used as model forcing. ORAS4 assimilates in situ vertical profiles of water temperature and salinity, data from buoy stations and sensors attached to marine animals, as well as satellite data on SST and sea ice concentration.

The GLORYS (Global Ocean Physics Reanalysis, 1993–2019)[5] global ocean reanalysis dataset is based on the NEMO model with atmospheric forcing from the ERA-Interim database. The temporal periodicity and spatial resolution of the reanalysis are month and 1/12°. The GLORYS reanalysis assimilates satellite data on altimetry, sea surface temperature, sea ice concentration and in situ data on temperature and salinity profiles.

[2]http://www.soda.umd.edu/
[3]https://www.ecmwf.int/
[4]https://www.cen.uni-hamburg.de/en/icdc/data/ocean/easy-initocean/ecmwf-ocean-reanalysis-system-4-oras4.html.
[5]https://marine.copernicus.eu/

Table 2.1. Spatial and temporal resolution of ARMOR-3D, SODA3 (versions 4.2 and 12.2), ORAS5, ORAS4, GLORYS data arrays, as well as the year since which the data has been available.

Data array	**Spatial resolution**	**Temporal resolution**	**Availability of data**
ARMOR-3D	0.25×0.25°	month	since 1993
SODA3 (versions 4.2 and 12.2)	0.5×0.5°	month	since 1980
ORAS5	1×1°	month	since 1958
ORAS4	1×1°	month	since 1958
GLORY	0.083×0.083°	month	since 1993

Heat content (OHC), freshwater content (FWC), oceanic heat convergence (ΔOHF) of the upper 500-meter layer, vertical turbulent flux (VHF) through the lower boundary of the studied upper layer (500 m), oceanic heat flux (OHF) and discharge (WT) through the section were calculated using the formulas:

$$OHC = \iiint \rho_0 C_p \left(T - T_{ref}\right) dz\, dx\, dy \quad (1)$$

$$FWC = \iiint \frac{S - S_{ref}}{S_{ref}} dz\, dx\, dy \quad (2)$$

$$\Delta OHF = \int \oint \rho_0 C_p \left(T - T_{ref}\right) V\ dl\ dz \quad (3)$$

$$OHF = \iint \rho_0 C_p \left(T - T_{ref}\right) V\, dx(dy)dz \quad (4)$$

$$WT = \iint V\, dz\, dx(dy) \quad (5)$$

$$VHF = \iint \rho_0 C_p K_z \frac{dT}{dz}\, dx\, dy, \quad (6)$$

where $\rho_0$is the basic density of sea water (1027 kg/m^3) , $C_p$is the specific heat capacity of sea water (3900 J/(kg*°C)), T is the temperature of water in situ (°C), T_{ref} is the base water temperature (in Chapter 4 for the Irminger Sea the base water temperature is 3.5°C, for the other chapters the base water temperature is -1.8°C), S is the water salinity, S_{ref} is the base salinity (in Chapter 4 for the Irminger Sea the base water salinity is 34.9), V *is* the current velocity perpendicular to the section (m/s), dl is the

distance along the boundary of the closed integration region (m), $dx(dy)$ – distance along the section (zonal or meridional), K_z= 10^{-4} m^2/s – coefficient of vertical turbulent heat diffusion (Belyaev and Soloviev, 1996). In Chapter 4, for the Irminger Sea, the average values of these characteristics at 500-1000 m were taken as the base temperature and salinity of sea water (Björk et al., 2001; Piron et al., 2016; Sarafanov et al., 2012). The choice reduces the contribution of the lower layers of the Irminger Sea to horizontal heat advection, where the reliability of the thermohaline characteristics and current velocities of the ARMOR-3D array decreases. $\frac{dT}{dz} = \frac{T_{500} - T_{600}}{100}$ was calculated as the temperature difference between 500 and 600 m (the next closest horizon). The 500-meter layer was chosen as the layer in which the main heat transfer by currents in the study regions is concentrated. The depth of 500 m in the considered convective basins represents the boundary of intermediate and deep water masses, conditionally dividing the areas of weak and moderate convection.

The heat balance for the Irminger Sea was calculated as the sum of oceanic heat convergence, latent and sensible ocean-atmosphere heat exchange fluxes, sea surface radiation balance, and vertical heat flux through the lower boundary of the upper 500-m layer.

The data sets (ARMOR-3D, ORAS5, SODA3.4.2, SODA3.12.2) demonstrate similar decadal variability of heat content in the selected study areas (Appendix 1), although the mean values may differ (Appendix 2). The largest differences in the mean heat content are observed in the shelf part of the Labrador Sea and in the area of the Norwegian and Greenland Seas (Appendix 2b, e, f). The SODA3.4.2 and SODA3.12.2 reanalysis show minor differences in the interannual variability of heat content in these study areas, with the exception of a slightly larger difference in the mean values of the upper ocean heat content in the Norwegian Sea (Appendix 2). Thus, the results based on the SODA3.4.2 and SODA3.12.2 data sets are largely independent of the atmospheric forcing model. The heat content calculated from ocean reanalysis for the period 1993–2016 shows high and significant correlations for all datasets with the ARMOR-3D reference dataset (see Taylor plots in Appendix 2, significance level 0.4 at 95%). SODA3 shows closer agreement with the ARMOR-3D results compared to ORAS5 (in terms of means and correlations, which are mostly close to 0.9, Appendix 2b, e, f). In the Labrador and Irminger Seas, the heat content decreases from the 1970s to the 1990s, then increases during the 1990s to early 2000s and then starts to decrease from the mid-2000s. This variability may be a manifestation of 20–30-year oscillations, although the time series are too short to draw a firm conclusion. In addition to these fluctuations, a general increase of about 0.1 J/m^2 has been observed since the 1980s. In the Norwegian and Greenland Seas, a general trend of increasing heat content has also been observed since the 1980s, with an average rate of about 1.5 J/m^2 (area 6 in Appendix 1), about 0.2 J/m^2 in the Norwegian Sea (area 5 in Appendix 1). This trend shows obvious variability on a time scale of 10–12 years (with local minima

in the early 1980s, 1990s and 2010s, and isolated maxima in the late 1970s, 1980s, early 2000s and late 2010s).

Although the integrated upper ocean heat content shows almost the same interannual variability among the four data sets (Appendix 2), the upper ocean heat transport through the selected transects (Appendix 1) can vary significantly between the data sets (Fig. 2.1). The ARMOR-3D results (Table 2.2) show that the average water transport in the upper 500 m into the Nordic Seas (through 64° N) is 6–10 Sv (according to Hansen et al., 2008; Sarafanov et al., 2012; Raj et al., 2018), in the Labrador Sea (at 44° W) — 9–12 Sv (according to Sarafanov et al., 2012; Dickson and Brown, 1994; Xu et al ., 2010), while the northward transfer of the Irminger Current into the Irminger Sea (through 58° N) is 4–7 Sv (according to Sarafanov et al ., 2012; Xu et al ., 2010). For ARMOR-3D, typical mean values of ocean heat transport (Tref = -1.8 °C) in the upper 300–350 TW to the Nordic Seas from the south and to the Labrador Sea from the east, while the Irminger Current transports about 150–200 TW to the north. The SODA3.4.2 reanalysis (using the ERA-Interim atmospheric forcing) better reflects absolute values, while the linear trends and interannual variability of ocean heat transport are better reflected by ARMOR-3D (Fig. 2.1). On average, over the analysis period (1993–2017), SODA and ORAS5 underestimate the water transports and heat fluxes for all sections by about 30–35% (Table 2.2). For SODA3.12.2. (using the JRA-55DO atmospheric reanalysis) a particularly strong underestimation (by 50%) of the polar modified inflow of Atlantic waters into the Labrador Sea through a meridional section south of Cape Farwell was obtained.

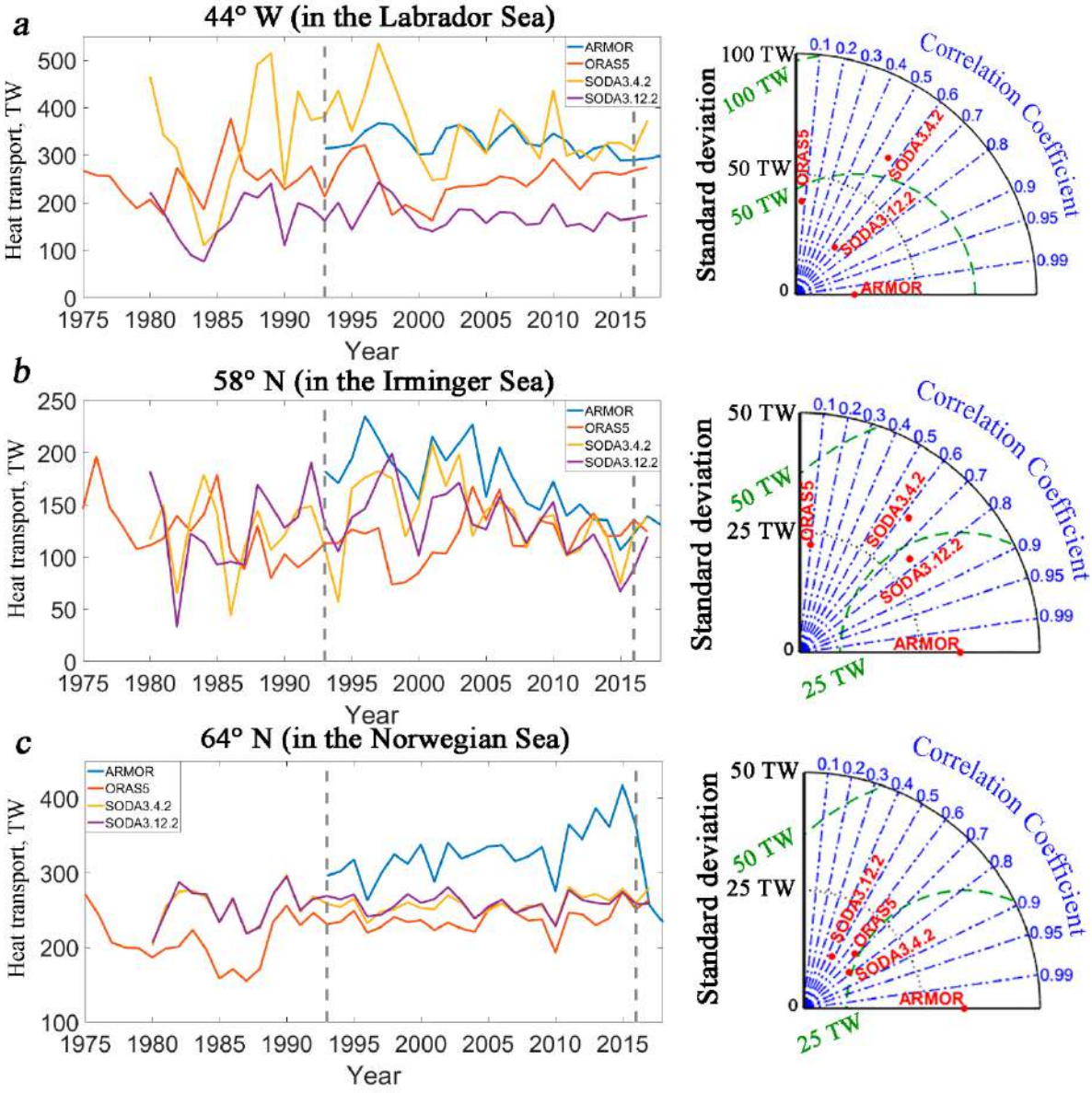

Figure 2.1. Interannual variability of annual mean oceanic heat flux values based on ARMOR - 3D, ORAS5, SODA3.4.2, SODA3.12.2 data: a – at 44° W (positive values mean that the flux is directed to the west), b – at 58° N (positive values mean that the flux is directed to the north), at 64° N (positive values mean that the flux is directed to the north, Appendix 1). Taylor diagrams are constructed for the period 1993–2016 (in the graphs, the period is limited by gray dotted lines) after subtracting the average for this period. Blue dash-dotted lines show correlations with the ARMOR-3D dataset, green dotted lines show the standard error with the ARMOR-3D results. The base water temperature for the calculation was taken as the freezing temperature of sea water (-1.8 °C).

Table 2.2. Average annual values of oceanic heat flux (TW), water transport (Sv) in the upper 500-meter layer at 44° W, 58° N, 64° N for the period 1993-2017. Standard deviation is given in brackets.

		ARMOR-3D	SODA3.4.2	SODA3.12.2	ORAS5
44° W, in the Labrador Sea to the east	Water transport (Sv)	12.6 (0.9)	6.1 (1.1)	5.9 (1.0)	10.2 (1.7)
	Heat flux (TW)	327 (25)	354 (69)	172 (25)	245 (39)
58° N, in the Irminger Sea from the south	Water transport (Sv)	5.6 (1.0)	4.6 (0.9)	4.5 (0.9)	3.8 (0.7)
	Heat flux (TW)	172 (34)	138 (36)	132 (30)	120 (23)
64° N, in the Nordic Seas from the south	Water transport (Sv)	10.0 (0.9)	7.8 (0.5)	7.9 (0.6)	7.2 (0.5)
	Heat flux (TW)	326 (37)	258 (13)	259 (12)	238 (17)

Sea level pressure and wind speed were obtained from the ERA-5 atmospheric reanalysis[6] database for the period 1993–2019 with a resolution of one month. The ERA-5 reanalysis has a spatial resolution of 0.25°. It is based on the Integrated Forecasting System (IFS) Cy41r2, which was introduced in 2016 (Dee et al., 2011). The interannual variability of Ekman surge and relative vorticity in the study area is calculated from the wind field. The Ekman surge is defined here as the Ekman transport towards the coast.

The vertical velocity formed as a result of coastal surge by Ekman transport (w_1, m/s) was estimated as:

$$w_1 = \frac{\tau_l}{\rho_0 f L}, \quad (7)$$

where $\tau_l$is the tangential wind stress along the coast (kg/m*s^2), f is the Coriolis parameter (s^{-1}), L is the distance from the coast to the point (m). The greater the value of the vertical velocity, the greater the deviation of the level from the average, associated with the Ekman surge.

The vertical velocity formed by the relative vorticity of the wind field (w_2, m/s) was estimated as:

$$w_2 = -\frac{1}{\rho_0 f} rot(\tau), \quad (8)$$

[6]https://climate.copernicus.eu/

where τ is the tangential wind stress. The greater the value of the vertical velocity, the greater the deviation of the level from the average, associated with the convergence/divergence of Ekman fluxes under the influence of the relative vorticity of the wind field.

The work also used radiation balance data, latent and sensible heat fluxes, which were obtained from the ERA- Interim[7] reanalysis on a 1/4×1/4˚ grid with monthly averaging (Dee et al., 2011). The radiation balance includes shortwave and longwave radiation (Hogan, 2015).

The fields of spatio-temporal variability of the upper ocean temperature were decomposed into characteristic modes of their variability using the Empirical Orthogonal Functions (EOF) method. The method allows one to identify characteristic spatial structures of parameter variations that have uniform variability over time, and to determine the contribution of each of these structures to the total variance of the initial temperature variability of the selected region (Lyakhov, 2006). The modes obtained using the EOF method are orthogonal to each other, i.e. one can expect that the physical processes describing different EOF modes are different, although this is not always the case. An additional complication in interpreting the EOF results is the fact that various natural processes that form water temperature variability are often interrelated.

The intensity of the Atlantic meridional overturning circulation over the entire observation period was characterized by both temperature and salinity indices (Chen and Tung, 2018). According to the cited work, the salinity indices were defined as the average salinity of the North Atlantic waters between 45–65° N in the 0–1500 m layer. One index was calculated based on the ISHII (1946–2015) and Scripps (2004–2020)[8] in situ databases[9], the other based on the EN4 database[10] (1946–2020). The HADIsst temperature index (1871–2020) is the difference between the SST in the Subpolar Gyre region and the global SST (Caesar et al., 2018). These indices reproduce well the AMOC variability obtained both from the analysis of RAPID observational data since 2004 and from the results of a joint analysis of altimetry data and Argo float trajectories since the early 1990s (Chen and Tung, 2018). The ensemble index of the AMOC characterizes the average between the three above-mentioned indices, pre-normalized (Fig. 2.2).

[7] https://www.ecmwf.int/
[8] http://www.argo.ucsd.edu/Gridded_fields.html
[9] http://rda.ucar.edu/datasets/ds285.3/
[10] https://www.metoffice.gov.uk/hadobs/en4/

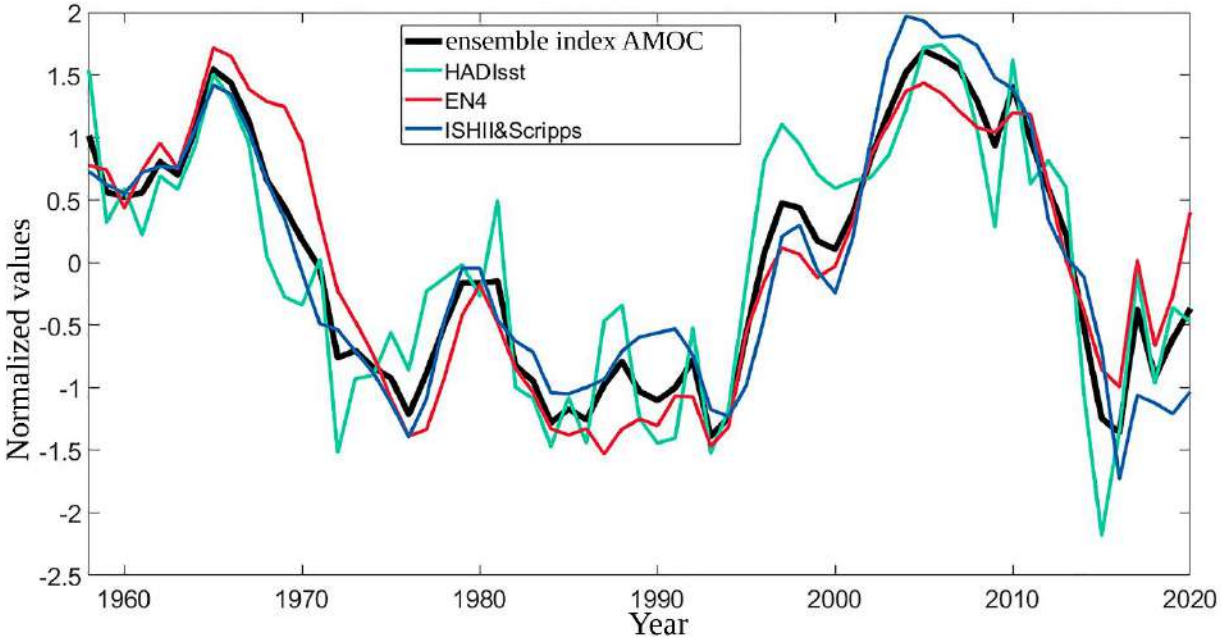

Figure 2.2. Interannual variability of normalized values of three AMOC indices for the HADIsst (temperature index), EN4 (salinity index), ISHII&Scripps (salinity index) arrays and the AMOC ensemble index since 1958.

The depth of the upper quasi-homogeneous layer (UHL) was determined based on ARMOR-3D data using three methods. The authors of the work (de Boyer Montégut et al., 2004) consider the depth of the UHL as the upper horizon where the difference between the potential density at a depth of 10 m and the underlying layer ($\Delta\sigma$) exceeds the selected critical value ($\Delta\sigma_c$): $\Delta\sigma > \Delta\sigma_c$. Deepening the upper boundary allows us to discard the possible influence of the daytime pycnocline. In the work (Kara et al., 2003) a threshold vertical temperature change ΔT is recorded, which is used to calculate $\Delta\sigma_c$ using the equation of state. With this approach, $\Delta\sigma_c$ decreases with decreasing water temperature, which provides a better recording of the UHL depth in smoothed winter density profiles. The method of Dukhovsky (Bashmachnikov et al., 2018) follows the principle outlined in the work (Piron et al., 2016). Here, the UHL depth is recorded at the horizon where the vertical density gradient of water exceeds two of its local standard deviations calculated in a 50-meter depth interval around the control point. In other words, the UHL depth is recorded at the upper point of the pycnocline, where the vertical density gradient begins to increase relatively rapidly with depth. Dukhovsky's method turned out to be the most accurate in determining the UHL depths in weakly stratified subpolar regions. According to the results of the work (Fedorov et al., 2023), the number of in-kind profiles available in open databases allows us to reliably estimate the maximum winter depth of the UHL in the Irminger Sea since the mid-1990s.

The values of the indices NAO, EAO, AOO, AO, AMO, EAWRP, TNHP, PEP, SP are downloaded from the NOAA website [11].

[11] http://www.cpc.ncep.noaa.gov/

CHAPTER 3. CAUSES OF VARIABILITY OF OCEANIC HEAT ADVECTION INTO THE NORWEGIAN SEA

This chapter examines the influence of regional atmospheric processes on the variability of heat advection and water temperature in the Norwegian Sea. The selected transect was 66.5° N, 4° W – 12.5° E (Fig. 3.1), which is located in close proximity to the Svinoy transect, where hydrological surveys are regularly carried out. Despite some discrepancies in the orientation of the selected transect relative to the transect where in situ observations were carried out, the transect will hereinafter be referred to as the Svinoy transect. Atlantic waters were identified from the sea surface to the 27.8 kg*m^{-3} isopycnal (Vesman et al., 2023). The depth of the 27.8 kg*m^{-3} isopycnal increases along the transect from approximately 100 m in the western part of the transect to 400 m in the eastern part (Fig. 3.2). The GLORYS array data (1993–2019) were used due to their higher resolution and assimilation of the satellite altimetry data array, which increases the reliability of the studied current velocity variability.

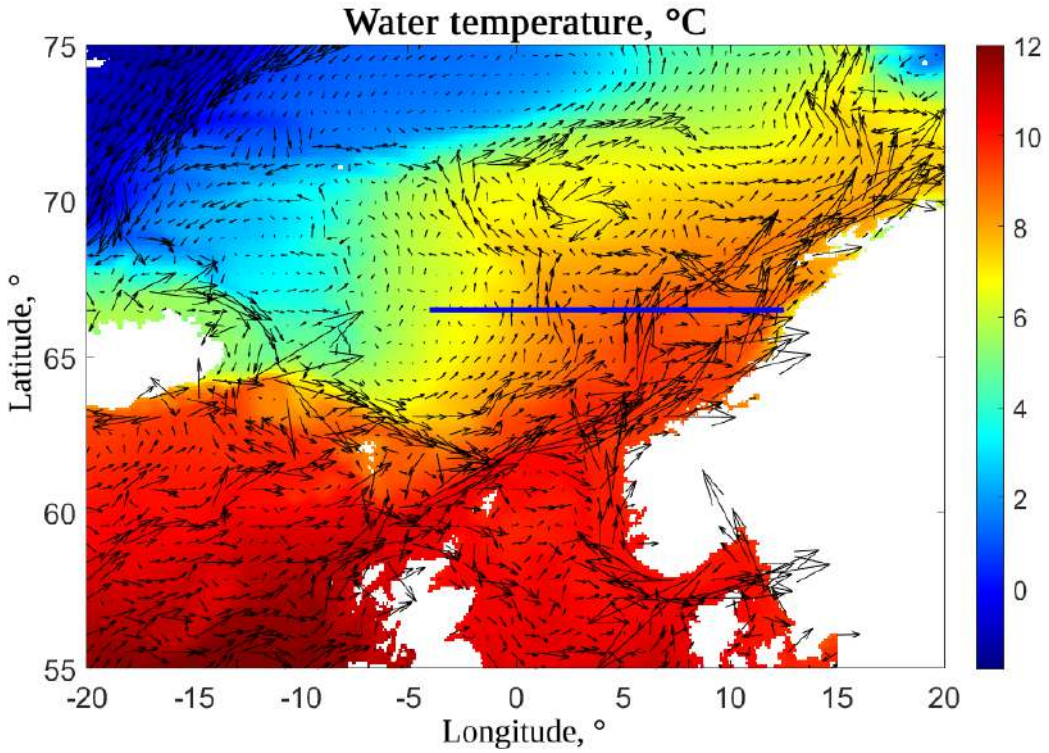

Figure 3.1. Spatial distribution of water temperature (°C) and sea surface current vectors averaged over the period 1993–2019 based on GLORYS data. The blue line shows the Svinoy section (66.5° N and 4° W – 12.5° E).

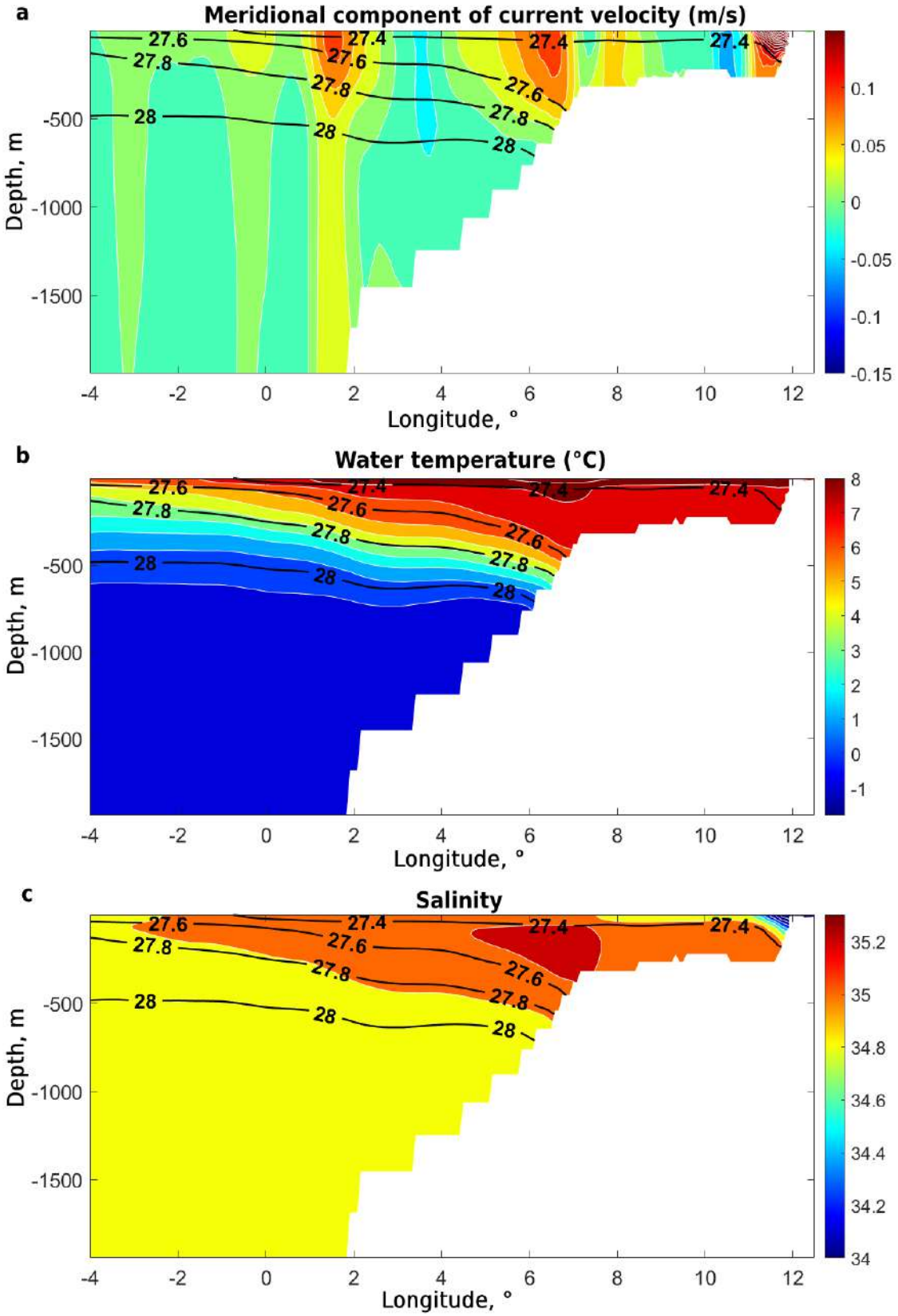

Figure 3.2. a – meridional component of current velocity (m/s); b – water temperature (°C); c – water salinity along the Svinoy section according to GLORYS data. The characteristics are averaged over the period 1993–2019. In Fig. 3.2a, 3.2b and 3.2c, the black lines show the isopycnals of potential density (kg*m^{-3}).

According to the GLORYS array, all three known branches of the Norwegian Current are distinguished (Fig. 3.2a): western (along the subpolar front), eastern (captured by the shelf edge), and coastal (along the coast). The first two branches bring Atlantic waters of the North Atlantic Current, and the last one brings shelf waters of the North Sea. The characteristic velocities of the western and eastern branches are about 10 cm/s. The layer of Atlantic waters was distinguished by a potential temperature of at least 4 °C, which corresponds to an isopycnal of 27.8 kg/m^3 (Fig. 3.2b) and salinity values of at least 35.0–35.2 (Fig. 3.2c). The coastal branch is significantly freshened (salinity 33.4), which is associated with the influence of the Baltic Sea waters and river runoff from the Scandinavian Peninsula. The vertical thickness of the layer varied from 150 m in the western part of the section to 500 m in the eastern part, near the continental slope of Scandinavia.

The results showed that, over the period 1993–2019, the Atlantic water discharge through the selected transect (Fig. 3.1) fluctuated between 6.5–7.5 Sv, without showing a significant trend (Fig. 3.3a). The water temperature averaged 7.3 °C; it increased by about 1 °C from 1995 to 2003, after which it stabilized (Fig. 3.3a). In agreement with in situ observations (Orvik, 2022), according to the GLORYS array, oceanic heat advection of both branches of the Norwegian Current in the Svinoy transect was determined by the variability of water discharge (correlation 0.90), but had a slight upward trend. The latter determined a low (but significant) correlation with the temporal variability of the average water temperature over the transect (0.39). The average values of oceanic heat advection for the period were 242 TW. The relatively high values are associated with the temperature T_{ref} = –1.8 °C. At T_{ref} = 0 °C, the oceanic heat flux through the Svinoy section is on average 193 TW, which corresponds to the estimates (Lebedev et al., 2019).

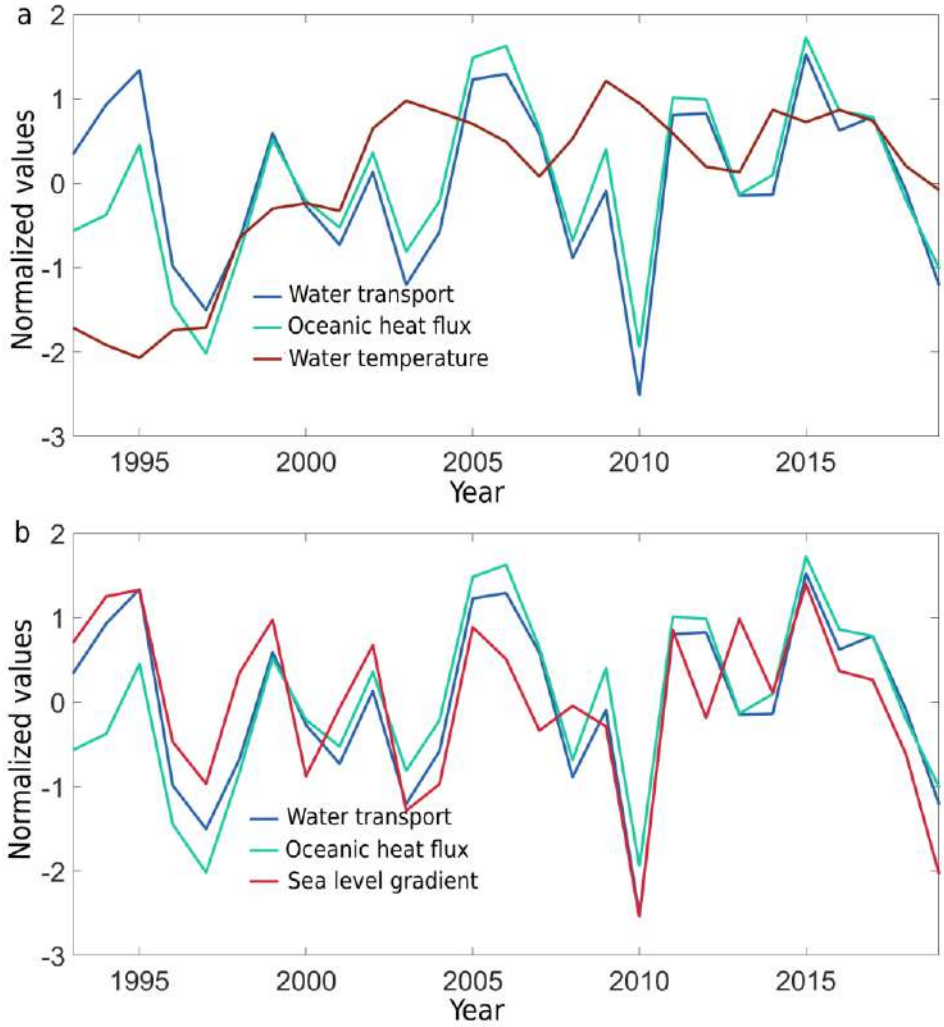

Figure 3.3. Interannual variability of average annual normalized values through the Svinoy section for the period 1993–2019 according to GLORYS data: a – water transport (blue line), oceanic heat flux (green line) and water temperature (red line) of Atlantic waters; b – water transport, oceanic heat flux and sea level gradient. The base water temperature for calculating the oceanic heat flux was taken as the freezing temperature of seawater (-1.8 °C).

In connection with the determining influence of water transport on heat advection (already identified by Orvik (2022)), we further investigated the causes of water transport variability. It turned out that the water transport variability is almost entirely determined by the variability of the sea level gradient through the Norwegian Current (Fig. 3.3b), which is reflected in the high values of the correlation coefficient of the sea level gradient with water transport (0.82), as well as with the oceanic heat flux (0.64). This suggests that the water transport (and oceanic heat advection) in the Svinoy section is determined by the wind field, which usually forms sea level gradients.

In connection with the above, correlations were calculated between the annual average advection of the Atlantic Ocean heat flux and the atmospheric circulation indices that determine the main modes of variability of the atmospheric pressure fields in the North Atlantic and adjacent regions, as well as

with the oceanic indices of the AMOC and AMO (Table 3.1). The results did not reveal a highly significant relationship with any of the indices. Previously, a low correlation between the Norwegian Current velocity and the NAO index (0.36) was obtained based on monthly average values for the period 1995–1999 (Skagseth, 2004). Since the indices used reflect the main modes of large-scale variability of the atmospheric pressure field (of such large regions as the entire or a significant part of the North Atlantic or the Arctic Ocean), we can assume a significant role of the regional component of the atmospheric pressure field in the interannual variability of the intensity of heat advection by the Norwegian Current.

Table 3.1. Correlations of the oceanic advection of Atlantic water heat, water transport through the Svinoy section, and the sea level gradient along the Svinoy section with the main atmospheric indices for the period 1993–2019. Significant correlations are highlighted in bold. EAP – East Atlantic Pattern, TNHP – Tropical/Northern Hemisphere Pattern, AMOC – Atlantic Meridional Overturning Circulation, AMO – Atlantic Multidecadal Oscillation, EAWRP – East Atlantic/Western Russia Pattern, NAO – North Atlantic Oscillation, PEP – Polar / Eurasia Pattern, SP – Scandinavian Pattern. All indices are averaged for January–March, except for AMOC and AMO, which are averaged over the year. Significance level = 0.38.

	EAP	TNHP	AMOC	AMO	EAWRP	NAO	PEP	SP
Heat advection	-0.21	0.22	0.00	0.43 (AMO is 1 year ahead)	-0.07	0.26	-0.18	-0.15
Water transport	-0.28	0.16	-0.25	-0.08	-0.05	0.44	-0.04	-0.21
Sea level gradient	-0.11	0.03	-0.30	-0.22	-0.07	0.33	0.05	-0.15

Composite maps of the pressure and wind fields in the years of the highest and lowest water transport values at the Svinoy section showed that in the years of the highest transports through the Svinoy section (1995, 2005, 2006, 2015), the Icelandic Low deepens and the low pressure area extends to the northeast across the entire Norwegian Sea (Fig. 3.4a). At the same time, the pressure gradients in the area of the Svinoy section increase and the southwesterly wind intensifies. This increases the coastal Ekman surge, as well as the regional values of the wind field rotor. In the years of the lowest transports through the Svinoy section (1996, 1997, 2003, 2010), the negative anomaly of atmospheric pressure in

the area of the Icelandic Low and the Norwegian Sea, as well as the wind strength in the study area, on the contrary, weaken (Fig. 3.4b). The most pronounced variability of atmospheric pressure anomalies is formed over the Norwegian Sea, which is only indirectly related to the NAO index (Fig. 3.4c). To determine the significance of the obtained anomalies, an analysis of variance (ANOVA) was performed for the series of average annual pressure values in the years of high and low transports at the Svinoy section. The analysis showed that in the central area of the most intense atmospheric pressure anomalies in the central part of the Norwegian Sea, the pressure differences in the years of high and low fluxes at the Svinoy section are statistically significant at the significance level (≥99%, i.e. p-statistics ≤0.01). In addition, correlations of the variability of transport through the Svinoy section with the variability of atmospheric pressure at sea level at each point in the study area were also calculated (Fig. 3.4d). The strongest negative correlations of about –0.7 (significantly above the significance level) outline approximately the same area of the central part of the Norwegian Sea as in Fig. 3.4c.

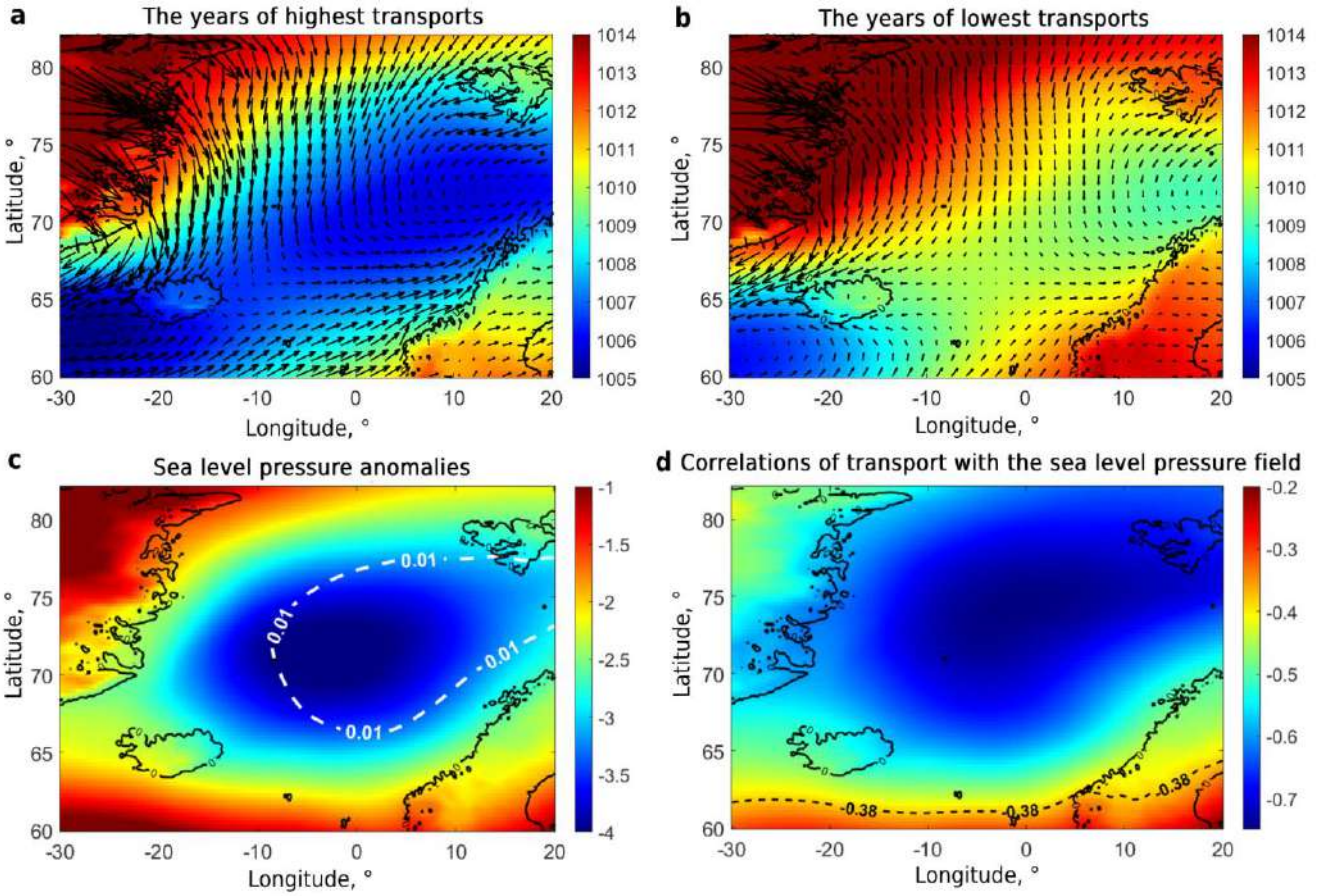

Figure 3.4. a – average sea level pressure field (hPa) and wind direction in the years of highest transports at the Svinoy section (1995, 2005, 2006, 2015); b – average sea level pressure field (hPa) and wind direction in the years of lowest transports at the Svinoy section (1996, 1997, 2003, 2010, 2019); c – sea level pressure anomalies (obtained as the difference between the average pressure in the years of highest transports and in the years of lowest transports at the Svinoy section); in the area inside the loop outlined by the white dotted line, the pressure differences are significant at a significance level of ≥99% (p-value ≤0.01); d – correlations of transport through the Svinoy section with the sea level pressure field with annual average averaging (the dotted line indicates a significance level of 0.38).

The correlations of the Norwegian Current water transport with the atmospheric pressure field in the Icelandic Low zone, which is one of the centers of atmospheric action for calculating the NAO and EAO indices, weaken by 1.5–2 times. This is the reason for the low correlation of the sea level gradient (and water transport) with these atmospheric indices (Table 3.1).

The wind field forms sea level gradients through the convergence (divergence) of Ekman fluxes, which manifest themselves both as a coastal Ekman surge and due to the local wind field rotor. The Ekman surge calculated using formula (7) rapidly decreases with distance from the coast, but even over the eastern branch of the Norwegian Current, at a distance of 250 km from the coast, the vertical velocities it creates are comparable to the vertical velocities under the action of the wind field rotor. The

vertical velocity gradients of the sea surface along the Svinoy section, which cause sea level variability, are significantly and positively correlated with each other for the Ekman surge and the wind field rotor (Fig. 3.5a), although the correlation coefficient is small (0.41). The effect of the Ekman surge dominates in the interannual variability of the sea level gradient along the section. On average over the section, the effect of the Ekman surge on the sea level gradient associated with the Ekman surge is approximately twice as large as the effect of the relative vorticity of the wind field. The correlation of the observed sea level gradient with the Ekman surge intensity is significant and positive, although small (0.46). A similar correlation with the sea level gradient formed by the wind field rotor is also positive, but does not exceed the significance level (0.30). The correlations of the interannual variability of the water transport and oceanic heat flux with the variability of the sea level gradient formed by the Ekman surge are also significant and positive, and amount to 0.54 and 0.46, respectively. The correlations of the interannual variability of the water transport and oceanic heat flux with the variability of the sea level gradient associated with the wind field rotor are insignificant (0.38 and 0.36, respectively). Joint consideration of the sea level gradient associated with both the wind field rotor and the Ekman surge slightly increases the correlations with both the water transport (0.57) and the oceanic heat flux (0.50).

The sea level gradient across the Norwegian Current had similar interannual variability with the steric oscillation gradient calculated for the 0–500 m layer (Fig. 3.5b). The average sea level gradient along the section was 6×10^{-7}, while the steric oscillation gradient was -1×10^{-7}. The correlation between them was significant and positive, 0.57. It should be noted that the strongest correlation (0.82) between the steric oscillation gradient and the sea level gradient was observed between 1995 and 2006, when the average annual temperature of the Norwegian Current waters increased monotonically (Fig. 3.3a). No significant correlations were found between the steric oscillation gradient and the water transport or oceanic heat flux.

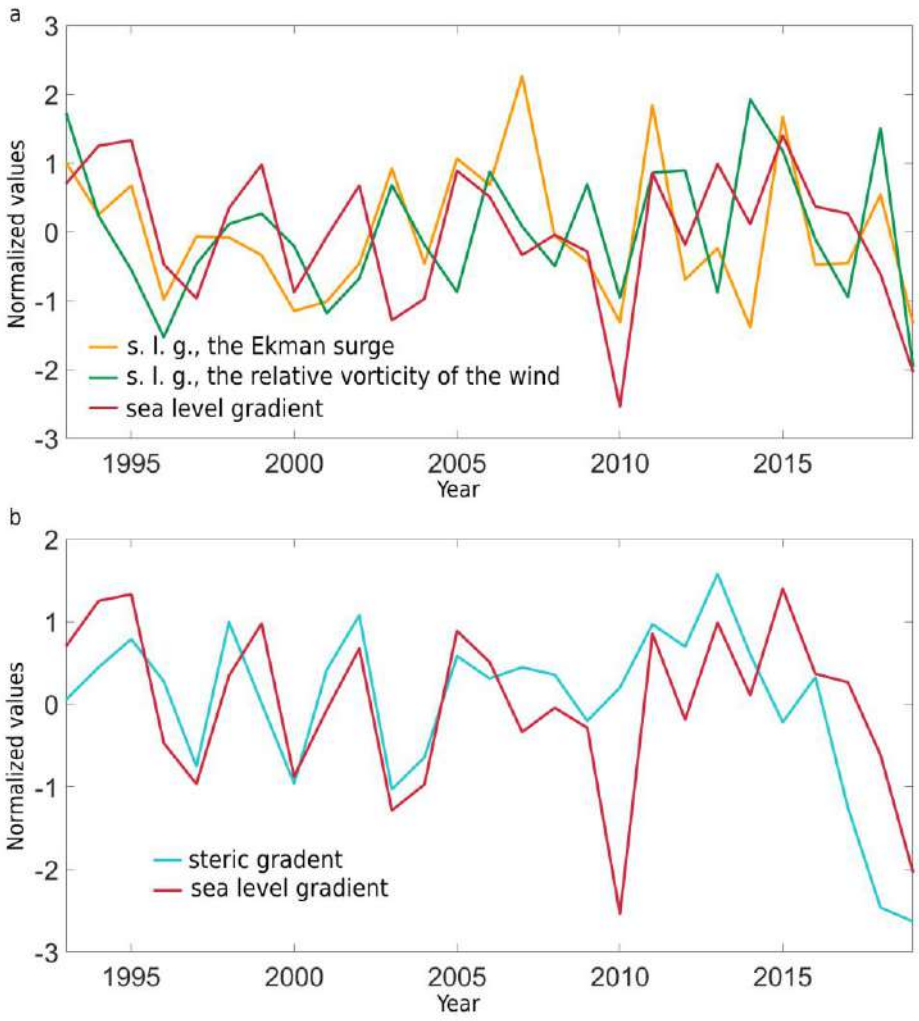

Figure 3.5. Interannual variability of the average annual normalized values of the sea level gradient at the Svinoy section for 1993–2019 (red) and (a) the sea level gradient associated with the Ekman surge (yellow), the sea level gradient associated with the relative vorticity of the wind field (green); and (b) the gradient of the steric component of the sea level (blue).

The total Sverdrup transport in the section averaged 0.4 Sv for the period 1993-2019, which is 6% of the average water transport. The correlation between the Sverdrup transport and the water transport is small and insignificant (0.35).

In the Lofoten Basin of the Norwegian Sea, winter convection in some years can reach 600 m and even 1000 m (Fedorov et al., 202). Deep convection in this area occurs when the ocean loses heat, which is associated with abnormally low air temperatures (Fedorov et al., 2021). In general, in December-May, westerly and southwesterly winds prevail over the region, which reduce heat loss from the ocean. The episodic manifestation of northern and northeasterly winds in winter leads to the short-term development of convection in a limited area of the central part of the Lofoten Basin. In particular, in the winter of 2010 and 2011, in the central part of the Lofoten Basin, the convection depth reached 1200 m for several days (Fedorov et al., 2021). The minimum of the water transport/ocean heat flux

(Fig. 3.3) corresponds to extremely deep convection (up to 1200 m) in 2010 in the Norwegian Sea (Fedorov et al., 2021). Also, a smaller Ekman surge is expected this year with strong northerly winds; the low pressure area is shifting towards the Barents Sea (Fedorov et al., 2021), which is also visible in Fig. 3.4b.

CHAPTER 4. INFLUENCE OF OCEANIC TRANSPORT ON HEAT CONTENT AND DEEP CONVECTION IN THE IRMINGER SEA

As noted in the introduction, the Irminger Sea is one of several areas in the North Atlantic where the North Atlantic Deep Water forms as a result of deep convection. For this area, a comparison of calculations for larger and smaller areas of the study region was made (Fig. 4.1a), which showed that the considered variability of the convergence of oceanic heat transport is not very sensitive to the choice of the boundaries of the region.

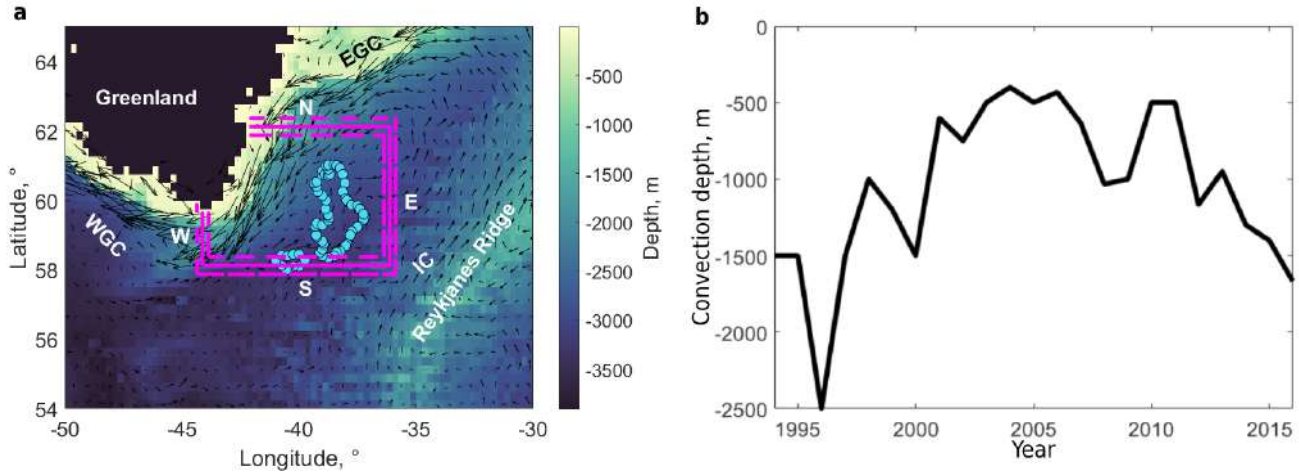

Figure 4.1. Study area: a – bathymetric map (m, color) and average field of surface currents (black arrows) for the analysis period (1993–2016). Blue dots show areas where winter convection greater than 1000 m was most frequently recorded, according to (Bashmachnikov et al., 2018). Solid pink lines (central) define the area where the heat balance parameters were calculated. Dashed pink lines (inner and outer) define the sections that were used to analyze the sensitivity of oceanic heat fluxes to the choice of regional boundaries. WGC – West Greenland Current, EGC – East Greenland Current, IC – Irminger Current; W – western section (44° W), N – northern section (62° N), E – eastern section (36° W), S – southern section (58° N). b – maximum convection depth in the Irminger Sea (m) during the cold season (January – April).

When analyzing the advection across the Irminger Sea boundaries, in addition to the relatively cold polar waters (with a temperature of 1.5–3 °C) of the East Greenland Current (with a velocity of 5-35 cm/s) (Fig. 4.2), a pronounced well-known recirculation was identified (Gladyshev et al., 2018; Våge et al., 2011a) warm (5–7 °C) and salty modified waters of the Irminger Current (Atlantic waters) entering the study area through the northern boundary of the study area (Fig. 4.1a). Some of these Atlantic waters leave the study area through the western boundary into the Labrador Sea, having a temperature of 4–6 °C. According to ARMOR-3D data, the average water transport through the northern boundary reaches 17 Sv, and the oceanic heat advection through the northern boundary is 104 TW (Fig. 4.3d). Only 14 Sv

and 64 TW leave the sea through the western boundary (Fig. 4.3d). The difference of 40 TW between the oceanic heat fluxes through these boundaries forms the main source of oceanic heat convergence in the study region (ΔOHF).

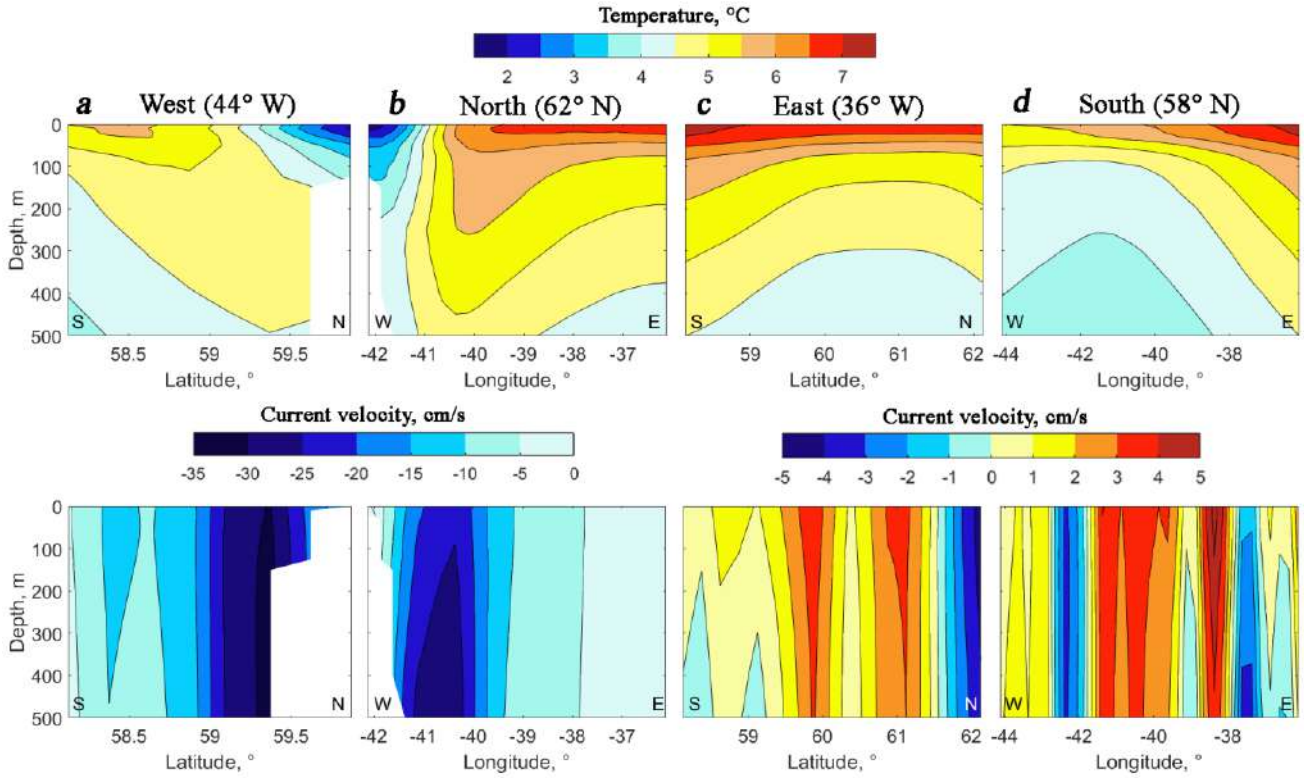

Figure 4.2. Water temperature (°C, top row) and current velocity (cm/s, bottom row) along the western (a), northern (b), eastern (c) and southern (d) sections (see Fig. 4.1a). Water temperature and current velocity are presented as an average for the period 1993-2016 in the upper 500-meter layer according to ARMOR -3D data. S – south, N – north, W – west, E – east.

Despite significant heat losses by Atlantic waters as they cross the western part of the selected region of the Irminger Sea, the oceanic heat fluxes through the northern and western boundaries are highly correlated (-0.96). The average annual imbalance in the water transports is 3±0.5 Sv in the upper layer and is most likely the result of a regional increase in the deep water flux below the considered 500-m layer, which can arise due to the development of deep convection in the central part of the Irminger Sea and at the eastern boundary of the East Greenland Current. This is consistent with previous estimates (Le Bras et al., 2020) outflow of locally formed lower fraction intermediate waters from the Irminger Sea, which below 500 m is estimated at 2–5 Sv.

In addition, Atlantic waters enter the study area from the south. This flux is less intense (current velocities in the upper layer are 1–5 cm/s at a water temperature of 4–7 °C). These waters leave the study area through its eastern boundary (Fig. 4.1a). Heat fluxes through the southern and eastern boundaries are strongly interrelated (correlation -0.90) and largely compensate for each other. On average, 2 Sv and 10 TW come through the southern boundary, while 2 Sv and 13 TW are removed through the eastern

boundary (Fig. 4.3d). The oceanic heat fluxes across the northern/western and southern/eastern boundaries are much less closely related (correlations of 0.5 and 0.4, on interannual scales of variability), indicating differences in the dynamics of the East Greenland Current and the western branch of the Irminger Current, which form the transport in question (Fig. 4.1a).

On seasonal scales (Fig. 4.3a), the variability of the upper ocean heat content reaches a minimum in March and coincides with the peak of deep convection intensity (Bashmachnikov et al., 2018). The maximum heat content is observed in September. On these time scales, the variability of the upper ocean heat content is a consequence of the seasonal variability of the ocean-atmosphere heat exchange (the sum of latent and sensible heat fluxes) and the radiation balance. The net effect on the sea surface indicates heat loss by the ocean over 7 months (from September to March). Oceanic heat convergence, being always positive, shows a pronounced minimum in February-March, which is replaced by a further increase until the end of December, which also affects the seasonal evolution of the upper ocean heat content.

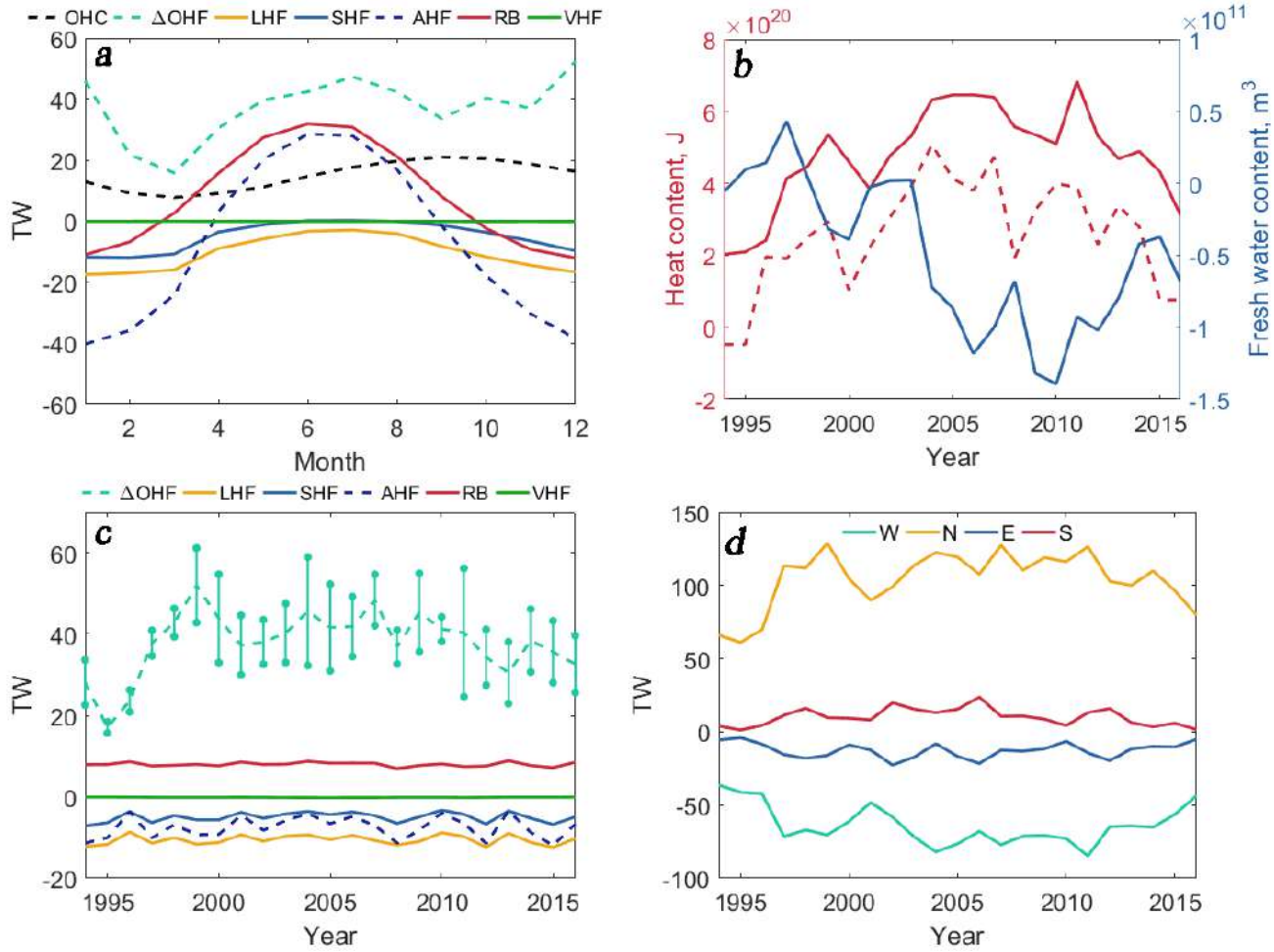

Figure 4.3. (a) Seasonal variability of characteristics in the central Irminger Sea: oceanic heat flux (ΔOHF), latent heat flux (*LHF*), sensible heat flux (*SHF*), vertical heat fluxes at the ocean-atmosphere boundary (the sum of latent, sensible heat flux and radiation balance, *AHF*), radiation balance (*RB*) and vertical turbulent heat diffusion (*VHF*) across the lower boundary of the domain at a depth of 500 m. (b) Interannual variability of heat content and freshwater content in the central Irminger Sea; solid lines – average from April of the previous year to March of the current year, dashed line – heat content for March. (c) Interannual variability of characteristics in the central Irminger Sea: oceanic heat flux (ΔOHF), latent heat flux (*LHF*), sensible heat flux (*SHF*), vertical heat fluxes at the ocean-atmosphere boundary (the sum of latent, sensible heat flux and radiation balance, *AHF*), radiation balance (*RB*) and vertical turbulent heat diffusion (*VHF*) through the lower boundary of the domain at a depth of 500 m (average from April of the previous year to March of the current year). The error ΔOHF is the error of the average for each year, calculated over three domains with boundaries shown in Fig. 4.1a. (d) Interannual variability of oceanic heat fluxes through the boundaries: W – through the western boundary, N – through the northern boundary, E – through the eastern boundary, S – through the southern boundary (see Fig. 4.1a). The base water temperature for calculating oceanic heat fluxes and heat content was taken to be 3.5 °C; base salinity for calculating fresh water content 34.9.

On interannual scales, heat content generally shows an upward trend, reaching a maximum in 2004–2011 (Fig. 4.3b). Such an increase in the temperature of the upper layer of the Irminger Sea since the early 2000s was noted in previous studies (Gladyshev et al., 2016a). An increase in the salinity of the upper layer of the sea was also noted during this period. The interannual variability of the average annual values of heat content of the upper layer of the ocean is highly correlated (0.84) with the interannual variability in March, which indicates that the interannual variability is primarily formed by the winter season.

The interannual variability of oceanic heat content in March shows a high positive correlation (0.77) with the sum of the convergence of oceanic and atmospheric heat fluxes (Table 4.2), which are averaged since the end of active convection development for the previous period (from April of the previous year to March of the current year). Even in the winter months, when the highest variability of atmospheric heat fluxes from the ocean is observed, the interannual variability of oceanic heat convergence remains 1.5 times higher (Fig. 4.3c and Table 4.1). The correlation coefficient between the heat content and the convergence of oceanic heat fluxes is 0.77. The correlation coefficient between the heat content and the ocean-atmosphere heat fluxes is insignificant (0.20). It follows from this that the convergence of oceanic heat fluxes determines the interannual variability of the heat content of the upper layer of the sea.

Table 4.1. Average values (from April of the previous year to March of the current year) of the oceanic heat flux, latent heat flux, sensible heat flux, radiation balance, vertical turbulent heat diffusion at the 500 m boundary, and heat balance. The confidence interval of the averages and the standard deviation were calculated using the average annual values in the central region of the Irminger Sea (the region is highlighted by solid lines in Fig. 4.1a). The statistics were calculated for the period 1994–2016.

		Mean and confidence interval, TW	Standard deviation, TW
Oceanic heat advection convergence (*ΔOHF*)		38±3.4	7.9
Ocean-atmosphere heat fluxes	Latent (*LHF*)	-11±0.5	1.2 (3.0 in winter)
	Sensible (*SHF*)	-5±0.5	1.2 (3.6 in winter)
Radiation balance (*RB*)		8±0.2	0.5
Vertical turbulent transport across the 500 m horizon (*VHF*)		-0.1±0.02	0.04
Heat balance		**30 ±3.7**	**8.6**

Heat content, heat balance and convection depth show similar interannual variability (Fig. 4.4a, for convection depth smaller (negative) values on the graph correspond to greater convection depth (see

Fig. 4.1b)). The correlation coefficient between heat content and convection depth is -0.77, i.e. deeper convection corresponds to lower heat content in the central part of the Irminger Sea (Table 4.2). Freshwater content shows an unexpectedly positive correlation with convection depth, reaching a maximum (0.63) with a shift of 1 year (convection depth leads). This relationship is most likely induced and is explained by the correlation between freshwater content and heat content in the upper part of the Irminger Sea (the maximum cross-correlation reaches -0.79 if the heat content leads by 1 year). Thus, the mechanism of interannual variability of deep convection in the Irminger Sea is determined by the variability of the heat balance in the upper layer, which distinguishes it from the mechanism in the Greenland Sea, where the convection intensity is determined by the freshwater balance (Bashmachnikov et al., 2021). Also, a low (albeit significant) correlation (0.45) was found between deep convection in the Irminger Sea and the NAO index.

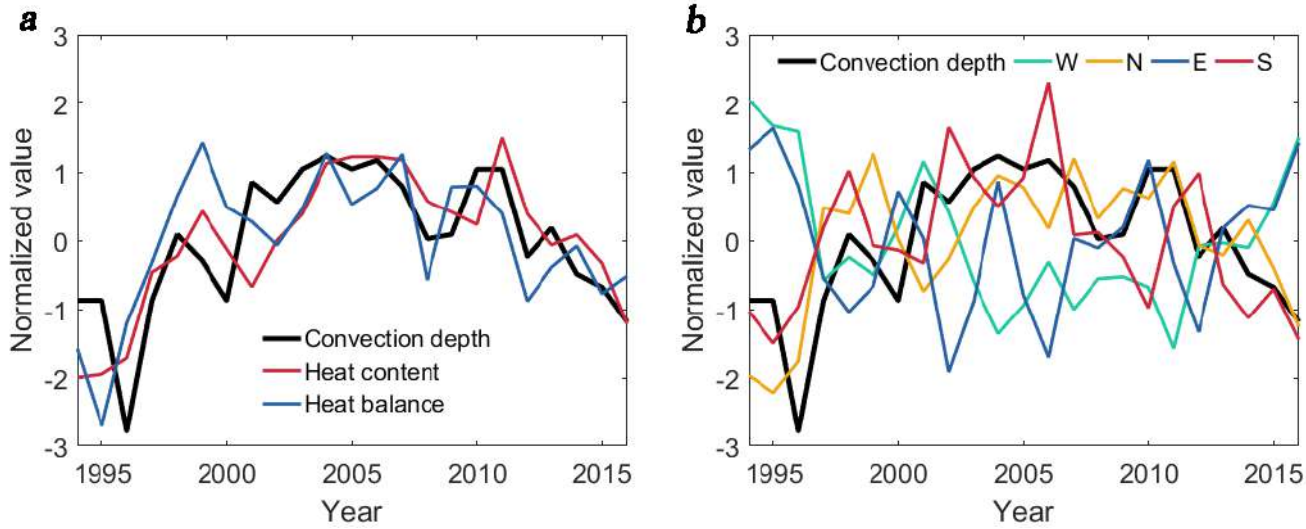

Figure 4.4. (a) Interannual variability of normalized values of convection depth, heat content, and heat balance (average from April of the previous year to March of the current year). It is worth noting that the convection depth axis is inverted: higher values of convection depth in Fig. 4.4a correspond to weaker convection (see also Fig. 4.1b). (b) Interannual variability of normalized values of convection depth and oceanic heat fluxes: W – through the western boundary, N – through the northern boundary, E – through the eastern boundary, S – through the southern boundary (see Fig. 4.1a). Normalization was performed by subtracting the mean value for the entire period and then dividing by the standard deviation. Oceanic heat fluxes through the western (W) and eastern (E) sections in Fig. 4.4b are presented with the opposite sign.

In the heat balance of the studied central region of the Irminger Sea, the correlation of the sum of heat fluxes at the ocean-atmosphere boundary (AHF) with the convection depth is insignificant (-0.34), whereas the oceanic heat convergence significantly and highly correlates with the convection depth (-0.57 at zero shear and -0.62 if the oceanic heat convergence is ahead of the convection by 1

year). Among the oceanic heat fluxes through the boundaries of the study area, the highest correlation coefficients with the convection depth were obtained with the oceanic heat flux through the northern and western boundaries (-0.64 and 0.68, respectively, see also Fig. 4.4b). The correlations with the heat fluxes through the southern and eastern boundaries are somewhat smaller, although also significant (-0.58 and 0.44, respectively). This result shows the importance of the oceanic heat influx with the recirculating waters of the Irminger Current from the north, which then penetrates into the central part of the cyclonic circulation of the Irminger Sea and forms the prerequisites for the development of convection. This confirms the hypothesis that it is the advection of heat from the north that causes the variability of water density in the central part of the Irminger Sea (Pickart et al., 2003a).

Table 4.2. Cross-correlations of the oceanic heat flux (ΔOHF), ocean-atmosphere boundary heat fluxes (*AHF = LHF + SHF + RB*), latent heat flux (*LHF*), sensible heat flux (*SHF*), radiation balance (*RB*), vertical heat flux at 500 m (*VHF*), heat balance, oceanic heat content (*OHC*) and convection depth (higher values characterize shallower convection depth – see Fig. 4.1b). The significance level is 0.37. The correlation coefficients were calculated based on annual average values (average from April of the previous year to March of the current year) for the period 1994–2016.

	AHF	*LHF*	*SHF*	*RB*	*VHF*	*Heat balance*	*OHC*	*Convection depth*
ΔOHF	0.11	0.06	0.24	-0.10	**-0.72**	**0.95**	**0.77**	**-0.57**
AHF	–	**0.98**	**0.98**	**0.79**	-0.25	**0.42**	0.20	-0.34
LHF		–	**0.96**	**0.70**	-0.22	**0.37**	0.17	-0.30
SHF			–	**0.71**	-0.36	**0.53**	0.34	**-0.44**
RB				–	-0.00	0.16	-0.11	-0.10
VHF					–	**-0.74**	**-0.90**	**0.73**
Heat balance						–	**0.77**	**-0.63**
OHC							–	**-0.77**

Figure 3 shows the water temperature and salinity anomalies, which were calculated as the difference in the average water temperature/salinity in years when the convection depth exceeded 1000 m and in years when the convection depth was less than or equal to 1000 m. For the upper layer (the 100 and 400 m horizons are shown), the water temperature anomalies are negative, and in some areas, including the central regions of the Irminger Sea, the difference at the 100 m horizon reached -1 °C (Fig. 4.5a), and at the 400 m horizon it was -0.6 °C (Fig. 4.5c). Salinity anomalies in the Irminger Sea were lower than temperature anomalies by almost two orders of magnitude (Figs. 4.5b, 4.5d), indicating their

insignificant contribution to the density variability of the upper layer. Salinity variability will have a more significant impact on density variability in the Labrador Sea (Fig. 4.5b, 4.5d).

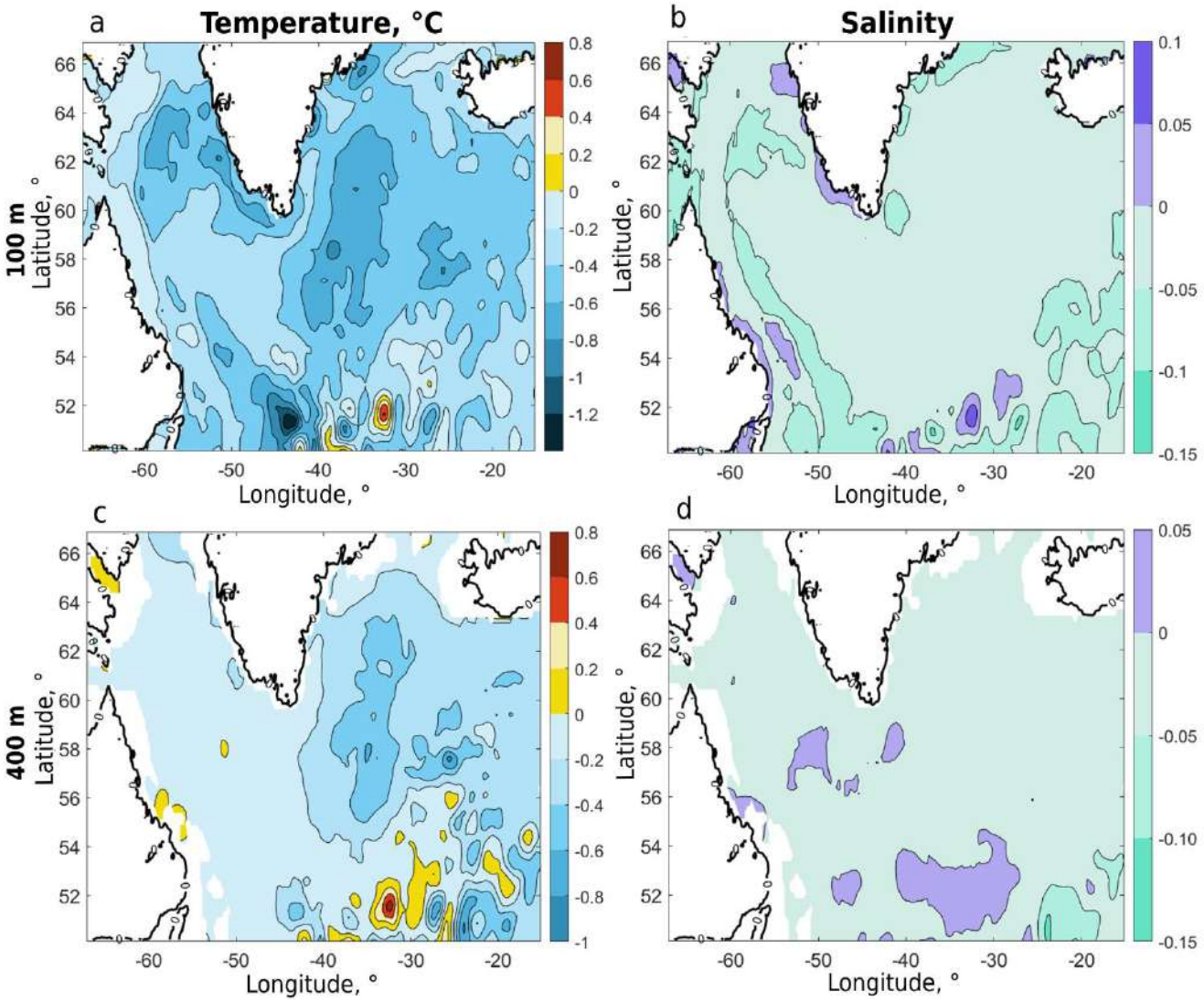

Figure 4.5. Spatial distribution of water temperature (a, c) and salinity (b, d) anomalies at 100 m (a, b) and 400 m (c, d) horizons according to GLORYS data. The anomalies were calculated as the difference in the average water temperature/salinity in the years when the maximum convection depth in the Irminger Sea exceeded 1000 m (11 years) and when it was less than or equal to 1000 m (12 years). Averaging was carried out for October–December, before the onset of intense convection. The period 1993–2016 was considered.

The heat expended in melting ice in the Irminger Sea (Fig. 4.6) is small compared to the heat fluxes. The heat expended in melting ice (IF) in the Irminger Sea was calculated using the formula:

$$IF = \int I\rho \; Cpi \; IT \; IC \; Vi \; dl\,, \tag{9}$$

where $I\rho$ is the density of ice (920 kg/m^3), Cpi is the specific heat of fusion of ice (3.3×10^5 J/kg), IT is the thickness of ice (m), IC is the concentration of ice (%), Vi is the velocity of ice perpendicular to the

section (m/s). Ice thickness, ice concentration and ice velocity are obtained from PIOMAS Arctic Sea Ice Volume Reanalysis[12].

Almost all of the incoming ice that comes with the East Greenland Current melts in the Irminger Sea. The average sea surface heat loss due to ice melting for January–March is about 0.04 TW. Due to such small values of heat loss due to ice melting compared to heat fluxes, their influence on the variability of deep convection was not considered.

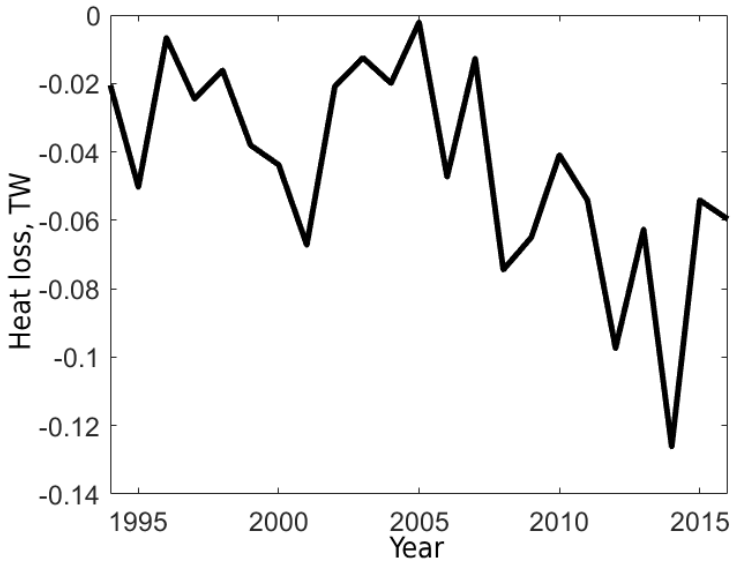

Figure 4.6. Interannual variability of heat (average for January-March) spent on melting ice (IF, TW). The calculation was made using a zonal section at 62° N.

[12] https://psc.apl.uw.edu/research/projects/arctic-sea-ice-volume-anomaly/

CHAPTER 5. INTERANNUAL VARIABILITY OF HEAT CONTENT IN THE LABRADOR SEA

In this chapter, the interannual variability of heat content and freshwater content in the Labrador Sea basin, 55–63° N and 44–60° W (Fig. 5.1) was investigated. The area covers the cyclonic gyre region of the Labrador Sea, including the area of deep convection and LSW formation (Falina et al., 2017; Fedorov et al., 2018).

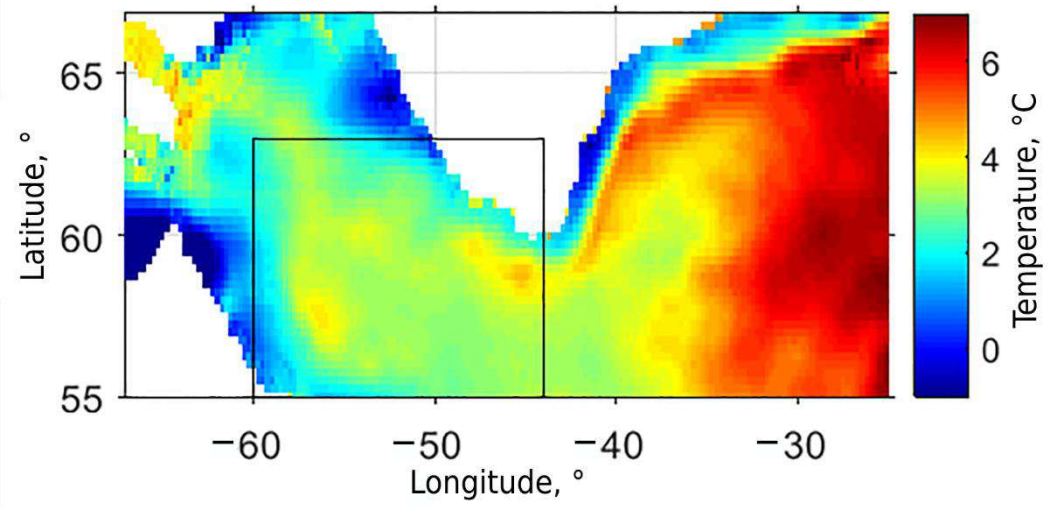

Figure 5.1. Map of water temperature distribution (°C) at a depth of 100 m in March 1996 based on ARMOR-3D data. The rectangle indicates the study area of the Labrador Sea.

On average, in the study area, the seasonal variability of water temperature at the sea surface has a pronounced maximum in August, when the maximum amount of incoming solar radiation is observed. At 100 m and deeper, the temperature maximum shifts in time to November-December and is weakly expressed. The temperature minima at all depths occur in March-April, the period of maximum development of deep convection (Fedorov et al., 2018). However, at a depth of 500 m, the temperature continues to decrease slightly until June. The amplitude of seasonal fluctuations in surface temperature is 5.72 °C, decreasing to 1.48 °C at the 100 m horizon, and is 0.3 °C at the 500 m horizon. Seasonal changes in water salinity at the surface have the opposite course: the maximum occurs in March, and the minimum in August. This course is consistent with the seasonal dynamics of freshwater export from the Arctic (Serreze et al., 2006), which primarily determines the dynamics of surface salinity in the subpolar seas of the North Atlantic (Peterson et al., 2006). At the horizon of 200 m and deeper, the seasonal course is insignificant and is almost in phase with the seasonal course of temperature, which is associated with the freshening of the subsurface layers as a result of deep convection (Holte et al., 2017). The amplitude of seasonal variability on the surface is 0.59, and at the horizon of 500 m it decreases to 0.03. In summer, vertical gradients of temperature and salinity indicate stable stratification of waters, in winter and spring

there is a temperature inversion and a weakening of the salinity gradient, which suggests the regular development of convection in the upper 500-meter layer.

Anomalies of interannual variability of temperature and salinity are formed on the sea surface and then spread downwards. For example, on the sea surface the highest average annual water temperature was observed in 2010, while at the 500 m horizon the interannual maximum of water temperature shifted in time to 2011. At the same time, a decrease in water temperature in the period after 2011 at the 500 m horizon is observed in all seasons, and on the sea surface – mainly in winter. Such interannual variability is characteristic of the development of convection as a result of cooling of the surface layer at abnormally low winter air temperatures.

The average annual values of heat content in the upper 500-meter layer (Fig. 5.2a) increased from 1.18×10^{10} to 1.39×10^{10} J*m^{-2} (i.e. by 18%) from 1993 to 2010, after which it began to decrease. The maximum of the quadratic trend in water temperature was reached in 2006–2007. After removing the quadratic trend, the characteristics of the interannual variability of heat content and fresh water content still show a fairly high negative correlation (–0.56).

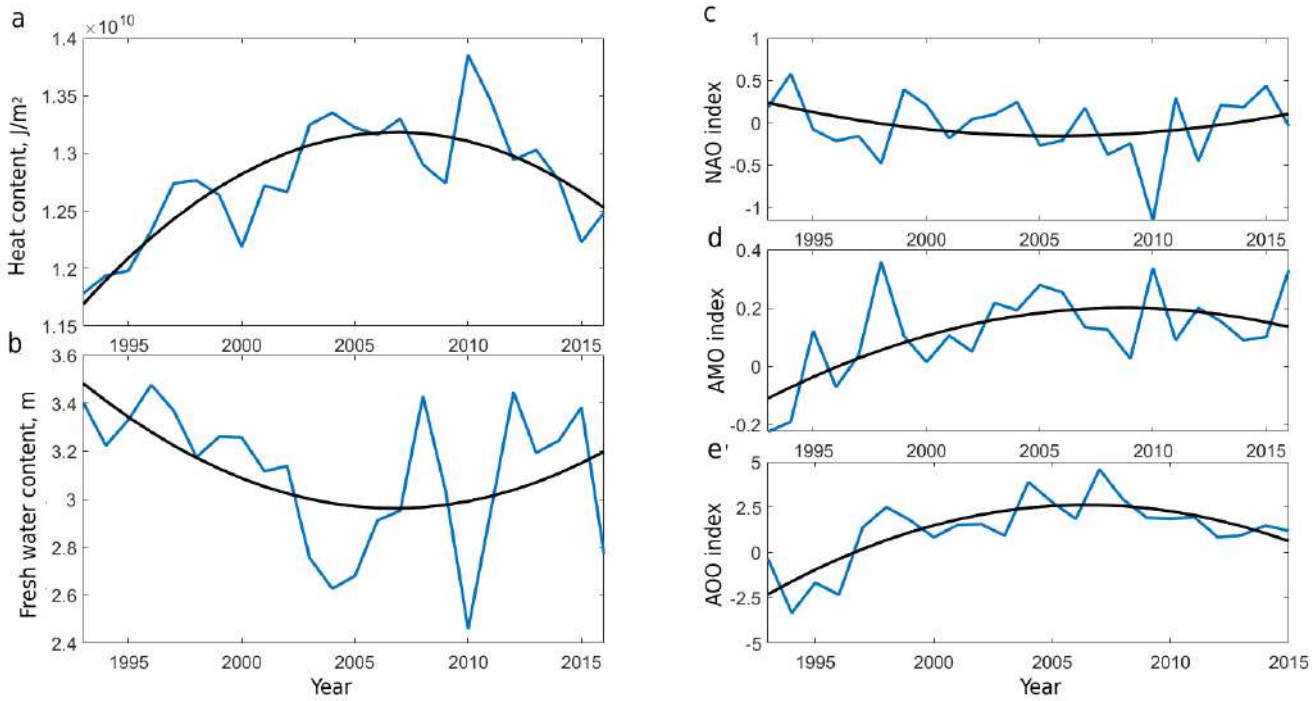

Figure 5.2. Interannual variability: a — heat content, b — fresh water content, c — NAO index, d — AMO index, e — AOO index; blue line — average annual values, black — quadratic trend, respectively. The base water temperature for calculating the heat content was taken as the freezing temperature of seawater -1.8 °C; the base salinity for calculating the fresh water content was 35. See the area in Fig. 5.1.

The extremes of the trends in the NAO (Fig. 5.2c), AMO and AOO indices correspond to those in the heat content and freshwater content of the Labrador Sea. Many interannual extremes also often

coincide. The growth of the NAO leads to a shift in the axis of the westerly winds to the eastern Atlantic, and cold and dry air from the Canadian Arctic Archipelago begins to dominate over the Labrador Sea (Fig. 5.4). During periods of low NAO index values, these winds weaken. At this time, there is often a westward shift in the axis of the southwesterly atmospheric transport, which passes through the central and eastern parts of the Labrador Sea. Such a change in atmospheric circulation can be the cause of anomalously warm and salty water in the Labrador Sea during periods of low NAO values. An increase in the AMO index indicates a general increase in the temperature (and salinity) of the surface waters of the North Atlantic, and an increase in the AOO index indicates a decrease in the flow of cold and freshened waters from the Arctic (Proshutinsky et al., 2015). This can also lead to an increase in the temperature and salinity of waters in the Labrador Sea during periods of high AMO and AOO values (Fig. 5.2).

The correlations of the winter NAO index (January-March) with the heat content (-0.64) and with the fresh water content (0.46) are significant. At the same time, the short-term interannual variability of the characteristics of the upper 500-meter layer of the Labrador Sea weakly correlates with the AMO and AOO, but correlates with the NAO. With the quadratic trend removed, the correlation coefficients of the relationship between the heat content and the fresh water content with the AOO index are 0.16 and -0.04, respectively. The corresponding correlation coefficients of the relationship of these characteristics with the AMO index are slightly higher (0.38 and -0.42), but are also insignificant.

Latent and sensible heat fluxes over the Labrador Sea increase during periods of high NAO index (NAO index > 0.9) (Fig. 5.3), with the sensible heat flux increasing particularly strongly (Fig. 5.3d). This occurs because at high NAO values, cold and dry air from the Canadian Arctic Archipelago is intensively transported into the Subpolar Gyre region (Fig. 5.4a). During the negative NAO phase (NAO index < -0.1), weaker southwesterly winds bring warmer and more humid air into the Subpolar Gyre region (Fig. 5.4b), which leads to a decrease in heat loss from the Labrador Sea surface (Fig. 5.3).

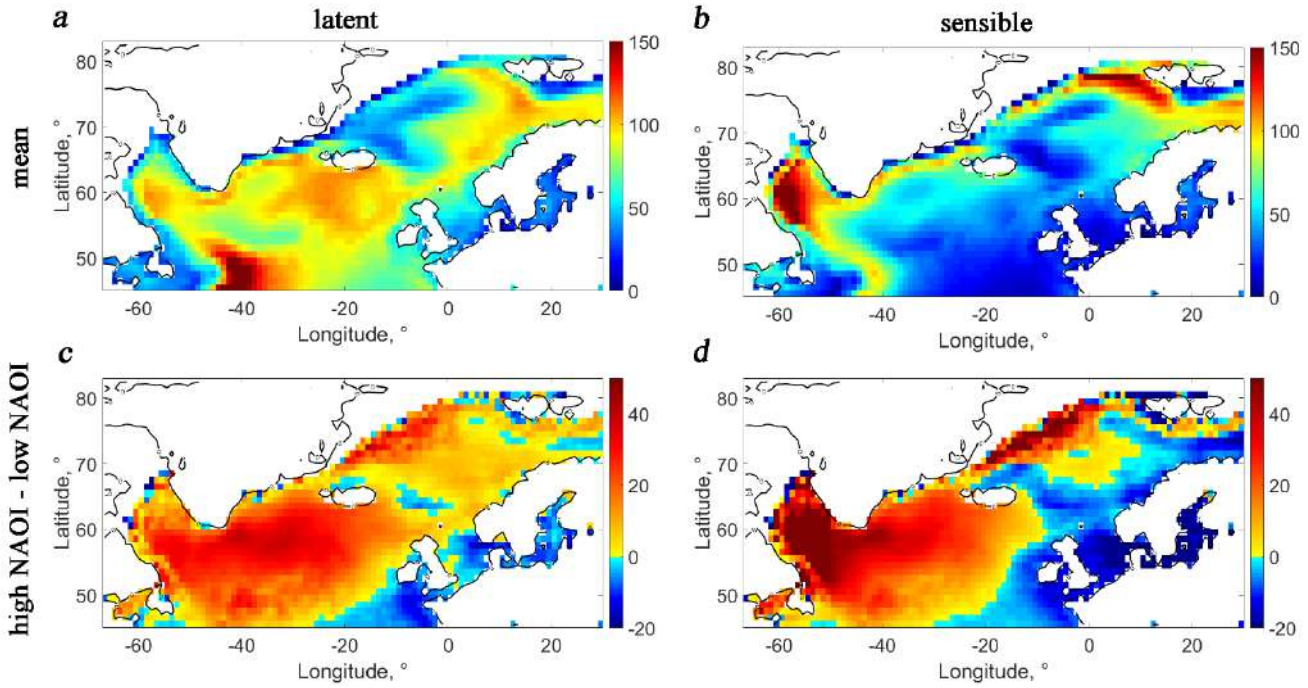

Figure 5.3. Spatial distribution of average ocean–atmosphere heat fluxes (January–March, W/m^2) based on OAFlux data (positive values – from the ocean) for the period 1975–2016: a – average latent heat flux, b – average sensible heat flux, c – latent heat flux anomalies, d – sensible heat flux anomalies. The anomalies were calculated as the difference between the heat flux in years with a high NAO index and a low NAO index.

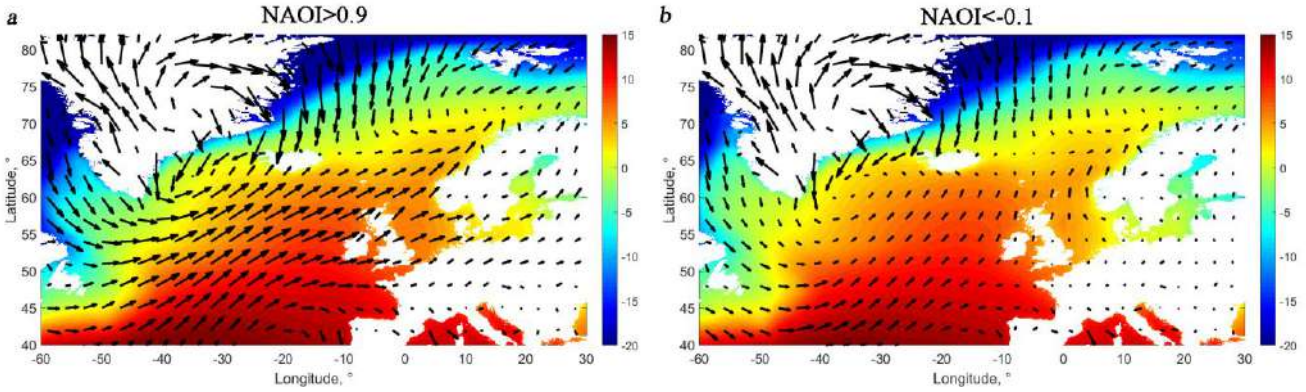

Figure 5.4. Spatial distribution of air temperature (color, °C) and wind (vectors) over the North Atlantic for January–March 1993–2016, obtained based on the ERA -5 reanalysis: a – at high values of the NAO index (>0.9), b – at low values of the NAO index (<-0.1).

When identifying periodicities in time series of natural parameters, instability of the amplitudes and periods of dominant interannual cyclicities is often observed. In this regard, instead of classical Fourier analysis, it is advisable to use wavelet analysis, which allows for the non-stationarity of dominant cyclicities (Astafieva, 1996; Kumar and Foufoula-Georgiou, 1997). The wavelet analysis of the original series with monthly discreteness showed (Fig. 5.5) that in both heat content and fresh water content, in addition to seasonal variability, cycles of 5–8 years duration are distinguished (Fig. 5.5a,b), and since

2000 a cycle of 2–4 years duration has also appeared. These same cycles are present in the variability of the NAO, AMO and AOO indices (Fig. 5.5c–d).

The amplitudes of 2-4-year cycles in heat content and fresh water content increase from 2009 to 2011, simultaneously with the increase in the amplitudes of the NAO and AMO indices, whereas the increase in the amplitudes of 2-4-year oscillations for the AOO index occurred somewhat earlier, in 2004–2007. This may be due to the remoteness of the Beaufort Sea, where the AOO index is estimated, from the Labrador Sea. A similar, although not so synchronous, increase in the amplitudes of the NAO and AMO indices occurred at the beginning of the observation period, but it did not lead to an increase in the amplitudes of oscillations in heat content and fresh water content in the Labrador Sea. This indicates the instability of possible links between these indices and the thermohaline characteristics of the Labrador Sea, and may also be associated with a change in the nature of the climate regime of the North Atlantic in the early 2000s, when cyclogenesis intensified with an increase in zonal westerly transport and heat loss from the ocean to the atmosphere in the North Atlantic increased (Byshev et al., 2011).

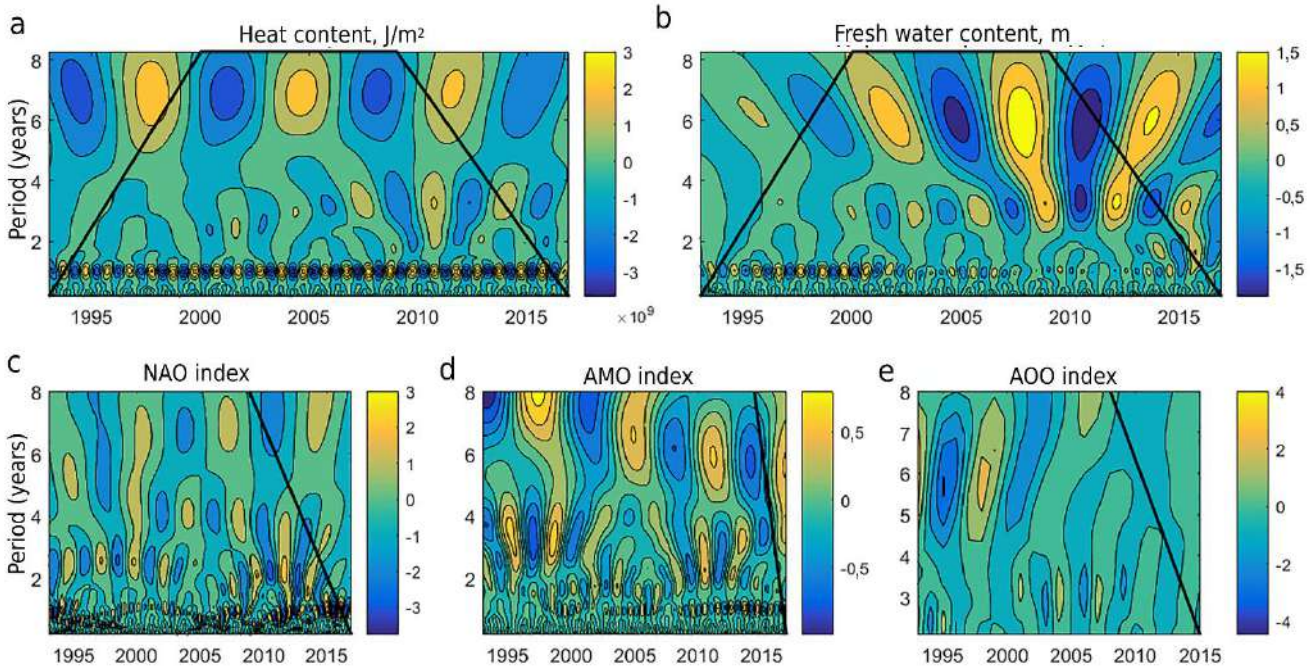

Figure 5.5. Results of wavelet analysis: a – heat content, b – fresh water content, c – NAO index, d – AMO index, e – AOO index. Graphs a – d show series with initial monthly discreteness, graph d – with initial annual discreteness; black lines are reliability triangles.

Cross-wavelet analysis of the heat content and the NAO index (Fig. 5.6a) shows high coherence for 2-year and 5–8-year cycles. Significant coherence in the periods of seasonal variability is manifested only in the years of increased values of the amplitudes of the seasonal variation of the NAO index. Almost in all periods, a delay of the NAO index oscillations by a quarter of the period is observed

compared to the heat content oscillations. It can be assumed that just as the NAO index affects the heat content, the heat content in the Labrador Sea indirectly affects the NAO index (Gnatiuk et al., 2018). The freshwater content also shows coherence with the NAO index, but only in 7–8-year cycles with a phase difference close to 0. The relationship between the heat content/freshwater content and the AMO index is observed, first of all, in 5–8-year periods. The connection for 2-4-year periods began to manifest itself towards the end of the observation interval, when the amplitudes of cyclic fluctuations in heat content/fresh water content increased (Fig. 5.5). For 5-8-year cycles, the AMO index changes almost in phase with the heat content, and for cycles lasting 2-4 years and seasonal cycles, the AMO index outpaces the heat content by approximately 1/8 of the period. There is practically no coherence between the ocean characteristics under consideration and the AMO index.

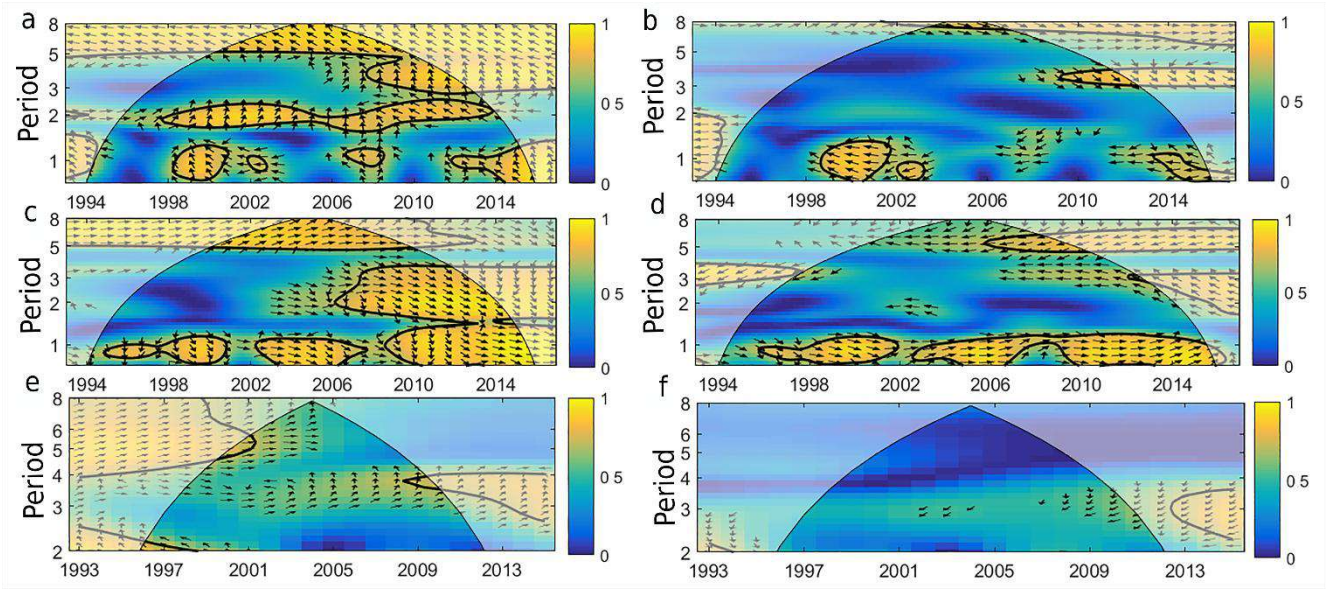

Figure 5.6. Wavelet coherences: a – heat content and NAO, b – fresh water content and NAO, c – heat content and AMO, d – fresh water content and AMO, e – heat content and AOO, f – fresh water content and AOO.

The trends we have identified (Fig. 5.2a,b) are consistent with the calculations of the nature of variability in the heat (Barrier et al., 2015) and freshwater (Serreze et al., 2006; Myers et al., 2007; Haine et al., 2015) balances of the Arctic and subarctic regions, performed by other authors. According to these calculations, changes in the nature of atmospheric circulation lead to a decrease in heat transfer to the atmosphere in the Labrador Sea, as well as a regional convergence of oceanic heat fluxes (Barrier et al., 2015). A parallel increase in the AMO index by the mid-2000s (and its further decrease after 2007–2008) indicates an increase (and further decrease) in the temperature and salinity of subtropical waters entering the Labrador Sea with the Irminger Current and its extension. In the freshwater balance of the region, a significant decrease in freshwater runoff from the Arctic from the 1980–1990s to the 2000s (due to both an increase in the salinity of polar waters and a decrease in ice export) is not compensated

by a slight increase in precipitation in the subpolar seas (Serreze et al., 2006; Myers et al., 2007; Haine et al., 2015), which leads to the observed decrease in the freshwater content in the near-surface layers of the sea. Together, these processes explain the observed intradecadal trends in changes in heat content and freshwater content in the upper 500-m layer.

When examining the wavelet coherences between the heat content and the oceanic heat flux across the 44° W meridian in the Labrador Sea (Fig. 5.7a), a relationship is distinguished on seasonal scales and on 3-4-year periods with a phase difference close to 0; on 6-8-year periods, the oceanic heat flux in the Labrador Sea is ahead of the heat content by 1/8 of the period. Between the heat content and the sensible heat flux, a high relationship is distinguished on seasonal and 3-4-year periods with a lag of the sensible heat flux by 1/4 of the period, on 7-8-year periods, the sensible heat flux is lagged by 3/8 of the period.

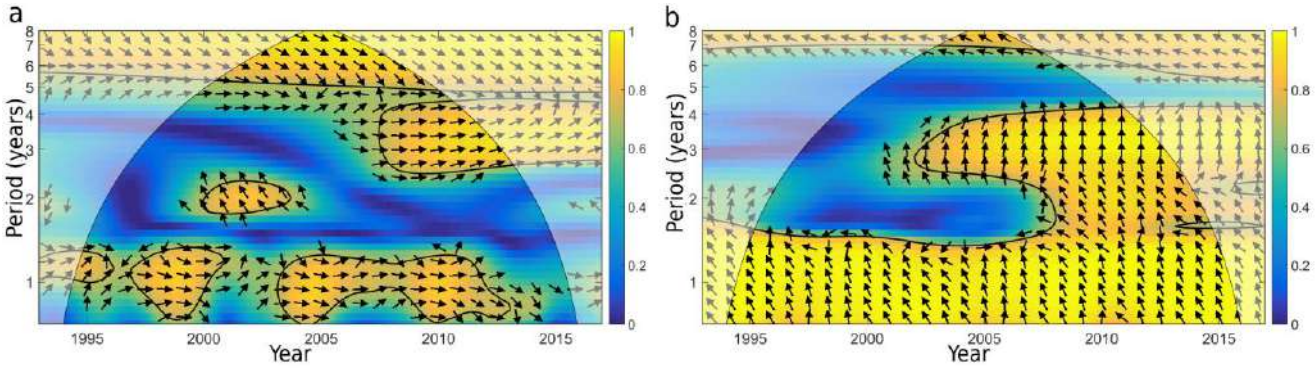

Figure 5.7. Wavelet coherences in the Labrador Sea: a – heat content and oceanic heat flux through the meridian of 44° W, b – heat content and sensible heat flux.

Despite the significant relationship between heat content and convection depth (-0.47, -0.59 with 3-year smoothing) and a fairly high significant relationship between heat content and sensible heat flux from the sea surface (-0.56), the correlation between convection depth and sensible heat flux is small and insignificant (0.06). Oceanic heat transport across the eastern boundary of the Labrador Sea (44° W) also does not have a high correlation with either convection depth (0.03) or heat content (0.05) at zero shear. Despite the similar course of interannual variability between heat content in the Labrador Sea and the Irminger Sea, the interannual variability of deep convection (Fig. 5.8) in these two seas is not similar, which is reflected in the low and insignificant correlation (0.16).

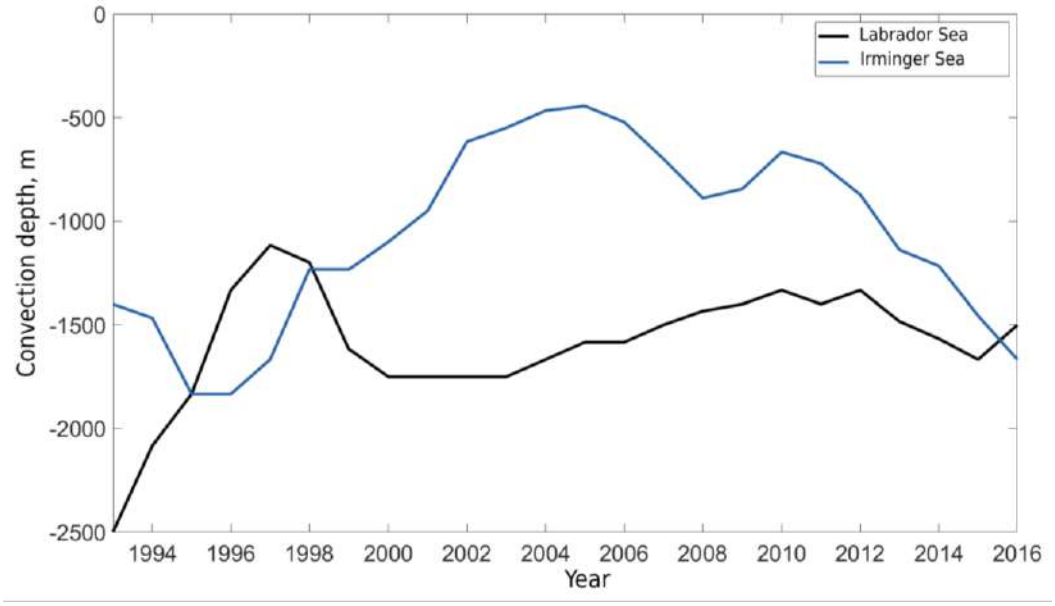

Figure 5.8. Interannual variability of convection depth (m) in the Labrador Sea and the Irminger Sea, smoothed by a 3-year moving average of ARMOR-3D data.

Figure 5.9 shows the temperature (a) and salinity (b) anomalies of water at a horizon of 100 m, which are obtained as the difference in the average water temperature/salinity in October–December 1993 (before the onset of deeper convection in 1994 in the Labrador Sea) and in October–December 1997 (before the onset of shallower convection in 1998 in the Labrador Sea). Temperature anomalies can reach -1 °C in the Labrador Sea, salinity anomalies 0–0.2.

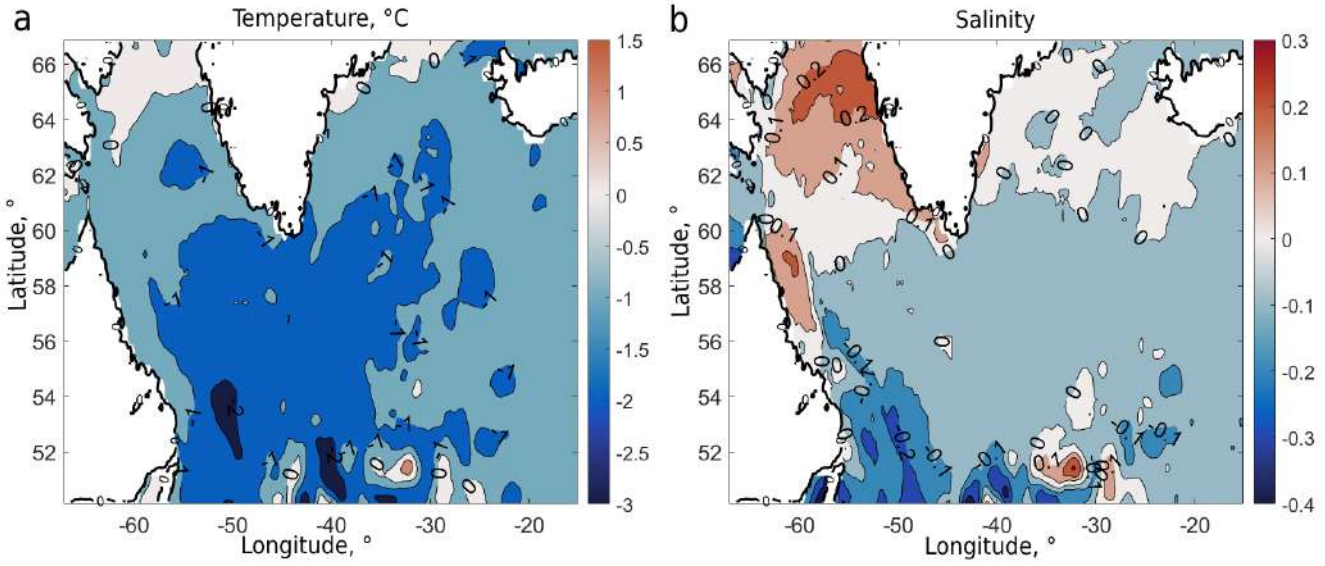

Figure 5.9. Spatial distribution of water temperature (a) and salinity (b) anomalies at the 100 m horizon based on ARMOR-3D data. The anomalies were calculated as the difference in mean water temperature/salinity in October–December 1993 (before the onset of intense deep convection in 1994 in the Labrador Sea) and in October–December 1997 (before the onset of relatively weak deep convection in 1998 in the Labrador Sea).

CHAPTER 6. SEESAW VARIABILITY OF OCEANIC HEAT TRANSFER TO THE NORWEGIAN SEA AND THE SEAS OF SUBPOLAR GYRE

In this Chapter, the EOF analysis of the water temperature of the upper 100-meter layer in the North Atlantic and the Arctic Ocean is carried out to search for connections with the AMOC. According to the results of the EOF analysis of the water temperature of the North Atlantic and the Arctic Ocean (45°–90° N and 70° W–140° E), the dispersions of the first three EOFs of water temperature in total exceed 70% for any of the three data sets used: ARMOR-3D, SODA3.4.2 and ORAS4 (Table 6.1).

Table 6.1. Dispersion (%) of the first three modes of the EOF of water temperature in the 0–100 m layer based on the ARMOR-3D, SODA3.4.2 and ORAS4 data sets.

	EOF1	EOF2	EOF3
ARMOR-3D	41	27	9
SODA3.4.2	43	21	8
ORAS4	41	20	10

The first mode of the EOF characterizes the general tendency of the upper sea temperature to increase over the entire observation period (Fig. 6.1a). This mode characterizes the process of warming of the upper ocean layer and, for all three databases, makes the largest contribution to the total dispersion, exceeding 40% (Table 6.1).

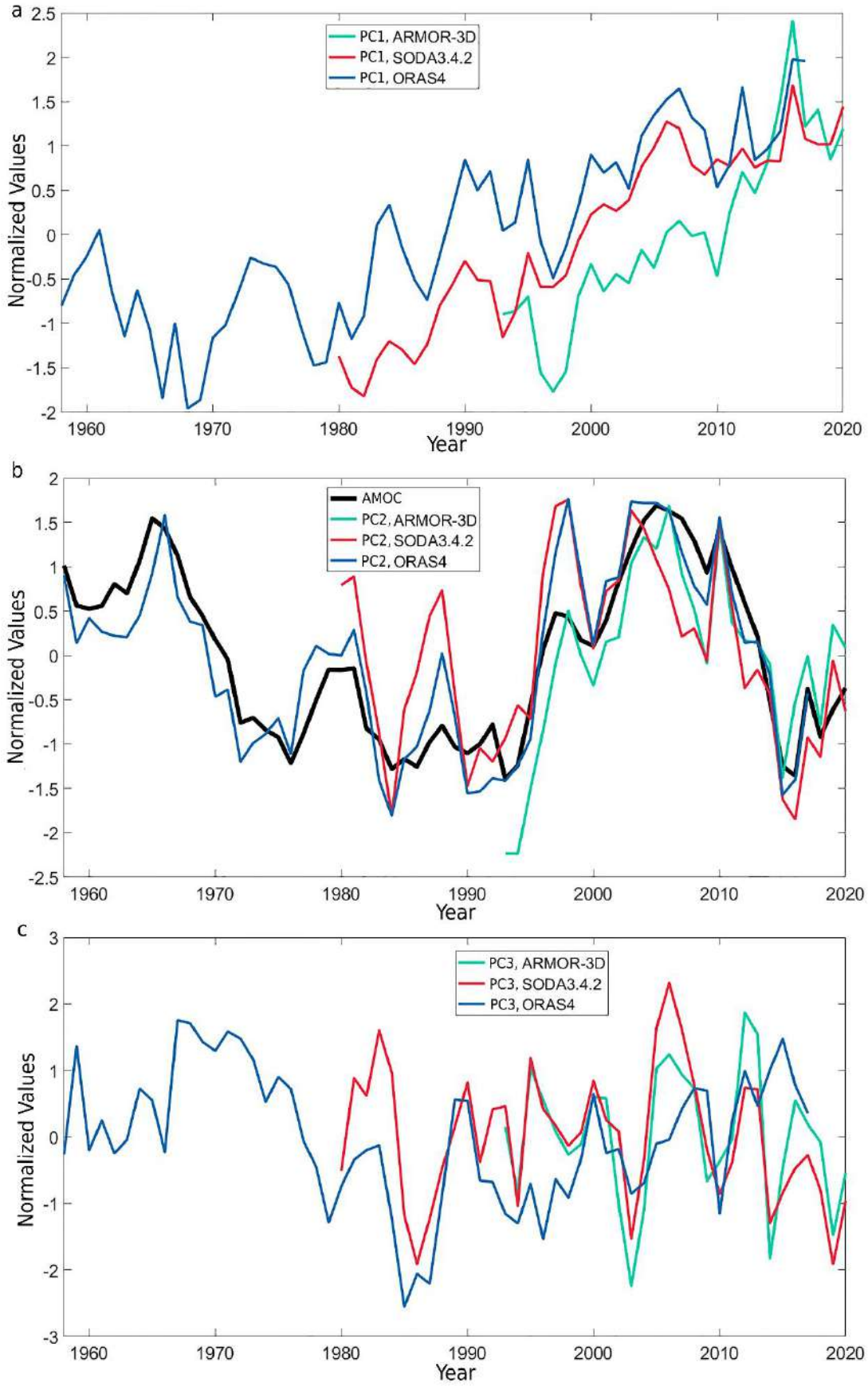

Figure 6.1. Interannual variability of the principal components of the EOF according to ARMOR-3D (since 1993), SODA3.4.2 (since 1980) and ORAS4 (since 1958) data: a – 1st mode, b – 2nd mode, c – 3rd mode.

The dispersion of the second mode of the EOF is also quite large and amounts to 27% for ARMOR-3D, 21% for SODA3.4.2, and 20% for ORAS4 (Table 6.1). The second mode of the EOF of water temperature is of the greatest interest to us, since its principal component (PC) has high (from 0.60 to 0.90) correlations with all AMOC indices, including the ensemble index (Table 6.2 and Fig. 6.1b). This mode determines mainly the interdecadal variability of the upper ocean temperature. The associated variability of water temperature reflects a tendency toward a decrease in the AMOC intensity from the mid-1960s to the mid-1970s, an increase in the AMOC intensity in the 1990s and until the mid-2000s, and a new weakening of the AMOC until the early 2010s and a weakly expressed tendency towards some strengthening of the AMOC in the late 2010s. The weakening and further strengthening of the AMOC at the beginning of the 21st century is consistent with direct observation data since 2004 (Volkov et al., 2020), while the weakening of the AMOC in the 1960s–1970s is supported by data from coral reef analysis and direct hydrographic observations for individual years (Rahmstorf et al., 2015).

Table 6.2. Correlations of the second PC of water temperature in the 0–100 m layer with the AMOC indices. The significance level of the correlations for each of the data sets is indicated in brackets in the last column of the table.

Data array\ AMOC index	AMOC HADIsst	AMOC ISHII&Scripps	AMOC EN4	AMOC Ensemble Index	Level of significance of correlations
ARMOR-3D, PC2	0.79	0.77	0.88	**0.86**	0.38
SODA3.4.2, PC2	0.80	0.66	0.61	**0.73**	0.31
ORAS4, PC2	0.92	0.85	0.80	**0.90**	0.25

The third mode of the EOF describes about 10% of the total value of water temperature dispersion (Table 6.1 and Fig. 6.1c). It characterizes shorter-term intra-decadal variability of water temperature.

The relationship between the variability of the second PC and the AMOC variability allows us to identify the influence of the AMOC on the spatial structure of the upper ocean temperature (Fig. 6.2). The spatial distributions of temperature anomalies associated with the AMOC dynamics are similar for all three data sets. In the subpolar North Atlantic and in the Nordic Seas, with an increase in the AMOC intensity, the temperature of the upper 100-meter ocean layer increases (Fig. 6.2). The strongest increase in water temperature is observed in the central part of the Irminger Sea, the northeastern part of the Labrador Sea and along the Labrador Current. At the same time, the southern and southeastern parts of the Norwegian Sea also become warmer. However, in the Greenland and Barents Seas, as well as north of Spitsbergen, the SODA3.4.2 and ORAS4 reanalyses show a decrease in the temperature of the upper 100-meter sea layer with an increase in the AMOC intensity. In ARMOR-3D, against the background

of a general increase in water temperature in a significant part of the Nordic Seas, a slight decrease in water temperature is also observed north of Spitsbergen and in the eastern part of the Barents Sea. In the upper layer of the Kara, Laptev and East Siberian seas, where the influence of Atlantic water advection is weak, no connection is observed between the upper water temperature and AMOC variability.

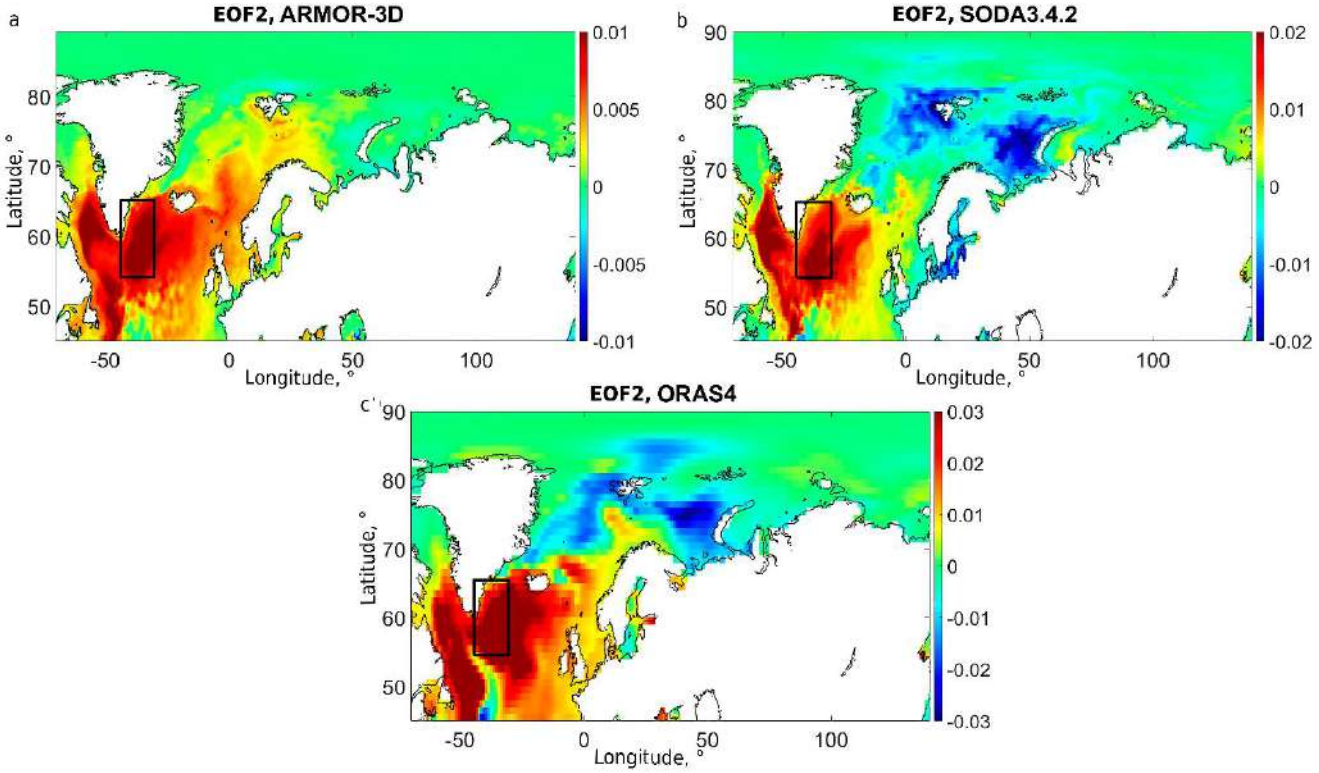

Figure 6.2. Spatial distributions of the amplitude of variability of the 2nd mode of the EOF water temperature in the 0–100 m layer, associated with the AMOC variability: a – according to ARMOR-3D data, b – according to SODA3.4.2 data, c – according to ORAS4 data. The Irminger Sea region is highlighted in black rectangle.

The differences in the manifestation of cold areas with the AMOC strengthening in the ARMOR-3D dataset may be associated with different lengths of the series. Thus, EOF2 of the relatively short ARMOR-3D series includes a part of the modern warming trend, which is evident from a certain slope of the second ARMOR-3D PC in relation to the corresponding SODA3.4.2 and ORAS4 PCs for the period 1993–2020 (Fig. 6.1b). The virtually absent variability in the high latitudes of the Arctic Basin of the second EOF of the ARMOR-3D dataset, in contrast to the SODA3.4.2 and ORAS4 reanalyses, is due to the fact that the ARMOR-3D data are based exclusively on satellite and observational data, which are extremely scarce in ice-covered regions, which does not allow for reliable identification of the spatiotemporal variability of water characteristics in these areas of the Arctic Ocean.

The amplitude of water temperature variations in the 0–100 m layer due to changes in the AMOC intensity in the deep convection region (see Bashmachnikov et al., 2018; Fedorov et al., 2018) of the central Irminger Sea is maximum and amounts to 1.5–2 °C. This result was confirmed by an additional

EOF analysis covering only the Irminger Sea (black rectangle in Fig. 6.2). In this limited region, the percentage of water temperature dispersion in the upper 100 m layer associated with the AMOC variability was 61% according to ORAS4, 78% according to SODA3.4.2, and 85% according to ARMOR-3D. The correlations of the AMOC ensemble index with the corresponding PCs of any of the three data sets were 0.9.

As noted earlier, the AMOC contribution to water temperature variability in the seas of the Subpolar Gyre of the North Atlantic and in the Norwegian Sea is significant. The contribution to water temperature variability is especially large in the Irminger Sea. In addition to ocean circulation, interaction with the atmosphere plays an important role in the variability of the upper ocean temperature. The influence of the atmosphere on the variability of oceanic heat fluxes and heat content of the upper ocean layer is analyzed below.

The interannual variability of oceanic heat fluxes at three transects at 44° W, 58° N, and 64° N (Appendix 1) are shown in Fig. 2.1, and the average oceanic heat fluxes (and expenditures) at the transects based on four data sets are presented in Table 2.2. For this Chapter, the oceanic heat fluxes are calculated at a base temperature equal to the freezing point of seawater (Tref = -1.8 °C). Overall, there is a relatively stable amount of oceanic heat entering the Labrador Sea from the east (Fig. 2.1), while in the Irminger Sea, oceanic heat transport appears to precede the corresponding change in heat content. Like the heat content, oceanic heat advection in the Norwegian Sea (Fig. 2.1) shows an increasing trend from 1980 to 2015. However, the quasi-decennial cycles observed in heat content (Appendix 2) are not evident in heat transport.

The NAO is the leading mode of the EOF of atmospheric variability over the North Atlantic. Heat exchange between the ocean and the atmosphere and oceanic advection from the south should lead to an increase in the upper ocean heat content in the Subpolar Gyre at low NAO and in the Norwegian Sea at high NAO. In fact, correlations between the annual mean upper ocean heat content and the NAO index (January-March) in the Irminger Sea and the Labrador Sea are high and negative (Table 6.3, see also Hauser et al., 2015; Li et al., 2015). However, all data sets show a weak relationship between the upper ocean heat content in the Nordic Seas and the NAO index (Table 6.3, see also Skagseth et al., 2008; Hauser et al., 2015). These results are fundamentally independent of whether annual means, January–March means, or combinations of both are used to calculate the correlation coefficients. However, since the upper ocean heat content is the result of heat accumulation since at least the previous winter, and the influence of atmospheric circulation on the ocean is mainly determined by the cold-season NAO index (Visbeck et al., 2003), only correlations of the January–March NAO index with the annual mean heat content are shown here.

Table 6.3. Correlation coefficients between average annual values of heat content in the studied areas (Appendix 1) with winter values of the NAO index (January-March). Significant correlations are highlighted in bold. The significance level for each data set is indicated in brackets.

	ARMOR-3D (0.39)	SODA3.4.2 (0.32)	SODA3.12.2 (0.32)	ORAS5 (0.30)
the central part of the Labrador Sea	**-0.70**	-0.28	-0.28	**-0.62**
the shelf part of the Labrador Sea	**-0.70**	-0.26	-0.25	**-0.43**
the central part of the Irminger Sea	**-0.62**	**-0.41**	**-0.41**	**-0.64**
the shelf part of the Irminger Sea	**-0.65**	**-0.53**	**-0.53**	**-0.50**
the Norwegian and Greenland Seas	-0.00	-0.04	-0.00	0.09
the Norwegian Sea	-0.17	-0.09	-0.03	0.03

The cross-correlation between the upper ocean heat content and the winter NAO index (January–March) was calculated in each grid cell of the ARMOR-3D dataset for different time shifts. The upper 500 m layer was divided into the 0–100 m layer (where a high influence of ocean–atmosphere heat exchange can be expected) and the 300–500 m layer (where oceanic heat advection should dominate, especially in summer). The results from the ARMOR-3D data were similar for both selected layers (Figure 6.3), and similar results were obtained using SODA (not shown).

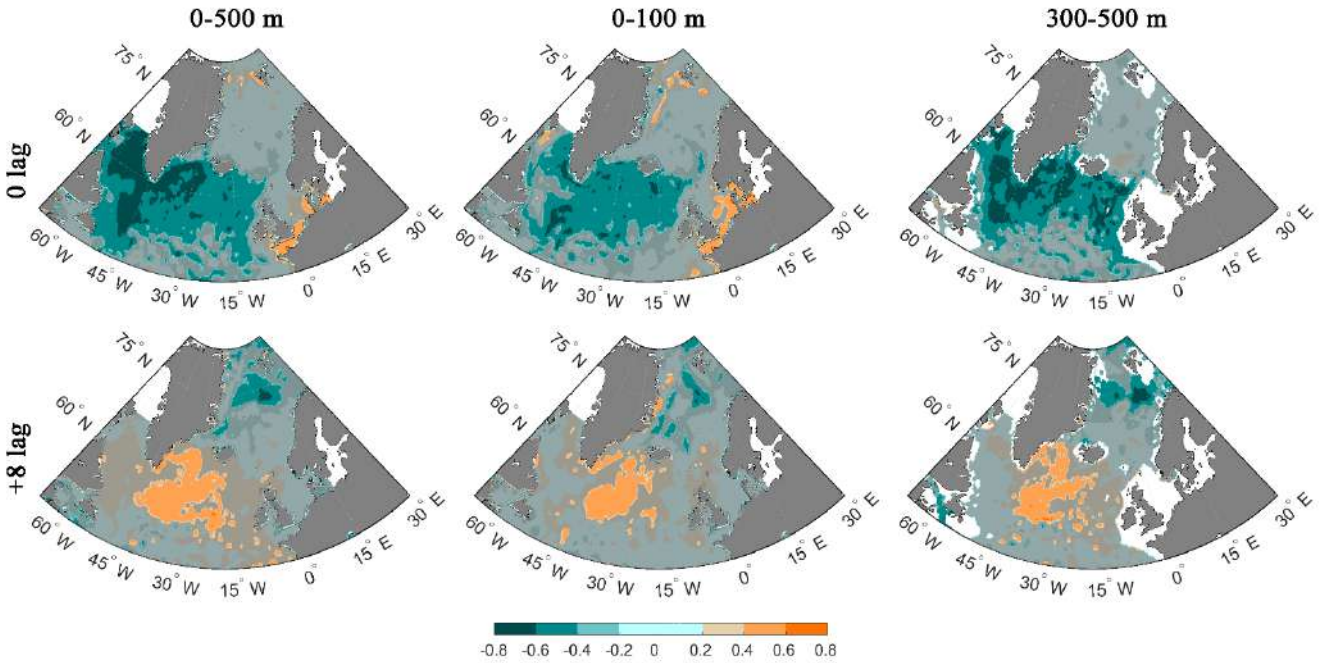

Figure 6.3. Spatial distribution of correlation coefficients between winter values of the NAO index (January–March) and the upper ocean heat content (ARMOR-3D): upper row – correlation coefficients with a shift of 0; lower row – correlation coefficients with a shift of 8 years (the positive sign of the shifts indicates that the NAO index is leading). The shifts of the NAO index (in years) relative to the heat content are shown on the left. Between these two shifts, the areas with a significant correlation between the variables are greatly reduced, decreasing to zero over almost the entire study area at shifts of 3–7 years. The first column corresponds to the 0–500 m layer (average annual values); the second column – to the 0–100 m layer (January–March); the third column – to the 300–500 m layer (June–September). The areas where the correlations are insignificant are shown in gray.

Large areas with significant correlation coefficients are obtained with a shift of 0 and 8 years (a positive shift means that the NAO index leads). Negative correlations with the NAO index cover the entire Subpolar Gyre and adjacent areas to the south and east (from 40 to 65° N). This is an immediate response of the upper ocean to changes in the NAO index, mainly caused by corresponding changes in the ocean-atmosphere heat exchange, whereas a delayed (opposite sign) response can result from changes in the intensity of oceanic heat transport (Visbeck et al., 2003). The results also show that the increase in the oceanic heat flux into the Irminger Gyre in 1995–2005 (Fig. 2.1b) precedes the maximum of the Irminger Sea heat content in 2000–2010. In the Nordic Seas, the correlations are mostly insignificant, but positive correlations are observed along the path of recirculating Atlantic waters along western Spitsbergen and on the northeastern Greenland shelf. The latter situation may be caused by the 10–15-year cycle in the Nordic Seas, previously discussed by Proshutinsky et al. (2015).

On average, during 1993-2018, the total heat flux into the atmosphere over the entire Subpolar Gyre (areas 1-4, Appendix 1) was 162 TW, which averages 86 W/m^2, while over the Norwegian Sea (area 5, Appendix 1) it was 55 TW and 94 W/m^2, respectively. The convergence of the annual mean oceanic heat flux depends on the selected parameter Tref (Formula 1). For further comparison with the ocean-atmosphere heat exchange, Tref was taken equal to 5 °C, which characterizes the average annual surface water temperature in the Subpolar Gyre and the Norwegian Sea. With Tref above, it follows that the oceanic heat flux entering the Subpolar Gyre (areas 1-4, Appendix 1) is 113 TW, predominantly through the southern boundary, and 29 TW leaving the area, which is mainly cold water transported through its northern boundary. In the Norwegian Sea (area 5, Appendix 1), the oceanic heat flux brings 53 TW (through the southern boundary) and 33 TW leaves the area (through the northern boundary). It is worth noting that in both study areas, the oceanic heat advection and heat release to the atmosphere are of the same order of magnitude.

During the high NAO index (NAO index > 0.9), the latent and sensible heat fluxes increase compared to the low NAO index period over the Subpolar Gyre and the western Nordic Seas (Figure 5.3), as cold and dry air from the Canadian Arctic Archipelago reaches the Subpolar Gyre and cyclonic circulation intensifies over the Greenland and Norwegian Seas (Figure 5.4a). During the negative NAO phase (NAO index < -0.1), the opposite situation occurs (Figure 5.4b). Weaker southwesterly winds bring warmer and more humid air into the Subpolar Gyre region, both of which reduce heat release over the sea. Compared with the low NAO index period, periods of high NAO index are characterized by a decrease in mean air temperature over the Labrador and Irminger Seas by 2-3 °C and an increase in wind speed by about 2 m/s, both of which increase ocean heat loss. Over the Norwegian Sea, where high NAO index periods are accompanied by more humid and warm air from the south, the mean air temperature increases by 0.3 °C compared with the low NAO index period, which is partially offset by the effect of an increase in wind speed by about 1 m/s (Visbeck et al., 2003). As a result, a clear intensification of ocean surface heat loss is observed over the Subpolar Gyre during high NAO index periods, while the total heat loss remains virtually unchanged over the Norwegian Sea (Table 6.4).

Table 6.4. Annual mean values of the upper 500-m oceanic heat convergence (TW) and the ocean-atmosphere heat exchange (TW) (positive values indicate that the flux is directed into the ocean) in the Subpolar Gyre and the Norwegian Sea for periods of high and low NAO index (1993-2018). The oceanic heat flux is calculated based on ARMOR-3D data. Standard deviations are given in brackets.

	Ocean-atmosphere heat exchange, TW		Oceanic convergence heat, TW	
	High NAO index	Low NAO index	High NAO index	Low NAO index
the Subpolar Gyre	-161 (21)	-147 (19)	80 (18)	89 (18)

the Norwegian Sea	-56 (3)	-56 (5)	24 (16)	19 (8)

The interannual variability of the oceanic heat flux is usually controlled by the variability of current velocities, which is often related to the NAO phase (Kwok, 2000; Bersch, 2002; Skagseth et al., 2004; Raj et al., 2018). During winter values (January–March) of the low NAO index (NAO index < -0.1), the current velocities in the Subpolar Gyre decrease, but the velocities of the Irminger and East Greenland Currents increase (Fig. 6.4). This situation was highlighted in all data sets. The increase in the intensity of the Subpolar Gyre and the cyclonic gyre of the Nordic Seas corresponds to the strengthening of the atmospheric circulation over the North Atlantic (Figs. 5.3 and 6.4, Foukal and Lozier, 2017). The northwest branch of the North Atlantic Current, which feeds the Irminger Current, on the contrary, weakens (Fig. 6.4).

As a result, in the Irminger Sea (and in the Labrador Sea), periods with a high NAO index are characterized by less intense advection of warmer waters of the Irminger Current (and West Greenland Current waters), and more intense advection of cold polar waters with the East Greenland Current (and Baffin Bay Current). This leads to a weakening of the convergence of oceanic heat with oceanic advection, which occurs in parallel with an increase in heat loss from the ocean surface (Table 6.4 and Appendix 3). Both factors contribute to a decrease in the heat content in the upper ocean in the Subpolar Gyre at high NAO index values, whereas the opposite heat flux anomalies lead to warming of the Subpolar Gyre at low NAO index values. This explains the high negative correlations of the heat content with the NAO index (Fig. 6.3 and Table 6.3). It should be noted that in the Subpolar Gyre, the anomaly of oceanic heat transfer convergence (9 TW), formed as a result of the change in the NAO, is only slightly less than the anomaly of ocean-atmosphere heat exchange equal to 14 TW (Table 6.4).

In the Norwegian Sea, there is also a slight increase in the convergence of oceanic heat transport during periods of high NAO index values (the anomaly reaches 5 TW), while the heat release to the atmosphere remains virtually unchanged (Table 6.4). However, this difference does not result in a clear increase in the heat content of the upper Norwegian Sea, suggesting that the heat content is controlled not only by the NAO effect but also by other processes (see also Appendix 3).

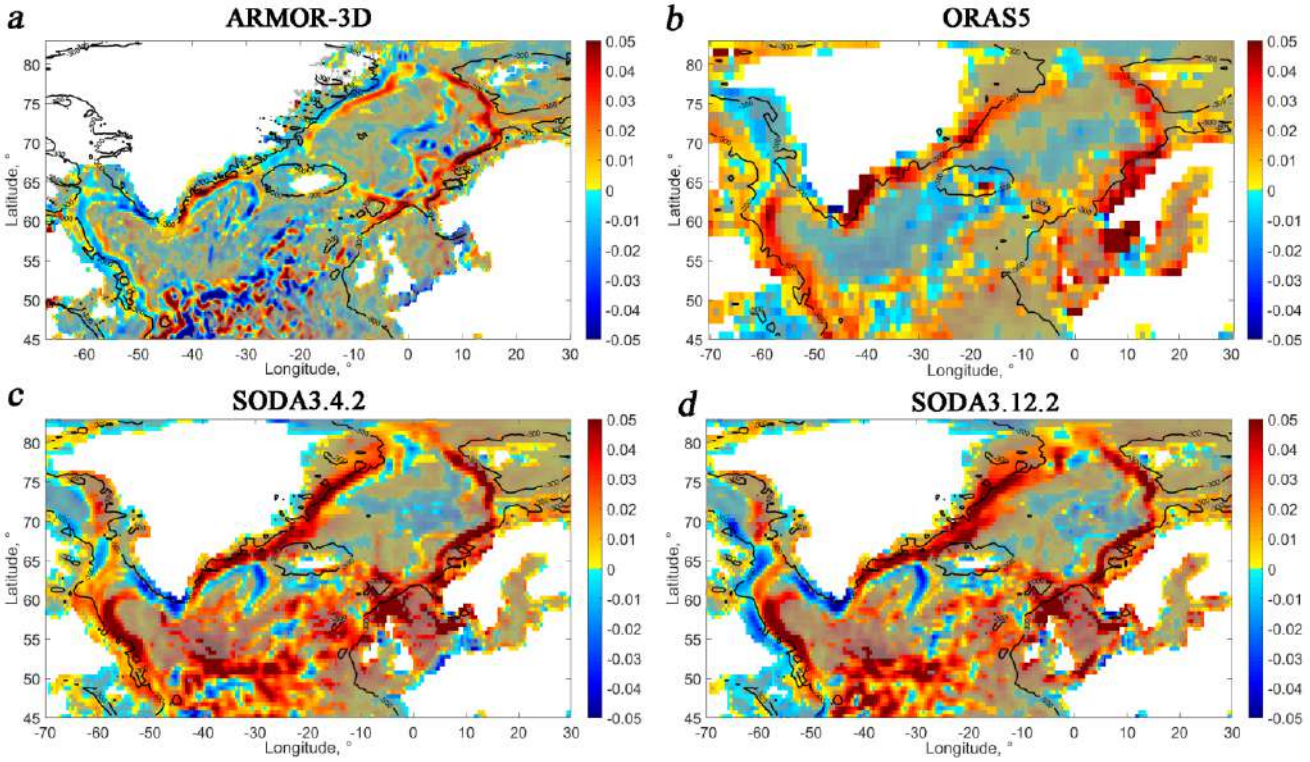

Figure 6.4. Spatial distribution of surface current velocity module anomalies (m/s) on average for January–March based on 4 data sets: a – ARMOR-3D (1993–2018), b – ORAS5 (1975–2017), c – SODA 3.4.2 (1980–2017), d – SODA 3.12.2 (1980–2017). The anomalies are obtained as the difference between the velocity module in years with a high NAO index (>0.9) and a low NAO index (<-0.1). Areas with current velocities less than 0.05 m/s are shown in gray. The 300 m isobath is shown in black.

CONCLUSION

Chapters 1 and **2** are introductory. They provide a physical-geographical description of the study areas, materials and methods.

In **Chapter 3,** the causes of the interannual variability of the advective heat flux with Atlantic waters in the Norwegian Sea were investigated. It was shown that the interannual variability of heat advection is entirely determined by the variability of water transport. The water transport was determined by the sea level gradient across the transect, which in turn was shaped by the Ekman surge and, to a lesser extent, by the local rotor of the wind field. The period of weak surge in 2010 was also a period of strong northerly winds and strong cooling of the sea surface. Together, this led to anomalously high convection in the central Lofoten Basin in that year.

Chapter 4 shows that in the central Irminger Sea there is a strong correlation between the convection depth and the heat content of the upper 500 m layer (correlation coefficient -0.77) for the period 1994–2016. On interannual scales, the main contribution to the variability of the heat content in the central Irminger Sea is made by oceanic heat advection (correlation coefficient 0.77), while the interannual variability of the heat content depends weakly on the variability of heat fluxes at the ocean-atmosphere boundary (correlation coefficient 0.20). From the above it follows that the convection intensity of the Irminger Sea is determined primarily by the convergence of oceanic heat advection (correlation coefficient -0.57), i.e. the less heat is brought to the sea with the recirculating waters of the Irminger Current over the previous period, the greater will be the maximum convection depth. At the same time, the interannual and interdecadal variability of the convergence of oceanic heat advection itself can be caused by the corresponding variability in the atmospheric circulation over the North Atlantic, as evidenced by the moderate correlation of the convection depth in the Irminger Sea with the NAO index, as well as the relationship between the heat content of the Irminger Sea and the AMOC intensity.

Chapter 5 shows that in the upper 500 m of the Labrador Sea, heat content and salt content have generally increased since 1993, possibly representing part of a longer-term (approximately 30 years) cyclicity. Wavelet analysis of heat content and freshwater content allows us to identify two dominant interannual cycles: one lasting 5–8 years (during the entire observation period) and one lasting 2–4 years (since 2000). Wavelet coherence showed the significance of the relationship between these cycles and similar cycles in the NAO index. The relationship between the variability of the thermohaline characteristics of the Labrador Sea and the NAO index is determined by the strengthening of ocean-atmosphere heat exchange and the simultaneous weakening of oceanic heat advection into the Labrador Sea with a decrease in the NAO index.

In **Chapter 6**, based on the analysis of several different data sets of different durations, it is shown that the AMOC forms the second mode of the EOF of the upper layer temperature of the North Atlantic and the Atlantic sector of the Arctic Ocean, the contribution of which is 20–27% of the total water temperature variance. In particular, it is shown that the AMOC makes a significant contribution to the decrease in the upper ocean temperature from the mid-1960s to the mid-1970s, the increase from the 1990s to the mid-2000s, and a new decrease from the mid-2000s to the mid-2010s. Previously, similar dependencies were obtained only for certain areas of the Atlantic and the southeastern part of the Nordic Seas of the Arctic Ocean (see, for example, Alekseev et al. al., 2021; Bryden et al., 2020; Caesar et al., 2021).

The results show that AMOC variability has the strongest impact on the upper-layer temperature of the central Irminger Sea. Here, the observed variability in AMOC intensity in recent decades can lead to an amplitude of 1.5–2 °C in the upper 100-meter sea layer temperature fluctuations. This significantly affects the convection intensity in this key region.

Chapter 6 also examines the influence of the main atmospheric circulation modes on the intensity of heat advection to the studied areas. This chapter shows that the velocities of the North Atlantic, Norwegian, East Greenland and Labrador Currents increase with increasing NAO index, while the velocities of the Irminger and West Greenland Currents, on the contrary, decrease. This forms a redistribution of the nature of heat advection of the North Atlantic Current between the Irminger and Labrador Seas (Subpolar Gyre) and the Nordic Seas. In the Subpolar Gyre, during periods of a high NAO index, this negative anomaly of oceanic heat convergence enhances the heat flux from the ocean to the atmosphere, which together effectively reduces the heat content of the upper layers of the Subpolar Gyre, enhancing convection. The heat content of the upper layers of the Norwegian Sea, despite some increase in the oceanic heat flux through its southern boundary, turned out to be practically unrelated to the NAO. This suggests that the NAO is not the leading mode of variability in heat transport in this region, and may also be a result of the heat redistribution processes of the Norwegian Current in the Norwegian Sea, associated with the high intensity of eddy heat transport in this region.

LIST OF ABBREVIATIONS

AMO – Atlantic Multidecadal Oscillation

AMOC – Atlantic Meridional Overturning Circulation

AO - Arctic Oscillation

AOO – Arctic Oceanic Oscillation

EAP – East Atlantic Pattern

ULSW – Upper Labrador Sea Water

PC – main component

EOF – Empirical Orthogonal Functions

LWM – “classic” Labrador Sea Water (CLSW – Classical Labrador Sea Water, or LSW – Labrador Sea Water)

NAO – North Atlantic Oscillation

NADW – North Atlantic Deep Water

AO – Arctic Ocean

SPWM – subpolar surface water mass (SPMW – SubpolarModeWater)

EAWRP – East Atlantic/Western Russia Pattern

PEP – Polar/Eurasia Pattern

SP – Scandinavian Pattern

TNHP – Tropical/Northern Hemisphere Pattern

LIST LITERATURES

1. Aksenov P. V., Ivanov V. V. "Atlantification" as a probable cause of the reduction in the area of sea ice in the Nansen Basin in the winter season // Problems of the Arctic and Antarctic. - 2018. - V. 64. - No. 1. - P. 42-54.
2. Alekseev G. V., Aleksandrov E. I., Glock N. I., et al. Evolution of the Arctic sea ice cover area under modern climate change conditions // Earth Research from Space. – 2015. – No. 2. – P. 5-5.
3. Alekseev G. V., Vyazilova A. E., Glock N. I., et al. The Impact of Water Temperature Anomalies in Low Latitudes of the Ocean on Arctic Climate Fluctuations and Their Predictability // Arctic: Ecology and Economics. - 2019. - Vol. 3. - No. 35. - P. 73–83.
4. Alekseev G. V., Kuzmina S. I., Glock N. I., et al. The influence of the Atlantic on warming and reduction of sea ice cover in the Arctic // Ice and Snow. - 2017. - Vol. 57. - No. 3. - P. 381–390.
5. Astafieva N. M. Wavelet analysis: fundamentals of theory and application examples // Uspekhi fizicheskikh nauk. – 1996. – V. 166. – No. 11. – P. 1145-1170.
6. Bashmachnikov I. L., Fedorov A. M., Vesman A. V., et al. Thermohaline convection in the subpolar seas of the North Atlantic and the Nordic Seas of the Arctic Ocean based on satellite and in situ data. Part 1: localization of convection regions // Modern Problems of Remote Sensing of the Earth from Space. – 2018. – Vol. 15. – No. 7. – P. 184–194. doi: 10.21046/2070-7401-2018-15-7-184-194
7. Bashmachnikov I. L., Fedorov A. M., Vesman A. V., et al. Thermohaline convection in the subpolar seas of the North Atlantic and the Nordic Seas of the Arctic Ocean based on satellite and in situ data. Part 2: convection intensity indices // Modern Problems of Remote Sensing of the Earth from Space. - 2019. - Vol. 16. - No. 1. - P. 191–201.
8. Belonenko T. V., Fedorov A. M., Bashmachnikov I. L., Fuchs V. R. Trends in the intensity of currents in the Labrador Sea and the Irminger Sea based on satellite altimetry data // Earth Research from Space. - 2018. - No. 2. - P. 3–12.
9. Belyaev K. P., Soloviev V. N. On numerical calculations of thermohydrodynamic equations simulating ocean currents in the region of the subpolar front of the North Atlantic // Mathematical Modeling. – 1996. – V. 8. – No. 11. – P. 87-95.
10. Byshev V. I., Neiman V. G., Romanov Yu. A., Serykh I. V. On the phase variability of some characteristics of the modern climate in the North Atlantic region // Reports of the Academy of Sciences. – Federal State Budgetary Institution "Russian Academy of Sciences", 2011. – V. 438. – No. 6. – P. 817-822.

11. Falina A. S., Sarafanov A. A., Dobrolyubov S. A. et al. Convection and stratification of waters in the North Atlantic Ocean based on measurements in the winter of 2013/14 // Bulletin of Moscow University. Series 5. Geography. - 2017. – No. 4. – P. 45-54.
12. Fedorov A. M., Bashmachnikov I. L., Belonenko T. V. Localization of deep convection regions in the Nordic Seas, Labrador and Irminger // Bulletin of St. Petersburg University. Earth Sciences. - 2018. - V. 63. - No. 3. - P. 345–362.
13. Gladishev S. V., Gladishev V. S., Gulev S. K., Sokov A. V. Anomalously deep convection in the Irminger Sea in winter 2014–2015 // Reports of the Academy of Sciences. – 2016a. – Vol. 469. – No. 3. – P. 351–355.
14. Gladyshev S. V., Gladyshev V. S., Sokov A. V., et al. Average long-term structure and water transport by the system of western boundary currents east of Greenland // Reports of the Academy of Sciences. - 2017. - Vol. 473. - No. 1. - P. 93–97.
15. Gladyshev S. V., Gladyshev V. S., Falina A. S., Sarafanov A. A. Winter convection in the Irminger Sea in 2004–2014. // Oceanology. – 2016b. – T. 56. – No. 3. – P. 353–363.
16. Gladyshev S. V., Sokov A. V., Gulev S. K., et al. The role of circulation mechanisms and variability of intermediate waters in the Irminger Sea during deep convection // Reports of the Academy of Sciences. - 2018. - Vol. 483. - No. 5. - P. 549–553.
17. Iakovleva D. A., Bashmachnikov I. L. Interannual variability of heat content and fresh water content in the cold water dome of the Labrador Sea // Bulletin of St. Petersburg University. Earth Sciences. - 2019. - Vol. 64. - No. 1. - P. 136-158. doi: 10.21638/spbu07.2019.108.
18. Iakovleva, D. A., Bashmachnikov, I. L. The Role of Regional Atmospheric Circulation in Interannual Variability of Heat Advection into the Nordic Seas // Bulletin of the Russian Academy of Sciences. Atmospheric and Oceanic Physics. - 2023. - Vol. 59. - No. 5. - P. 539–548.
19. Iakovleva D. A., Bashmachnikov I. L., Kuznetsova D. A. Influence of the Atlantic Meridional Oceanic Circulation on the Temperature of the Upper Layer of the North Atlantic and the Atlantic Sector of the Arctic Ocean // Oceanology. - 2023. - Vol. 63. - No. 2. - P. 173–181.
20. Ivanov V. V., Alekseev V. A., Repina I. A. Increasing impact of Atlantic waters on the ice cover of the Arctic Ocean // Turbulence, dynamics of the atmosphere and climate. - 2014. - P. 336-344.
21. Kuznetsova D. A., Bashmachnikov I. L. On the mechanisms of variability of the Atlantic meridional ocean circulation (AMOC) // Oceanology. - 2021. - Vol. 61. - No. 6. - P. 843–855.
22. Lebedev K. V., Filyushkin B. N., Kozhelupova N. G. Water exchange of the Polar seas with the Atlantic and Arctic oceans based on Argo observations // Oceanological studies. - 2019. - Vol. 47. - No. 2. - P. 183-197.

23. Lyakhov A. N. Modern methods of data processing in geophysics // Proceedings of the International Baikal Youth Scientific School on Fundamental Physics and the Conference of Young Scientists “Physical Processes in Space and the Near-Earth Environment”. Irkutsk: Editorial and Publishing Department of ISTP SB RAS, 2006. – P. 39–46.
24. Mikhailova N. V., Yurovsky A. V. East Atlantic Oscillation: mechanism and influence on the climate of Europe in winter // Marine Hydrophysical Journal. - 2016. - No. 4 (190). - P. 27-37.
25. Mokhov I. I., Semenov V. A., Khon V. Ch., et al. Relationship of climate anomalies in Eurasia and the North Atlantic with natural variations in the Atlantic thermohaline circulation according to long-term model calculations // Reports of the Academy of Sciences. – Federal State Budgetary Institution "Russian Academy of Sciences", 2008. – V. 419. – No. 5. – P. 687-690.
26. Nesterov E. S. On the East Atlantic Oscillation of Atmospheric Circulation // Meteorology and Hydrology. - 2009. - No. 12. - P. 32-40.
27. Semenov V. A. Influence of oceanic inflow into the Barents Sea on climate variability in the Arctic // Reports of the Academy of Sciences. – Federal State Budgetary Institution "Russian Academy of Sciences", 2008. – V. 418. – No. 1. – P. 106-109.
28. Soviet Arctic (Seas and islands of the Arctic Ocean) / Acad. Sciences of the USSR, Institute of Geography; ed.: Ya. Ya. Gakkel, L. S. Govorukha, I. P. Gerasimov. – M.: Nauka, 1970. – 526 p.
29. Treshnikov A.F., Balakshin L.L., Belov N.A. et al. Geographical names of the main parts of the bottom relief of the Arctic basin // Problems of the Arctic and Antarctic. – 1967. – No. 27. – P. 5.
30. Alekseev G. V., Smirnov A. V., Pnyushkov A. V. et al. Changes of fresh water content in the upper layer of the Arctic Basin in the 1950s-2010s // Fundamentalnaya I Prikladnaya Gidrofzika. – 2021. – V. 14. – № 4. – P. 25–38.
31. Ardyna M., Babin M., Gosselin M. et al. Recent Arctic Ocean sea ice loss triggers novel fall phytoplankton blooms //Geophysical Research Letters. – 2014. – V. 41. – №. 17. – P. 6207-6212.
32. Bacon S., Reverdin G., Rigor I. G., Snaith H. M. A freshwater jet on the east Greenland shelf // Journal of Geophysical Research: Oceans. – 2002. – V. 107. – № C7. – P. 5-1–5-16.
33. Bakalian F., Hameed S., Pickart R. Influence of the Icelandic Low latitude on the frequency of Greenland tip jet events: Implications for Irminger Sea convection // Journal of Geophysical Research: Oceans. – 2007. – V. 112. – № C4.
34. Balmaseda M. A., Mogensen K., Weaver A. T. Evaluation of the ECMWF ocean reanalysis system ORAS4 // Quarterly Journal of the Royal Meteorological Society. – 2013. – V. 139. – № 674. – P. 1132–1161.

35. Barnston A. G., Livezey R. E. Classification, seasonality and persistence of low-frequency atmospheric circulation patterns // Monthly weather review. – 1987. – V. 115. – №. 6. – P. 1083-1126.
36. Barrier N., Cassou C., Deshayes J., Treguier A. M. Response of North Atlantic Ocean circulation to atmospheric weather regimes //Journal of Physical Oceanography. – 2014. – V. 44. – №. 1. – P. 179-201.
37. Barrier N., Deshayes J., Treguier A. M., Cassou C. Heat budget in the North Atlantic subpolar gyre: Impacts of atmospheric weather regimes on the 1995 warming event // Progress in Oceanography. – 2015. – V. 130. – P. 75-90.
38. Bashmachnikov I., Belonenko T. V., Koldunov A. V. Intra-annual and interannual non-stationary cycles of chlorophyll concentration in the Northeast Atlantic // Remote sensing of environment. – 2013. – V. 137. – P. 55-68.
39. Bashmachnikov I. L., Fedorov A. M., Golubkin P. A. et al. Mechanisms of interannual variability of deep convection in the Greenland Sea // Deep Sea Research Part I: Oceanographic Research Papers. – 2021. – V. 174. – P. 103557.
40. Bashmachnikov I. L., Raj R. P., Golubkin P., Kozlov I. E. Heat transport by mesoscale eddies in the Norwegian and Greenland seas // J. Geophysical Research: Oceans. – 2023. – P. e2022JC018987.
41. Bersch M. North Atlantic Oscillation–induced changes of the upper layer circulation in the northern North Atlantic Ocean //Journal of Geophysical Research: Oceans. – 2002. – V. 107. – №. C10. – P. 20-1-20-11.
42. Beszczynska-Möller A., Fahrbach E., Schauer U., Hansen E. Variability in Atlantic water temperature and transport at the entrance to the Arctic Ocean, 1997–2010 //ICES Journal of Marine Science. – 2012. – V. 69. – №. 5. – P. 852-863.
43. Beszczynska-Moller A., Woodgate R. A., Lee C. et al. A synthesis of exchanges through the main oceanic gateways to the Arctic Ocean // Oceanography. – 2011. – V. 24. – № 3. – P. 82–99.
44. Björk G., Gustafsson B. G., Stigebrandt A. Upper layer circulation of the Nordic seas as inferred from the spatial distribution of heat and freshwater content and potential energy // Polar Research. – 2001. – V. 20. – №. 2. – P. 161-168.
45. Billet D. S. M., Lampitt R. S., Rice A. L., Mantoura R. F. C. Seasonal sedimentation of phytoplankton to the deep sea benthos // Nature. – 1986. – V. 302. – P. 520–522.
46. Bingyi W., Jia W. Possible impacts of winter Arctic Oscillation on Siberian high, the East Asian winter monsoon and sea–ice extent // Advances in Atmospheric Sciences. – 2002. – V. 19. – №. 2. – P. 297-320.

47. Brambilla E., Talley L. D., Robbins P. E. Subpolar mode water in the northeastern Atlantic: 2. Origin and transformation // Journal of Geophysical Research: Oceans. – 2008. – V. 113. – №. C4.
48. Bryden H. L., Johns W. E., King B. A. et al. Reduction in ocean heat transport at 26 N since 2008 cools the eastern subpolar gyre of the North Atlantic Ocean // Journal of Climate. – 2020. – V. 33. – № 5. – P. 1677–1689.
49. Buckley M. W., Marshall J. Observations, inferences, and mechanisms of the Atlantic Meridional Overturning Circulation: A review // Reviews of Geophysics. – 2016. – V. 54. – №. 1. – P. 5-63.
50. Buongiorno Nardelli B., Guinehut S., Pascual A. et al. Towards high resolution mapping of 3-D mesoscale dynamics from observations // Ocean Science. – 2012. – V. 8. – №. 5. – P. 885-901.
51. Caesar L., McCarthy G. D., Thornalley D. J. R. et al. Current Atlantic meridional overturning circulation weakest in last millennium // Nature Geoscience. – 2021. – V. 14. – № 3. – P. 118–120.
52. Caesar L., Rahmstorf S., Robinson A. et al. Observed fingerprint of a weakening Atlantic Ocean overturning circulation // Nature. – 2018. – V. 556. – № 7700. – P. 191–196.
53. Carton J. A., Chepurin G. A., Chen L. SODA3: A new ocean climate reanalysis //Journal of Climate. – 2018. – V. 31. – №. 17. – P. 6967-6983.
54. Chafik L., Rossby T. Volume, heat, and freshwater divergences in the subpolar North Atlantic suggest the Nordic Seas as key to the state of the meridional overturning circulation // Geophysical Research Letters. – 2019. – V. 46. – № 9. – P. 4799–4808.
55. Chanut J., Barnier B., Large W. et al. Mesoscale eddies in the Labrador Sea and their contribution to convection and restratification // Journal of Physical Oceanography. – 2008. – V. 38. – №. 8. – P. 1617-1643.
56. Chen X., Tung K. K. Global surface warming enhanced by weak Atlantic overturning circulation // Nature. – 2018. – V. 559. – № 7714. – P. 387–391.
57. Curry R. G., McCartney M. S., Labrador sea water carries northern climate signal south // Oceanus-Woods Hole Mass. – 1996. – V. 39. – P. 24-28.
58. de Boyer Montégut C., Madec G., Fischer A. S. et al. Mixed layer depth over the global ocean: An examination of profile data and a profile-based climatology // Journal of Geophysical Research: Oceans. – 2004. – V. 109. – № C12.
59. de Jong M. F., van Aken H. M., Våge K., Pickart R. S. Convective mixing in the central Irminger Sea: 2002–2010 // Deep Sea Research Part I: Oceanographic Research Papers. – 2012. – V. 63. – P. 36–51.

60. Dee D. P., Uppala S. M., Simmons A. J. et al. The ERA-Interim reanalysis: Configuration and performance of the data assimilation system // Quarterly J. royal meteorological society. – 2011. – V. 137. – № 656. – P. 553–597.
61. Desbruyères D., Mercier H., Thierry V. On the mechanisms behind decadal heat content changes in the eastern subpolar gyre // Progress in Oceanography. – 2015. – V. 132. – P. 262–272.
62. Dickson R. R., Brown J. The production of North Atlantic Deep Water: sources, rates, and pathways // Journal of Geophysical Research: Oceans. – 1994. – V. 99. – №. C6. – P. 12319-12341.
63. Drinkwater K. F., Miles M., Medhaug I. et al. The Atlantic Multidecadal Oscillation: Its manifestations and impacts with special emphasis on the Atlantic region north of 60 N // Journal of Marine Systems. – 2014. – V. 133. – P. 117-130.
64. Dukhovskoy D. S., Yashayaev I., Proshutinsky A. et al. Role of Greenland freshwater anomaly in the recent freshening of the subpolar North Atlantic // Journal of Geophysical Research: Oceans. – 2019. – V. 124. – № C5. – P. 3333–3360.
65. Eldevik T., Nilsen J. E. Ø., Iovino D. et al. Observed sources and variability of Nordic seas overflow // Nature Geoscience. – 2009. – V. 2. – № 6. – P. 406–410.
66. Emery W. J., Thomson R. E. Data Analysis Methods in Physical Oceanography // Elsevier, Amsterdam, 2001. – P. 1–634.
67. Falina A., Sarafanov A., Mercier H. et al. On the cascading of dense shelf waters in the Irminger Sea // Journal of Physical Oceanography. – 2012. – V. 42. – № 12. – P. 2254–2267.
68. Fedorov A.M., Bashmachnikov I.L., Iakovleva D.A. et al. Deep convection in the Subpolar Gyre: Do we have enough data to estimate its intensity? // Dynamics of Atmospheres and Oceans. – 2023. – V. 101. – P. 101338.
69. Fedorov A. M., Raj R. P., Belonenko T. V. et al. Extreme convective events in the Lofoten Basin // Pure and Applied Geophysics. – 2021. – V. 178. – №. 6. – P. 2379-2391.
70. Foukal N. P., Lozier M. S. Assessing variability in the size and strength of the North Atlantic subpolar gyre // Journal of Geophysical Research: Oceans. – 2017. – V. 122. – №. 8. – P. 6295-6308. https://doi.org/10.1002/2017JC012798.
71. Frajka-Williams E., Ansorge I. J., Baehr J. et al. Atlantic meridional overturning circulation: observed transport and variability // Frontiers in Marine Science. – 2019. – V. 6. – № 260.
72. Fried N., de Jong M. F. The role of the Irminger Current in the Irminger Sea northward transport variability // Journal of Geophysical Research: Oceans. – 2022. – V. 127. – № C3. – P. e2021JC018188.
73. Gnatuik N., Vihma T., Bobylev L. Inter-seasonal teleconnections between Earth surface temperature and near-surface air temperature // POLAR. – 2018. – P. 15-26.

74. Haine T. W. N., Curry B., Gerdes R. et al. Arctic freshwater export: Status, mechanisms, and prospects // Global and Planetary Change. – 2015. – V. 125. – P. 13-35.
75. Hansen B., Østerhus S., Turrell W.R. et al. The inflow of Atlantic water, heat, and salt to the Nordic seas across the Greenland–Scotland ridge // Arctic–subarctic ocean fluxes: Defining the role of the northern seas in climate. – 2008. – P. 15–43.
76. Hansen B., Larsen K. M. H., Hátún H. et al. Transport of volume, heat, and salt towards the Arctic in the Faroe Current 1993–2013 // Ocean Science. – 2015. – V. 11. – №. 5. – P. 743–757.
77. Hauser T., Demirov E., Zhu J., Yashayaev I. North Atlantic atmospheric and ocean inter-annual variability over the past fifty years–Dominant patterns and decadal shifts // Progress in Oceanography. – 2015. – V. 132. – P. 197-219.
78. Hogan R. Radiation quantities in the ECMWF model and MARS // ECMWF, 2016. – 2015.
79. Holte J., Straneo F. Seasonal overturning of the Labrador Sea as observed by Argo floats // Journal of Physical Oceanography. – 2017. – V. 47. – №. 10. – P. 2531-2543.
80. Iakovleva D. A, Bashmachnikov I. L. On the seesaw in interannual variability of upper ocean heat advection between the North Atlantic Subpolar Gyre and the Nordic Seas // Dynamics of Atmospheres and Oceans. – 2021. – V. 96. – P. 101263.
81. Iakovleva D. A., Bashmachnikov I. L., Diansky N. A. Coherence of Deep Convection in the Irminger Sea with Oceanic Heat Advection // Oceanology. – 2023. – V. 63. – №. Suppl 1. – P. S1-S10.
82. Jenkins W. J., Smethie Jr W. M., Boyle E. A., Cutter G. A. Water mass analysis for the US GEOTRACES (GA03) North Atlantic sections //Deep Sea Research Part II: Topical Studies in Oceanography. – 2015. – V. 116. – P. 6-20.
83. Jevrejeva S., Moore J. C., Grinsted A. Influence of the Arctic Oscillation and El Niño-Southern Oscillation (ENSO) on ice conditions in the Baltic Sea: The wavelet approach //Journal of Geophysical Research: Atmospheres. – 2003. – V. 108. – №. D21.
84. Josey S. A., de Jong M. F., Oltmanns M. et al. Extreme variability in Irminger Sea winter heat loss revealed by ocean observatories initiative mooring and the ERA5 reanalysis // Geophysical Research Letters. – 2019. – V. 46. – № 1. – P. 293–302.
85. Kara A. B., Rochford P. A., Hurlburt H. E. Mixed layer depth variability over the global ocean // Journal of Geophysical Research: Oceans. – 2003. – V. 108. – № C3. – P. 3079.
86. Karcher M. J., Gerdes R., Kauker F., Köberle C. Arctic warming: evolution and spreading of the 1990s warm event in the Nordic seas and the Arctic Ocean // Journal of Geophysical Research: Oceans. – 2003. – V. 108. – №C2.

87. Khatiwala S., Schlosser P., Visbeck M. Rates and mechanisms of water mass transformation in the Labrador Sea as inferred from tracer observations // Journal of Physical Oceanography. – 2002. – V. 32. – №. 2. – P. 666-686.
88. Kumar P., Foufoula-Georgiou E. Wavelet analysis for geophysical applications //Reviews of geophysics. – 1997. – V. 35. – №. 4. – P. 385-412.
89. Kwok R. Recent changes in Arctic Ocean sea ice motion associated with the North Atlantic Oscillation // Geophysical Research Letters. – 2000. – V. 27. – №. 6. – P. 775-778. https://doi.org/10.1029/1999GL002382.
90. Larnicol G., Guinehut S., Rio M. H. et al. The global observed ocean products of the French Mercator project. Proceedings of the Symposium on 15 Years of Progress in Radar Altimetry, 13–18 March 2006. Venice, Italy.
91. Latarius K., Quadfasel D. Water mass transformation in the deep basins of the Nordic Seas: Analyses of heat and freshwater budgets // Deep Sea Research Part I: Oceanographic Research Papers. – 2016. – V. 114. – P. 23–42.
92. Le Bras I. A., Straneo F., Holte J. et al. Rapid export of waters formed by convection near the Irminger Sea's western boundary // Geophysical Research Letters. – 2020. – V. 47. – № 3. – P. e2019GL085989.
93. Le Bras I. A. A., Straneo F., Holte J., Holliday N. P. Seasonality of freshwater in the East Greenland Current system from 2014 to 2016 // Journal of Geophysical Research: Oceans. – 2018. – V. 123. – № C12. – P. 8828–8848.
94. Levermann A., Born A. Bistability of the Atlantic subpolar gyre in a coarse-resolution climate model // Geophysical Research Letters. – 2007. – V. 34. – № 24. – P. L24605.
95. Li F., Jo Y. H., Yan X. H., Liu W. T. Varying temperature and heat content signatures in the central Labrador Sea at different layers and timescales // Deep Sea Research Part I: Oceanographic Research Papers. – 2015. – V. 103. – P. 114-124.
96. Lozier M. S., Li F., Bacon S. et al. A sea change in our view of overturning in the subpolar North Atlantic // Science. – 2019. – V. 363. – №. 6426. – P. 516-521.
97. Luo D., Diao Y., Feldstein S. B. The variability of the Atlantic storm track and the North Atlantic Oscillation: A link between intraseasonal and interannual variability //Journal of the Atmospheric Sciences. – 2011. – V. 68. – №. 3. – P. 577-601.
98. Marshall J., Johnson H., Goodman J. A study of the interaction of the North Atlantic Oscillation with ocean circulation // Journal of Climate. – 2001. – V. 14. – №. 7. – P. 1399-1421.
99. Mastropole D., Pickart R. S., Valdimarsson H. et al. On the hydrography of Denmark Strait // Journal of Geophysical Research: Oceans. – 2017. – V. 122. – № 1. – P. 306–321.

100. McCarthy G. D, Brown P. J., Flagg C. N. et al. Sustainable observations of the AMOC: methodology and technology // Reviews of Geophysics. – 2020. – V. 58. – № 1. – P. e2019RG000654.

101. McCartney M. S., Talley L. D. The subpolar mode water of the North Atlantic Ocean // Journal of Physical Oceanography. – 1982. – V. 12. – №. 11. – P. 1169-1188.

102. Mo K. C., Livezey R. E. Tropical-extratropical geopotential height teleconnections during the Northern Hemisphere winter // Monthly Weather Review. – 1986. – V. 114. – №. 12. – P. 2488-2515.

103. Mork K. A., Blindheim J. Variations in the Atlantic inflow to the Nordic Seas, 1955–1996 // Deep Sea Research Part I: Oceanographic Research Papers. – 2000. – V. 47. – № 6. – P. 1035–1057.

104. Myers P. G. Josey S. A., Wheler B., Kulan N. Interdecadal variability in Labrador Sea precipitation minus evaporation and salinity //Progress in Oceanography. – 2007. – V. 73. – №. 3-4. – P. 341-357.

105. Nansen F. Das bodenwasser und die abkühlung des meeres //Internationale Revue der gesamten Hydrobiologie und Hydrographie. – 1912. – V. 5. – №. 1. – P. 1-42.

106. Orvik K. A. Long-Term Moored Current and Temperature Measurements of the Atlantic Inflow Into the Nordic Seas in the Norwegian Atlantic Current; 1995–2020 // Geophysical Research Letters. – 2022. – V. 49. – № 3. – P. e2021GL096427.

107. Orvik K. A., Skagseth Ø. The impact of the wind stress curl in the North Atlantic on the Atlantic inflow to the Norwegian Sea toward the Arctic // Geophysical Research Letters. – 2003. – V. 30. – №. 17.

108. Orvik K. A., Skagseth Ø., Mork M. Atlantic inflow to the Nordic Seas: current structure and volume fluxes from moored current meters, VM-ADCP and SeaSoar-CTD observations, 1995–1999 // Deep Sea Research Part I: Oceanographic Research Papers. – 2001. – V. 48. – № 4. – P. 937–957.

109. Oziel L., Baudena A., Ardyna M. et al. Faster Atlantic currents drive poleward expansion of temperate phytoplankton in the Arctic Ocean // Nature Communications. – 2020. – V. 11. – №. 1. – P. 1705.

110. Peterson B. J., McClelland J., Curry R. et al. Trajectory shifts in the Arctic and subarctic freshwater cycle // Science. – 2006. – V. 313. – №. 5790. – P. 1061-1066.

111. Petit T., Lozier M. S., Josey S. A., Cunningham S. A. Atlantic deep water formation occurs primarily in the Iceland Basin and Irminger Sea by local buoyancy forcing // Geophysical Research Letters. – 2020. – V. 47. – № 22. – P. e2020GL091028.

112. Pickart R. S., Spall M. A., Ribergaard M. H. et al. Deep convection in the Irminger Sea forced by the Greenland tip jet // Nature. – 2003a. – V. 424. – № 6945. – P. 152–156.

113. Pickart R. S., Straneo F., Moore G. K. Is Labrador Sea water formed in the Irminger basin? // Deep Sea Research Part I: Oceanographic Research Papers. – 2003b. – V. 50. – № 1. – P. 23–52.

114. Piron A., Thierry V., Mercier H., Caniaux G. Argo float observations of basin-scale deep convection in the Irminger sea during winter 2011–2012 // Deep Sea Research Part I: Oceanographic Research Papers. – 2016. – V. 109. – P. 76-90.

115. Piron A., Thierry V., Mercier H., Caniaux G. Gyre-scale deep convection in the subpolar North Atlantic Ocean during winter 2014–2015 // Geophysical Research Letters. – 2017. – V. 44. – № 3. – P. 1439–1447.

116. Polyakov I., Johnson M. Arctic decadal and interdecadal variability // Geophysical Research Letters. – 2000. – V. 27. – № 24. – P. 4097–4100.

117. Pozo-Vázquez D., Esteban-Parra M. J., Rodrigo F. S., Castro-Díez Y. An analysis of the variability of the North Atlantic Oscillation in the time and the frequency domains // International Journal of Climatology: A Journal of the Royal Meteorological Society. – 2000. – V. 20. – №. 14. – P. 1675-1692

118. Proshutinsky A., Dukhovskoy D., Timmermans M. L. et al. Arctic circulation regimes // Philosophical Transactions of the Royal Society A: Mathematical, Physical and Engineering Sciences. – 2015. – V. 373. – №. 2052. – P. 20140160.

119. Rahmstorf S., Box J. E., Feulner G. et al. Exceptional twentieth-century slowdown in Atlantic Ocean overturning circulation // Nature climate change. – 2015. – V. 5. – № 5. – P. 475–480.

120. Raj R. P., Nilsen J. Ø., Johannessen J. A. et al. Quantifying Atlantic Water transport to the Nordic Seas by remote sensing // Remote Sensing of Environment. – 2018. – V. 216. – P. 758–769.

121. Rhein M., Kieke D., Hüttl-Kabus S. et al. Deep water formation, the subpolar gyre, and the meridional overturning circulation in the subpolar North Atlantic // Deep Sea Research Part II: Topical Studies in Oceanography. – 2011. – V. 58. – №. 17-18. – P. 1819-1832.

122. Rühs S., Oliver E. C., Biastoch A. et al. Changing spatial patterns of deep convection in the subpolar North Atlantic // Journal of Geophysical Research: Oceans. – 2021. – V. 126. – № 7. – P. e2021JC017245.

123. Sarafanov A., Falina A., Mercier H. et al. Mean full-depth summer circulation and transports at the northern periphery of the Atlantic Ocean in the 2000s // Journal of Geophysical Research: Oceans. – 2012. – V. 117. – № C1.

124. Schauer U, Fahrbach E., Osterhus S., Rohardt G. Arctic warming through the Fram Strait: Oceanic heat transport from 3 years of measurements // J. Geophysical Research: Oceans. – 2004. – V. 109. – № C6.

125. Serreze M. C., Barrett A. P., Slater A. G. et al. The large-scale freshwater cycle of the Arctic // Journal of Geophysical Research: Oceans. – 2006. – V. 111. – №. C11.

126. Skagseth Ø. Monthly to annual variability of the Norwegian Atlantic slope current: Connection between the northern North Atlantic and the Norwegian Sea // Deep Sea Research Part I: Oceanographic Research Papers. – 2004. – V. 51. – № 3. – P. 349–366.

127. Skagseth Ø., Furevik T., Ingvaldsen R. et al. Volume and heat transports to the Arctic Ocean via the Norwegian and Barents Seas // Arctic–subarctic ocean fluxes: Defining the role of the northern seas in climate. – 2008. – P. 45-64.

128. Skagseth Ø., Orvik K. A., Furevik T. Coherent variability of the Norwegian Atlantic Slope Current derived from TOPEX/ERS altimeter data // Geophysical Research Letters. – 2004. – V. 31. – №. 14.

129. Stramma L., Kieke D., Rhein M. et al. Deep water changes at the western boundary of the subpolar North Atlantic during 1996 to 2001 // Deep Sea Research Part I: Oceanographic Research Papers. – 2004. – V. 51. – №. 8. – P. 1033-1056.

130. Våge K., Pickart R. S., Moore G. W. K., Ribergaard M. H. Winter mixed layer development in the central Irminger Sea: The effect of strong, intermittent wind events // Journal of Physical Oceanography. – 2008. – V. 38. – № 3. – P. 541–565.

131. Våge K., Pickart R. S., Sarafanov A. et al. The Irminger Gyre: Circulation, convection, and interannual variability // Deep Sea Research Part I: Oceanographic Research Papers. – 2011a. – V. 58. – № 5. – P. 590–614.

132. Våge K., Pickart R. S., Spall M. A. et al. Significant role of the North Icelandic Jet in the formation of Denmark Strait overflow water // Nature Geoscience. – 2011b. – V. 4. – № 10. – P. 723–727.

133. Våge K., Pickart R. S., Thierry V. et al. Surprising return of deep convection to the subpolar North Atlantic Ocean in winter 2007–2008 // Nature Geoscience. – 2009. – V. 2. – № 1. – P. 67–72.

134. Vernet M., Ellingsen I. H., Seuthe L. et al. Influence of phytoplankton advection on the productivity along the Atlantic water inflow to the Arctic Ocean // Frontiers in Marine Science. – 2019. – V. 6. – P. 583.

135. Vesman A. V., Bashmachnikov I. L., Golubkin P. A., Raj R. P. The coherence of the oceanic heat transport through the Nordic seas: oceanic heat budget and interannual variability // Russian J. Earth Sciences. – 2023. – P. 1–24.

136. Visbeck M. Power of pull // Nature. – 2007. – V. 447. – № 7143. – P. 383–383.

137. Visbeck M., Chassignet E. P., Curry R. G. et al. The ocean's response to North Atlantic Oscillation variability // Geophysical Monograph-American Geophysical Union. – 2003. – V. 134. – P. 113-146.

138. Volkov D. L., Meinen C. S., Schmid C. et al. Atlantic meridional overturning circulation and associated heat transport // In: Blunden J., Arndt D.S. (eds.). State of the climate in 2019. American Meteorological Society. – 2020. – P. 159–163.

139. Walczowski W., Piechura J., Goszczko I., Wieczorek P. Changes in Atlantic water properties: an important factor in the European Arctic marine climate // ICES Journal of Marine Science. – 2012. – V. 69. – №. 5. – P. 864-869.

140. Wallace J. M., Gutzler D. S. Teleconnections in the geopotential height field during the Northern Hemisphere winter // Monthly weather review. – 1981. – V. 109. – №. 4. – P. 784-812.

141. Wang Y. H., Magnusdottir G., Stern H. et al. Decadal variability of the NAO: Introducing an augmented NAO index //Geophysical Research Letters. – 2012. – V. 39. – №. 21.

142. Xu X., Schmitz Jr. W. J., Hurlburt H. E. et al. Transport of Nordic Seas overflow water into and within the Irminger Sea: an eddy-resolving simulation and observations. // Journal of Geophysical Research: Oceans. – 2010. – V. 115. – №. C12.

143. Yang Q., Dixon T. H., Myers P. G. et al. Recent increases in Arctic freshwater flux affects Labrador Sea convection and Atlantic overturning circulation // Nature communications. – 2016. – V. 7. – № 1. – P. 10525.

144. Yashayaev I. Hydrographic changes in the Labrador Sea, 1960–2005 // Progress in Oceanography. – 2007. – V. 73. – № 3–4. – P. 242–276.

145. Yashayaev I., Clarke A. Evolution of North Atlantic water masses inferred from Labrador Sea salinity series // Oceanography. – 2008. – V. 21. – №. 1. – P. 30-45.

146. Yashayaev I., Loder J. W. Recurrent replenishment of Labrador Sea Water and associated decadal-scale variability // Journal of Geophysical Research: Oceans. – 2016. – V. 121. – № C11. – P. 8095–8114.

147. Yashayaev I., Seidov D. The role of the Atlantic Water in multidecadal ocean variability in the Nordic and Barents Seas // Progress in Oceanography. – 2015. – V. 132. – P. 68-127. https://doi.org/10.1016/j.pocean.2014.11.009.

148. Yashayaev I., Seidov D., Demirov E. A new collective view of oceanography of the Arctic and North Atlantic basins // Progress in Oceanography. – 2015. – V. 132. – P. 1–21.

149. Zunino P., Mercier H., Thierry V. Why did deep convection persist over four consecutive winters (2015–2018) southeast of Cape Farewell? // Ocean Science. – 2020. – V. 16. – № 1. – P. 99–113.

150. Zuo H., Balmaseda M. A., Tietsche S. et al. The ECMWF operational ensemble reanalysis–analysis system for ocean and sea ice: a description of the system and assessment // Ocean science. – 2019. – V. 15. – №. 3. – P. 779-808.

Appendix 1

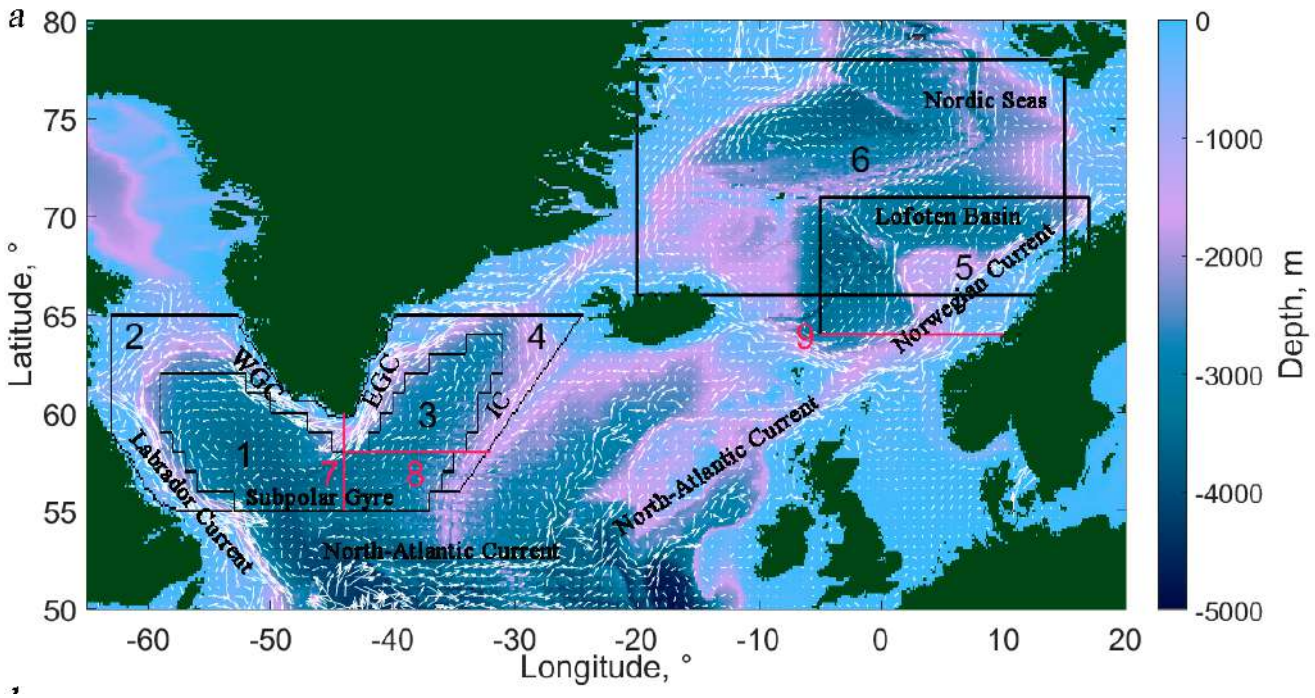

Map of the study area with regions and three sections for comparison of arrays (Fig. 2.1 and Appendix 2): 1 – central part of the Labrador Sea, 2 – shelf part of the Labrador Sea, 3 – central part of the Irminger Sea, 4 – shelf part of the Irminger Sea, 5 – Norwegian Sea, 6 – Norwegian and Greenland Seas, 7 – through 44° W (55-60° N), 8 – through 58° N (44-32° W), 9 – through 64° N (5° W – 12° E). EGC – East Greenland Current, WGC – West Greenland Current, IC – Irminger Current.

Appendix 2

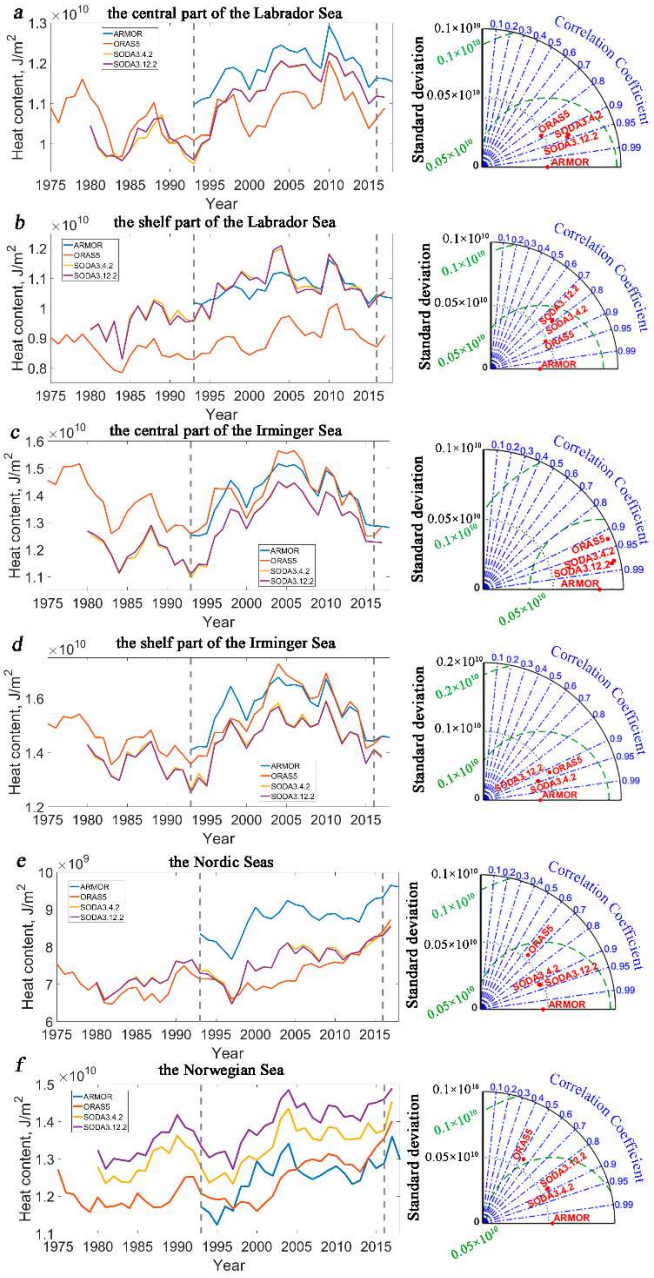

Interannual variability of annual mean heat content in the upper 500 m layer according to ARMOR-3D, ORAS5, SODA3.4.2, SODA3.12.2 data and the Taylor diagram: a – central Labrador Sea, b – shelf Labrador Sea, c – central Irminger Sea, d – shelf Irminger Sea, e – Norwegian and Greenland Seas, f – Norwegian Sea (see Appendix 1 for area boundaries). Taylor diagrams are constructed for the period 1993–2016 (limited by gray dotted lines) after removing the mean for the entire period. Blue dashed-dotted lines show correlations with the ARMOR-3D data-set, green dotted lines show the root-mean-square error from the ARMOR - 3D data-set. The base water temperature for calculating heat content was taken as the freezing temperature of sea water -1.8 °C.

Appendix 3

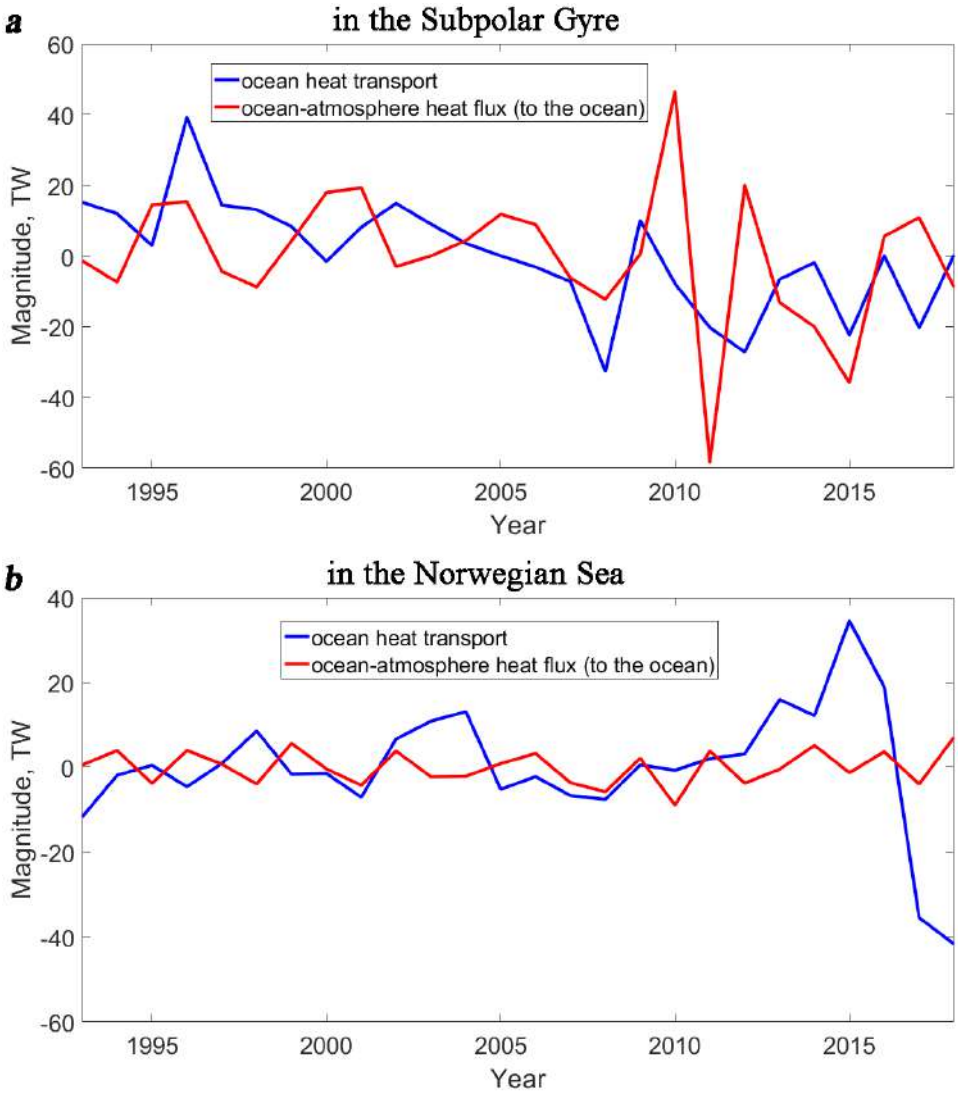

Interannual variability of the convergence of oceanic heat fluxes and ocean-atmosphere heat fluxes (mean values removed): a – in the Subpolar Gyre (Labrador and Irminger Seas, region 1–4 in Appendix 1), b – in the Norwegian Sea (region 5 in Appendix 1). The convergence of oceanic heat fluxes is calculated as the sum of oceanic heat fluxes across all boundaries of the region. The base water temperature for calculating the oceanic heat fluxes was taken as the freezing temperature of seawater (-1.8 °C).